SCIENTIFIC CONFERENCE

Le Bourget-du-Lac – July 2022

PRE-PRINT 2021

SYMPOSIUM 04
Geomorphology and speleogenesis

Speleogenesis of juvenile serial sinkhole-resurgence systems in the karsts of the Amazonian side of the Andes Mountains, Peru

Jean-Yves BIGOT[(1)], Jean Loup GUYOT[(2)] & Philippe AUDRA[(3)]

(1) Association française de karstologie (AFK), jeanbigot536@gmail.com (corresponding author)
(2) Groupe Spéléologique Bagnols-Marcoule (GSBM), Bagnols-sur-Cèze, jean-loup.guyot@ird.fr
(3) Polytech'Lab - UPR 7498, Université Côte d'Azur, France, Philippe.AUDRA@univ-cotedazur.fr

Résumé

Spéléogénèse des systèmes juvéniles de type doline-résurgence en série, dans les karsts de la face amazonienne de la Cordillère des Andes, Pérou. Les systèmes perte-résurgence en série, traversés par une même rivière, sont fréquents dans le nord du Pérou. Deux exemples dans la région d'Amazonas sont présentés, situés dans les karsts de Cerro Shipago (Prov. d'Utcubamba) et de Soloco (Prov. de Chachapoyas). Les rivières se perdent parfois jusqu'à trois fois sous terre en seulement 10 km de distance. Les tronçons souterrains se développent tantôt selon le pendage, tantôt selon la fracturation. Dans tous les cas, ces tronçons restent à proximité de la surface, sans pénétration à grande profondeur. Ces systèmes perte-résurgence en série sont typiques des hautes montagnes en forte surrection, bénéficiant de précipitations importantes. Ils correspondent à des réseaux juvéniles apparaissant avec la première karstification d'ensemble des calcaires. Les écoulements de surface soutenus par la présence de couvertures imperméables sont progressivement capturés par des pertes. Au-delà de la structure géologique, l'évolution des systèmes juvéniles de perte-résurgence en série est contrôlée principalement par la dynamique de surface, notamment l'épaisseur des couvertures imperméables, le gradient topographique et la dynamique d'incision des vallées.

Abstract

Serial sinkhole-resurgence systems, crossed by the river, are frequent in Northern Peru. We present here two examples from the Amazonas region, located in the karsts of Cerro Shipago (Utcubamba Prov.) and Soloco (Chachapoyas Prov.). The rivers flowing on the topographical surface sink underground rapidly in less than 10 km distance. The underground segments develop alternatively along dip or joints. They systematically remain at shallow depth. These series of sinkhole-resurgence systems are typical of mountains with high uplift rate and under a wet climate regime. Such karst features correspond to juvenile systems that appear during the first karstification phase of the limestone. Surface runoff occuring on low-permeability covers are gradually captured by sinkholes. Beyond the geological structure, the evolution of these sinkhole-resurgence systems is mainly controlled by surficial dynamic, especially the thickness of low-permeability covers, the topographic gradient and the incision dynamic of the valleys.

Resumen

Espeleogénesis de sistemas juveniles de sumidero-resurgimiento, en los karts de la vertiente amazónica de la Cordillera de los Andes, Perú. Los sistemas de pérdida-resurgencia en serie, cruzados por el mismo río, son comunes en el norte de Perú. Se presentan dos ejemplos en la región Amazonas, ubicados en los karsts de Cerro Shipago (Prov. de Utcubamba) y Soloco (Prov. de Chachapoyas). Los ríos a veces se pierden hasta tres veces bajo tierra en solo 10 km. Los tramos subterráneos se desarrollan a veces según el buzamiento, a veces según la fractura. En todos los casos, estos tramos permanecen próximos a la superficie, sin penetrar a gran profundidad. Estos sistemas de pérdida-resurgencia en serie son típicos de las altas montañas, que se benefician de precipitaciones importantes. Corresponden a redes juveniles que aparecen con la primera karstificación de todas las calizas. Los flujos superficiales, apoyados por la presencia de cubiertas impermeables, son capturados gradualmente por las pérdidas. Más allá de la estructura geológica, la evolución de los sistemas juveniles de pérdida-resurgencia en serie está controlada principalmente por la dinámica de la superficie, incluido la potencia de las cubiertas impermeables, el gradiente topográfico y la dinámica de la incisión del valle.

1. Introduction

Since 2003, the ECA club of Lima (Espeleo-club Andino) and French caving clubs, such as the Bagnols-Marcoule Speleological Group (GSBM), have been exploring continuously the karsts of Northern Peru. During numerous explorations in the Amazonian foothills of the Andes, the frequency of sinkhole-resurgence systems led us to look for the reasons behind the origin of the concentration of such karst phenomena in this area.

Are the series of sinkhole-resurgence systems a main characteristic of the Andino-Amazonian karsts of Peru?
We describe here two examples in the Amazonas Region (Fig. 1), the karsts of Cerro Shipago (Utcubamba) and the massif of Soloco (Chachapoyas), in order to identify similar features and that may provide an explanation for the frequency of these sinkhole-resurgence systems.

2. The slopes of Cerro Shipago

Figure 1: Location of the two provinces of Amazonas Region (Peru) and the sinkhole-resurgence systems of Cerro Shipago (Utcubamba) and Soloco (Chachapoyas).

a) Geological context

Cerro Shipago is one of the highest points (alt. 2849 m) of the limestone massif which extends to the south of the Bagua Grande city, in the Utcubamba Province. The Shipago massif appears as a large anticline fold, with a Permian sandstones core. It is capped by cretaceous series, including limestones, which form a monocline cover on the northern slope of the massif, from its summit to the bottom of the Bagua-Utcubamba syncline valley (alt. 430 m). The cretaceous formation, of several hundred meters thick, displays a steep dip to the north.
The massif is extensively karstified at high altitudes where higher rainfalls are more frequent. Indeed, the longest caves are located above 2000 m. The hilly topography rarely reveals the limestone outcrops, which is covered by thick weathering layers. However, sinkholes (locally called *tragaderos*) capture the streams at the bottom of closed sinks, making the caves active and crossed by streams (Fig. 2).

b) The series of sinkhole-resurgence system of the Río de las Tres Naranjas

The Tragadero del Río de las Tres Naranjas (alt. 2470 m) shows a complete set of passages forming a series of sinkhole-resurgence system of about 250 m in length each (BIGOT, 2019). The system has active and non-active passages over 739 m long and 17 m vertical range.

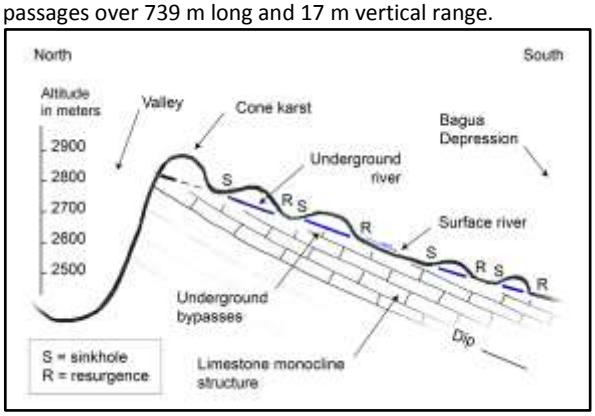

Figure 2: Schematic profile of the Shipago massif showing the shallow development of cave passages as a series of sinkhole-resurgence systems

Such caves are typical contact caves, developed along the dip, following a thin marly layer interbedded in Cretaceous limestones and locally guided by vertical fractures. These sinkhole-resurgence systems do not penetrate deep into the thick limestone and remain at shallow depth, below a thin layer of limestone. These karst systems are probably young, because they are still active.

3. The Soloco area

a) A series of sinkhole-resurgence systems in Soloco area

The series of sinkhole-resurgence systems in this area are extending over a distance of approximately 10 km, from the heights of Ancayrrumo down to the Sonche valley (Fig. 3).

From upstream to downstream, segments are: Ancayrrumo-Yacuñahui River, Chaquil-Río Seco, and Salcaquihua River-El Molino. Río Seco Cave is the main the segment, with 2095 m long and 42 m vertical range (-20, +22).

The nearby resurgence of the Río Seco is the largest in the area with an average discharge of about 1.2 m^3/s and a catchment area of about 40 km^2 (GUYOT, 2006). The system is probably fed by the river that sinks into the Tragadero de Chaquil (alt. 2986 m), located 300 m higher and 2.6 km upstream to the south.
Another underground system is developing parallel to Chaquil and Río Seco: the sinkholes of Parjugsha Grande, Parjugsha Alto, and Vaca Negra (Fig. 4). Underground segments were previously partly explored.

b) Hydrogeological and geomorphological context

Caves are developing in the Chambara Fm. limestone of Upper Triassic (BABY, 2006).
The general structure corresponds to a succession of thick limestone stripes between impermeable clastic formations. Sinkholes and resurgences are located at the contact of these formations. As a consequence, the three sinkhole-resurgence systems do not have direct morphological link, apart from the stream that crosses them.

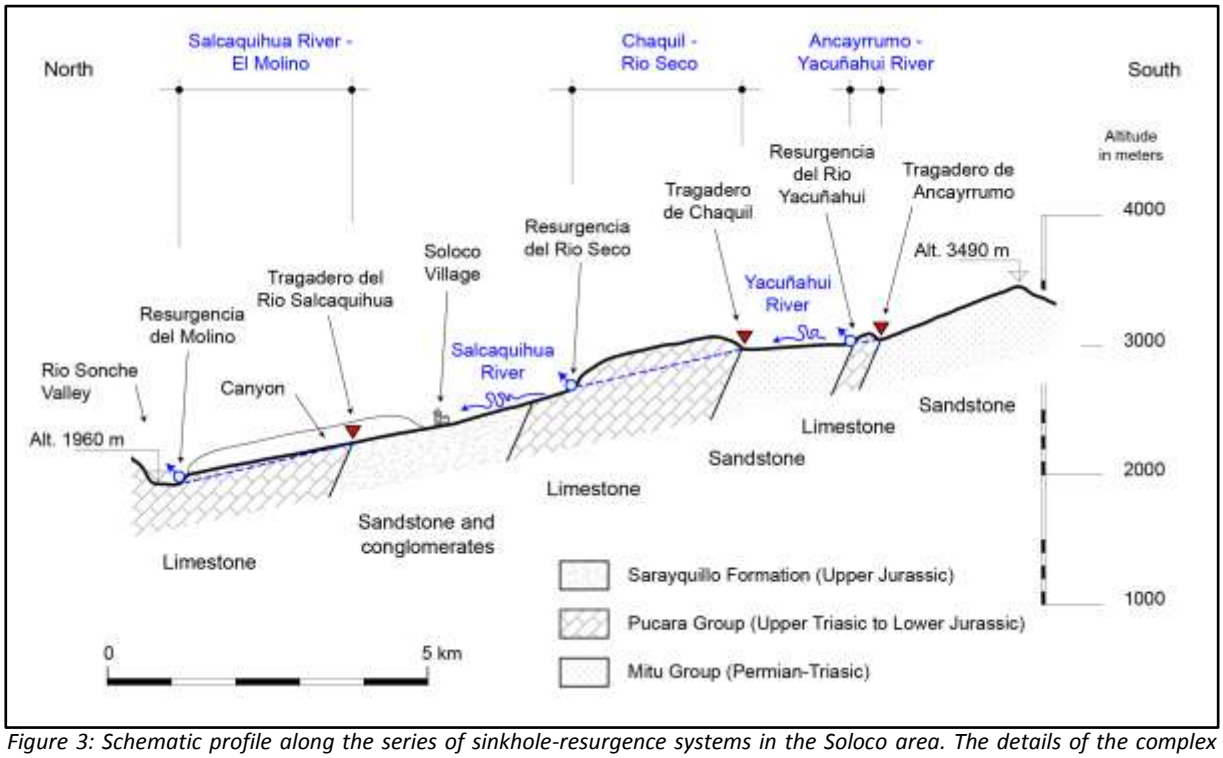

Figure 3: Schematic profile along the series of sinkhole-resurgence systems in the Soloco area. The details of the complex tectonic at the origin of the succession of stripes of the same limestone has not been indicated.

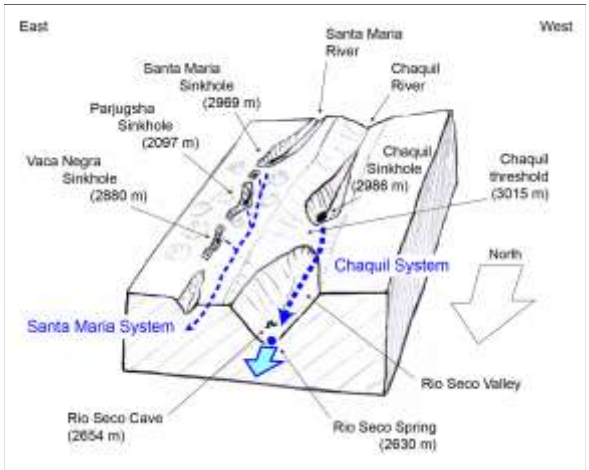

Figure 4: Simplified block diagram of the Soloco massif showing the two parallel underground systems.

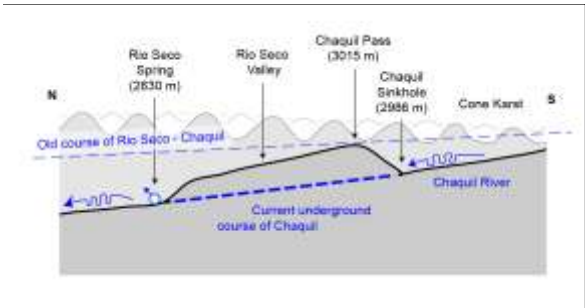

Figure 5: Simplified longitudinal profile of the Río Seco. The pass located at 3015 m attests to the ancient valley of Chaquil whose course has become underground.

The geomorphology of the massif shows that the surface river of Chaquil previously flowed in the Río Seco valley (Fig. 5). The underground captures gradually drained the valley, leaving a threshold upstream, which corresponds to the Chaquil pass (BIGOT, 2013).

4. Discussion and conclusion

In this area of Andino-Amazonia of Northern Peru, most of the caves are characterized by segments of underground bypasses, organized as a series of sinkholes-resurgences along the course of surficial rivers. Some cave waters of streams are crossing limestone stripes and reappear when arriving at the contact of impervious rocks (Soloco area). Others show the same trend even when crossing entirely limestone rocks (Cerro Shipago). In the latter, the cave systems are also guided by a thin marly inception horizon. Here, the underground segments are located along the dip of the limestone strata, locally guided by joints of similar direction as the general gradient. In all the explored caves, caves remain generally at shallow depth below the cone karst landscape. It seems that cave systems with vertical shafts are absent in this area, in opposite to the classical "alpine caves" model, whose caves reach great depth by using succession of fractures (AUDRA et al., 2002).

Such pattern of speleogenesis is typical of the juvenile cave type (AUDRA & PALMER, 2015). It is characteristic of recent karst areas with very fast uplift rates, conducting to important hilly landscapes and significantly eroded under a wet tropical climate such the case of the Amazonian side of the Andean Chain.

Consequently, the hypothesized story behind the karstification, since its early stage to the present-time as seen in both examples here-above, begin with a buried deep limestone which was initially not karstified.

As a consequence, before outcropping, the limestone masses were not karstified, being buried at great depth. This observation is supported by the high runoff largely present at the surface and still eroding or draining the thick weathering covers. Then caves begin to develop from the concentrated input of the streams. Caves follow prominent discontinuities, mainly bedding planes especially when inception horizons are present, fractures parallel to the slope, along the shortest path from sinkhole to resurgence. The resulting pattern shows a rectilinear plan with a moderate and constant slope from sinkhole to resurgence. Caves are always active whereas, abandoned passages are limited to some loops located at a moderate height above the active stream referring thus to their recent abandonment by the drainage system.

In some areas (Soloco), it is possible to follow the evolution stages, from shallow surface valley in the cone karst landscape, to progressive captures in underground segments, then to additional captures toward a new series of sinkhole-resurgence systems, whereas the first series of sinkhole-resurgence gradually tends toward an evolved landscape with large doline fields (Fig. 3, 5).

The new stream captures by sinkhole-resurgence systems are controlled by the dynamic of surface rivers, where those with the largest incision rate are gradually capturing the neighbouring catchment areas.

Finally, we conclude that the early development of underground karst conduits is initially controlled by the landscape characteristics and dynamic: i) the distribution, thickness, and evolution of the weathering covers controls the location of first sinkholes; ii) the topographic gradient controls the slope and extension of juvenile cave systems; iii) the large catchment areas produce surface rivers with higher incision rates that gradually capture the neighbouring catchment areas.

References

AUDRA P. & PALMER A.N. (2015) Research frontiers in speleogenesis. Dominant processes, hydrogeologic conditions and resulting cave pattern. *Acta Carsologica*, vol. 44, n° 3, pp. 315-348. https://ojs.zrc-sazu.si/carsologica/article/view/1960

AUDRA P., QUINIF Y. & ROCHETTE P. (2002) The genesis of the Tennengebirge karst and caves (Salzburg, Austria). *Journal of Cave and Karst Studies*, vol. 64, n° 3, pp. 153-164. https://caves.org/pub/journal/PDF/V64/cave_64-03-fullr.pdf

BABY P. (2006) Géologie des massifs de Soloco. Geología de los macizos de Soloco. *Bull. hors-série du GSBM Spécial* Chachapoyas 2004 & Soloco 2005 et *« Ukupacha » El Mundo Subterraneo*, n° 2, pp. 82-83.

BIGOT J.-Y. (2013) Note géomorphologique sur le massif calcaire de Soloco (Pérou). *Actes de la 22e Rencontre d'Octobre*, La Caunette 2012, *S. C. Paris édit.*, pp. 48-52.

BIGOT J.-Y. (2019) Les systèmes perte-résurgence en série des pentes du Cerro Shipago. *In* Nor Perú 2019. Expédition spéléologique au Pérou du 20 août au 9 octobre 2019. *ECA, GSBM, GS Vulcain, GS Dolomites édit.*, pp. 72-79.

GUYOT J. L. (2006) Hydro-climatologie du massif de Soloco. Hidro-climatología del macizo de Soloco. *Bull. hors-série du GSBM*, Spécial Chachapoyas 2004 & Soloco 2005 et *« Ukupacha » El Mundo Subterraneo*, n° 2, pp. 86-89.

The Peruvian cave files with topographies are available on the website http://www.cuevasdelperu.org

All topographic data and drawings for *TheRíon* are available at https://github.com/robertxa/Mapas_Cavernas_Peru

Speleogenesis and geomorphology of caves in conglomerate rocks in the Eastern Sayan

Anatoliy BULYCHOV

Institute of Geology and Mineralogy, SB RAS, Koptyug av., 3/4 Novosibirsk 630090 Russia

Abstract

Big Oreshnaya and Badjeiskaya caves in conglomerates (Siberia, Manskiy trough, Narva's suite) are unique as their length is about 50 km and 10 km respectively, while in general, there is no significant development of caves in such rocks. The reasons for the local karstification of the Narva's suite conglomerates are high porosity and fracturing of the rocks, high content of limestone and dolomite pebbles, boulders of gravelite rocks with quartz-calcite-dolomite filler, and the location of the cave massif which is favorable for infiltration and discharge of ground waters. The length of the passages in Big Oreshnaya cave is increasing year by year. Our geomorphological observations show the presence of large linear faults, which played an obvious role in karstogenesis, and the presence of signs of a near-surface cave level, which has not been discovered yet.

1. Introduction. Badjeiskiy site of Manskiy trough

The area of Manskiy trough (East Sayan) represents a part of a large synclinorium. The layer of conglomerates 2000m thick belongs to Narva's suite of lower Ordovician and covers 132 km² but the karst area occupies only 36 km² (TSYKIN 2004).

The rocks correspond to calcareous-dolomitic clays and marls, in which caves are not developed (TSYKIN 1990), and Narva's conglomerates which contain large cavities, undoubtedly of karst origin (TSYKINA & TSYKIN 1971). This is due to the structure of the rock, consisting of debris and cement, where dissolution of any of the components leads to a selective loss of strength. The cement of the rock has a high porosity, which is exemplified by intensive dripping from dead-end domed tubes. The rock composing boulders is fine-grained and crossed by 2-3 systems of fractures.

2. Geology of Big Oreshnaya and Badjeiskaya caves

The site with the largest caves is subject to tectonic fragmentation. In the caves, there are interlayer fracturing, and a network of faults. The conglomerate layers dip south-west-ward with an inclination from 45 to sometimes 80°. The entrances to the caves are located at an altitude of 600 m, relative elevations are up to 250 m. The relief of the surface is formed by erosion and denudation. Karst is heavily turfed and poorly expressed on insignificant fragments of the flatten surfaces.

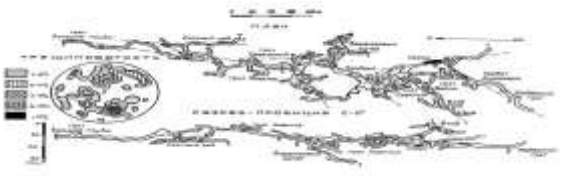

Figure1: Badjeiskaya cave (by Burmak I., Krasnoyarsk)

The main elements of the cave system are galleries of vaulted and triangular cross-sections 4-15 m wide, 2-30 m high, passages and squeezes with blocky and loamy deposits. Isometric rooms sometimes reach more than 30 m in diameter. Genesis of voids is erosional and tectonic-denudational with accumulation of loam and blocks of debris. Occasionally in the rooms, there are snow-white and reddish stalactites, stalagmites, draperies and cascades. Vertical shafts and chimneys with a depth of 6-40 m, elliptical and slit-shaped, connect the underlying and overlying parts of the cave system.

The main factor of the dynamic system is corrosion due to condensation, infiltration of water and transfer of water vapor, so Badjeiskaya and Big Oreshnaya caves are still developing (new systems and rooms that were either impossible to get into 45 years ago or that were dug open). The presence of calcium bicarbonate in water vapor is evidenced by numerous exudates: spherulites, grains, flowers, and the Crystals Gallery, discovered in 1978, all consist of crystalline sheaf-like aggregates. The number of luminescent moon-milk in «Galaxy way» and in «Siberian system» has increased. Moon-milk is probably a white cement of vein calcite with 88Sr impurities (TSYKIN & TSYKINA 1978).

Permanent watercourses have little flow rate (up to 3.5 l/sec). Most of the streams are cut into loams, but the Porcelain Creek in Badjeiskaya and the streams in the rooms of Dreams, Mazodrom, Adventure, Columnar in Big Oreshnaya are cut into the bedrock. Temporary streams are intensively eroding in vertical cracks. Active infiltration of karst waters is represented by intense dripping.

Permanent small lakes were formed by the clogging of the bottom of rooms or galleries with loam. Large lakes are located at the lower levels of the caves, but their drainage towards the surface was not found.

The deposits are represented by loams, consisting of sandy, silty and clayey particles interspersed with pebbles. The clay mineral is represented by hydromica (TSYKIN 1985). The accumulation of loams continues in the passages along their longitudinal axis in the form of swelling.

The morphology of the area shows that Badjeiskaya cave (Fig. 1) was opened by a nival-corrosive shaft (23 m deep) and developed initially at the same level (the impressive volumes of the Broadway gallery are about 0.5 km long), Big Oreshnaya was opened by slope denudation and developed simultaneously at different levels.

3. History of speleogenesis

Speleogenesis at the initial stage is associated with the formation of a Miocene peneplain (TSYKIN 1990) and occurred due to the structural factors of rocks with selective high water permeability.

In the Neogene, the conglomerate was saturated with water. As the neotectonic uplift increased and karst discharge decreased, the water saturation of the speleosystem dwindled. Fluctuations in climatic conditions significantly influenced the formation of karst waters. In the caves, the pluvial of the Middle-Upper Pleistocene can be traced by following the tracks of lake levels and relics of thick drip crusts.

At the contemporary (Late Quaternary) stage of speleogenesis, the leading factor is the complex denudation and development of cave systems along tectonic faults.

From the main entrance, Big Oreshnaya cave is 155 meters deep. The bottom sump is 35 m deep. The highest point of the cave (system "Zastrem") is situated 44 meters above the main entrance. So the recent amplitude of Big Oreshnaya cave is 234 m. The total volume of voids is estimated to be over 400 000m^3. All separate parts and systems of the cave are mapped carefully and appear to be more than 60km totally. But it is still difficult to synthetize all of them to a general map (BOULYTCHOV 1999, Fig. 2), so an accomplished map doesn't exist completely yet. Persistent efforts to perform the entire map are being continued. Young cavers have been working a lot last 20 years but mostly digging a loam in narrows or excavating in breakdowns, and they have succeeded to discover new systems. But the mapping is hardly being done.

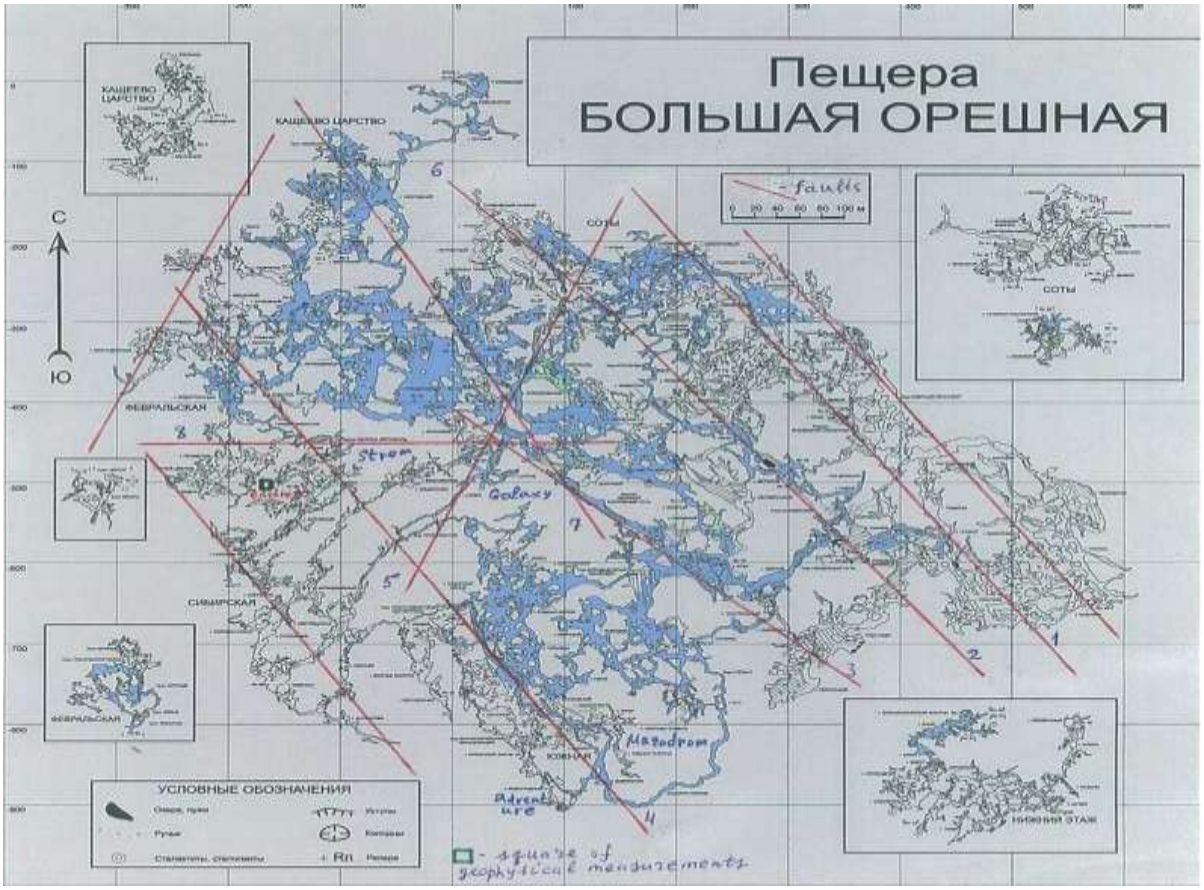

Figure 2: Preliminary map of Big Oreshnaya cave and deduced faults, along which the cave is developed

4. Geomorphological and geophysical observations

After our discovery of Siberian, Lotos and Strem systems where we had to free climb up 70 m vertical and overhanging walls (BULYCHOV & SOROKINA 2017), we proposed to search on the upper part of the mountain where Big Oreshnaya cave is developed. This prompted us to carry out seismic-electrical (BOULYTCHOV 1997, BOULYTCHOV 2000, SOROKINA & BOULYTCHOV 2001) measurements on the surface near the top of the mountain on a relatively flat area. As a result of processing the geophysical data, emptinesses were recorded at depths of 3-8 m. It gave enthusiasm to squeeze through a breakdown in the Strem system upwards to discover Zastrem system which appeared to be very close to the surface (3-5 m but totally blocked by calcite-cemented boulders).

The assumption about the possible continuation of the cave along the upper horizons led to the search for fragments of ancient alignment surfaces near the top of the mountain and in the direction of the significant Rucheinaya cave, which has been very actively extended towards Big Oreshnaya cave the last year. By means of deciphering aerial photographs, signs of destroyed peneplains and faults were deduced (Fig. 3).

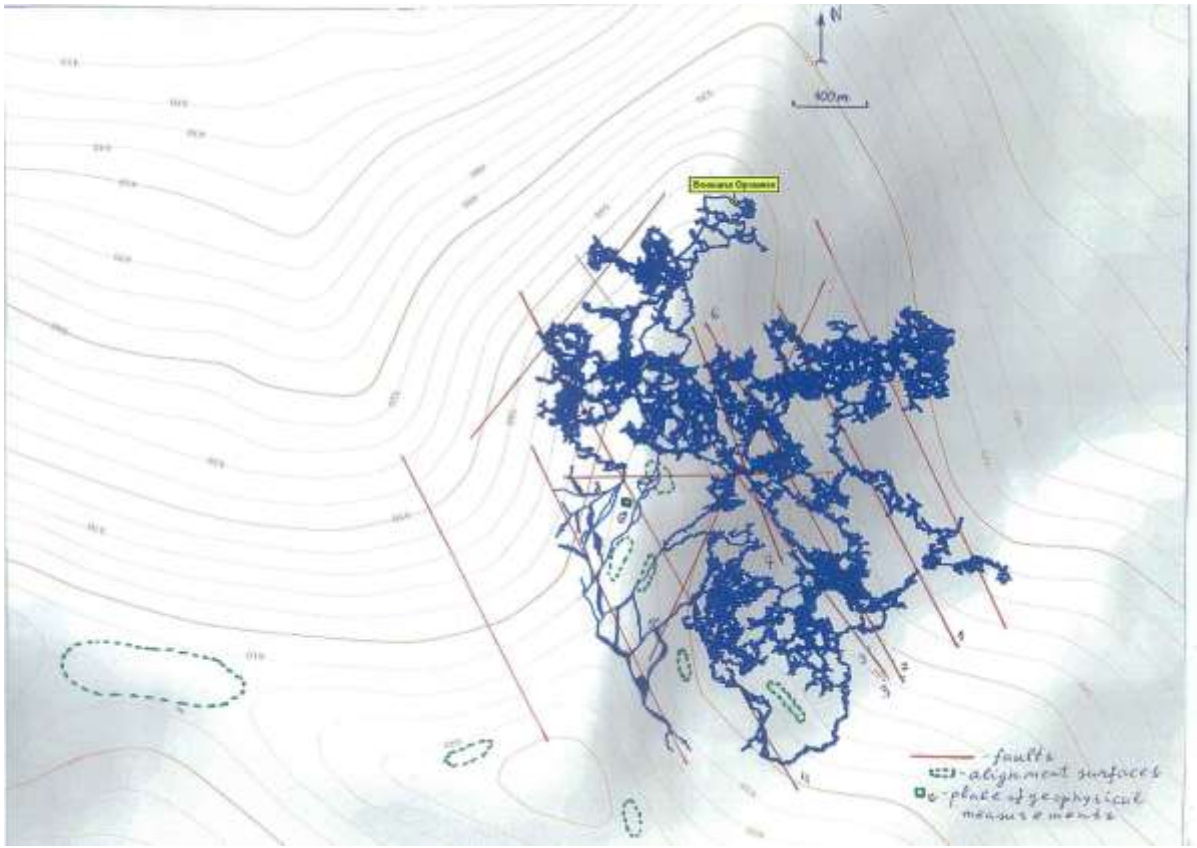

Figure 3: Deciphered faults and projection of the map of Big Oreshnaya cave to the surface.

5. Discussion

It is clearly seen (Fig. 3) that Big Oreshnaya cave is developed in a block bound by a network of faults, which is geomorphologically expressed by a sharp bend of the horizontal lines in the massif. Moreover, it was possible to clearly identify faults to the west of the main massif of the cave, along which the cavers have not yet found anything.
The assumption about the existence of a continuation of the cave is strengthened by the identified fragments of the peneplains located on the surface near the top of the mountain, and the deciphered faults to the west of the main massif of the cave.

Careful analysis of aerial photographs through high-resolution optical binoculars did not allow to identify geomorphological signs of faults and karst forms further to the west towards Rucheinaya cave, which is about 1.5 km away.
Since we have already discovered a very significant extension of the cave in the upper part of the Vertical fault, there is reason to try our luck to make new discoveries in the upper parts of other faults.

6. Conclusions

The study of the data obtained allowed us to infer the following conclusions:

- perspective for the development of Big Oreshnaya cave along upper levels storeys is quite possible (especially to the West towards Rucheinaya cave);
- a connection with Rucheinaya cave (Fig. 4), according to geomorphological analysis, is unlikely;
- the discovery of new systems should be attempted by climbing the walls (Fig. 2, 3) of faults (2- Ozerny, 5- Kolokolny, 7- Prohodnoy, 3- Convict, 4- NSU, 1- Extraterrestrial Galaxy, 6- Surdovsky, 8- Vertical, another part) from the bottom up, followed by the excavation of clay plugs or squeeze in the breakdowns, as well as by means of excavation at the base of the fault zones.

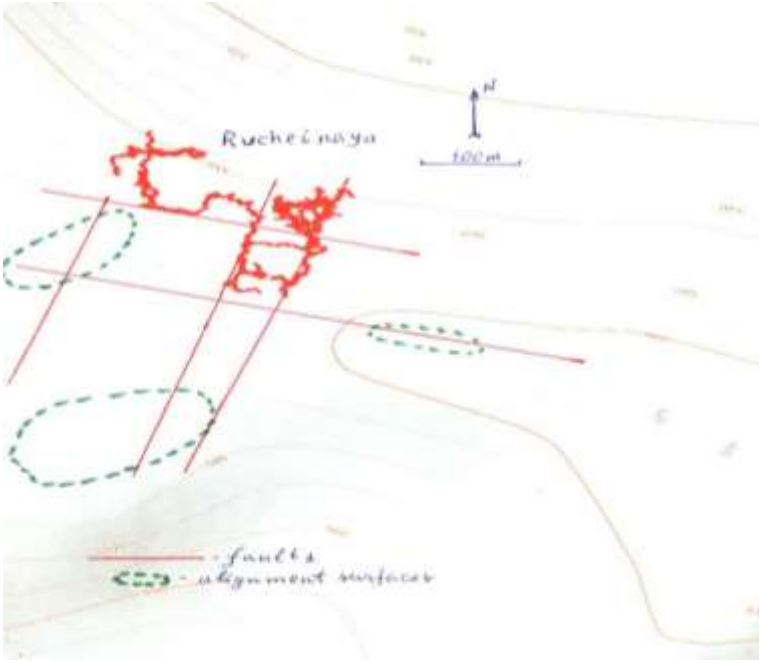

Figure4: *Deciphered faults and projection of the map of Rucheinaya cave to the surface.*

Acknowledgments

I would like to express my gratitude to Artem Barinov (Krasnoyarsk Speleo Club) for the scheme of projection of the Big Oreshnaya cave to the surface.

A separate profound reverence to my fellow colleagues, our fraternity of speleologists for the 45-year practice of joint exploration of the Big Oreshnaya and nearby caves of the Badjeiskiy site: Denis Rogozin, Alexey Zhdanov, Sergei Shundeev, Vasily Shcherbakov ...

References

BOULYTCHOV A.A. (1997) Geophysically predicted and discovered large cave emptinesses in Siberia. *Proceedings of the 12-th International Congress of Speleology*, La-Chaux-de-Fonds, Switzerland, v.5, 89-92.

BOULYTCHOV A.A. (1999) Kektash - the deepest cave of Siberia and Big Oreshnaya - the longest one. *Stalactite*, Bern, Switzerland, n° 49, 1, 47-48.

BOULYTCHOV A.A. (2000) Seismic-electric effect method on guided and reflected waves. *Physics and Chemistry of the Earth*, Journal of EGS, v.25, No 4, 333-336.

BULYCHOV A.A., SOROKINA T.V. (2017) Multi-faceted training of caver-explorer. *Proceedings of the 17-th International Congress of Speleology*, Sydney, Australia, v.1, 278-284.

SOROKINA T.V., BOULYTCHOV A.A. (2001) Seismic-electric benchmarking of shallow subsurface horizons and dome cavities. *Extended abstracts of EAGE*, Amsterdam, Netherlands, v.2, P133.

TSYKINA Z.L., TSYKIN R.A. (1971) Badjeiskie conglomerate caves, *Caves*, Perm, edition 10-11.

TSYKIN R.A. (1985) *Deposits and minerals of karst*, Science, Novosibirsk, 165 p.

TSYKIN R.A. (1990) *Karst of Siberia*, Krasnoyarsk, 154 p.

TSYKIN R.A. (2004) *Karst-speleological regions and caves of Krasnoyarsk district*, Krasnoyarsk, 129 p.

TSYKIN R.A., TSYKINA Z.L. (1978) *Karst of eastern part of Altai-Sayan folded region and its related minerals*, Science, Novosibirsk, 104 p.

Dissolution-corrosion measurements with limestone and gypsum tablets in active sulphuric acid caves of southern Italy

Ilenia M. D'ANGELI(1), Mario PARISE(2), Marco VATTANO(3), Giuliana MADONIA(3) & Jo DE WAELE(1)

(1) Dipartimento di Scienze Biologiche, Geologiche e Ambientali, Università di Bologna, jo.dewaele@unibo.it (corresponding author), dangeli.ilenia89@gmail.com
(2) Dipartimento di Scienze della Terra e Geoambientali, Università di Bari, mario.parise@uniba.it
(3) Dipartimento di Scienze della Terra e del Mare, Università di Palermo, marco.vattano@unipa.it, giuliana.madonia@unipa.it.

Abstract

Dissolution-corrosion (DC) represents an important factor for speleogenesis, and can be measured monitoring weight variation over time of carbonate and gypsum tablets exposed in underground environments. The oxidation of H2S produces H2SO4, which in carbonate host rock induces the surface of carbonate tablets to be rapidly corroded by sulphuric acid, whereby CaCO3 is replaced by CaSO4·2H2O, producing a significant weight gain. We describe preliminary results of DC monitoring in four still-active SAS systems, including Ninfe Cave and Terme Sibarite (Calabria), Fetida Cave (Apulia), and Acqua Fitusa Spring Cave (Sicily). The tablets have been set inside the caves, in three different conditions of exposure (i.e. underwater, air, interface zone) in the winter 2015-2016 to monitor DC in five years. The results show how the condition of exposure is an important control for the behaviour of weight variation. Tablets set underwater displayed significant weight loss during the first period of exposure, whereas those located at the interface zone exhibited a tendency of weight variation significantly dependent on time, and tablets in air showed weight gain.

1. Introduction

Dissolution-corrosion (DC) represents the key process to understand the speleogenesis and evolution of karst systems (GABROVŠEK & PERIC, 2006). Generally, in caves, geomorphological changes are slow and invisible, but observable over long time scales (PRELOVŠEK, 2012).

DC rates can be measured using: 1) micro-erosion meter (MEM) (HIGH & HANNA, 1970; MIHEVC, 2001) or Traversing micro-erosion meter (TMEM) (TRUDGILL *et al.*, 1981), 2) rock tablets (SWEETING, 1979), and 3) hydrogeological methods (CORBEL, 1959; PULINA & SAURO, 1993; FORD & WILLIAMS, 2007).

Rock tablets measure the weight loss throughout cave exposure. Weight loss/gain is calculated using a weight scale, and it is more precise than micrometer measurements. Since the size of the exposed surface is known, it is possible to convert weight loss into metric units, comparable to MEM measurements and hydrogeological balance calculations.

For sulphuric acid caves the most important factor is the oxidation of H_2S into H_2SO_4, which immediately tends to corrode carbonate rocks both underwater or in aerate conditions. In aerate conditions, calcium carbonate ($CaCO_3$) is replaced by gypsum ($CaSO_4 \cdot 2H_2O$), the most common secondary mineral in sulphuric acid speleogenetic (SAS) caves. In addition, active sulphuric acid caves are influenced by microbiological extremophiles which colonize waters, walls and ceilings (D'ANGELI et al. 2019b).

The study of DC rate in still-active SAS caves can give significant information on the evaluation of the different stages of cave formation, and to correlate them with landscape evolution (GALDENZI *et al.*, 1997; MARIANI *et al.*, 2007; GALDENZI, 2012).

Italy hosts 25% of the SAS caves known worldwide, and several of them are still-active (D'ANGELI *et al.*, 2019). Investigations on DC rates began in the winter 2015-2016, and are still ongoing in the following SAS caves of southern Italy (Fig. 1): 1) Ninfe Cave (Cerchiara di Calabria) and Terme Sibarite (Cassano allo Ionio) in Calabria; 2) Fetida Cave (Santa Cesarea Terme) in Apulia; 3) Acqua Fitusa Spring Cave (San Giovanni Gemini) in Sicily. The preliminary results of our DC monitoring are shown in this work.

Figure 1: Study area displaying caves location.

2. Materials and methods

Limestone, marble and gypsum tablets (7x4x1 cm with an initial mean weight of 74 g) were produced and placed in several locations of the caves (Fig. 2) to observe eventual differences in DC rate in various environmental conditions: 1) underwater (10-20 cm below water table); 2) at the water-air interface; 3) in the cave atmosphere (Fig. 2). In each site, we placed 2 tablets each per lithology: a) selenitic gypsum (G); b) Istria limestone (I); c) Carrara marble (M); and for Fetida and Acqua Fitusa Spring caves, also host rock which are, respectively, d) Altamura limestone (C) and Rudist breccias member of the Crisanti Formation (B).

In Fetida Cave the experiment started in October 2015 and it is still ongoing. Here two sites were monitored, both located in the innermost portion (B1 and B2), where we observe evidences of rising sulphidic waters (B1). In addition, in B2, three limestone tables were set horizontally in aerate conditions to observe possible changes of DC rate due to space orientation of the exposed surface.

In Fitusa, Terme Sibarite, and Ninfe caves the experiments started at the beginning of January 2016 and are still ongoing. Here the tablets were placed in a single site. In Acqua Fitusa Spring Cave, tablets were placed in the lower still-active level, where the sulphidic water table is currently located (Fig. 2E). In the Terme Sibarite Cave, tablets were placed in a small water body (Fig. 2B), and in Ninfe Cave in the innermost zone (Fig. 2A).

In all these locations, we also carried out water sampling. Water parameters (pH, T, EC) were measured using the multiparameter sensor Hanna HI991001, and in each location two samples (250 ml) were collected, one of which was acidified with 65% HNO_3. Water samples were analyzed in the laboratories of Politecnico di Torino. The saturation analysis showed (following Debye-Hückel equation) the index for calcite to be slightly undersaturated in almost all the locations, excluding Ninfe Cave which was oversaturated. Saturation index for dolomite was close to the equilibrium state, and for gypsum was undersaturated.

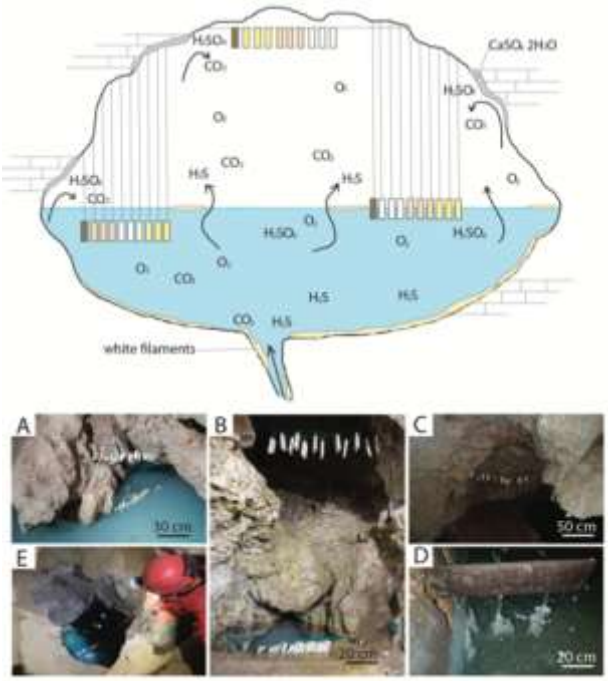

Figure 2: Sketch showing how tablets were placed in a cross-section. Pictures: A) Ninfe Cave; B) Terme SIbarite; C and D) Fetida Cave; E) Acqua Fitusa Spring *Cave.*

3. Results

Gypsum tablets showed different rates of dissolution depending on environmental conditions (i.e. underwater, interface water-air, air). In Fetida Cave (B1 and B2) gypsum weight loss reached a mean of 92% in 33 days in underwater conditions, and 60% at the interface. In aerate conditions the dissolution was slower: as a matter of fact, we observed 0.49% in 601 days of exposure.

In Terme Sibarite, in 2 days we recorded weight loss of 59 and 35%, respectively underwater and at the interface, whereas in Ninfe Cave in 10 days the loss reached 36% underwater and 5% at the interface.

In Acqua Fitusa Spring Cave, gypsum tablets after 40 days totally disappeared (100%), whilst at the interface and in aerate conditions they showed values of 72 and 0.9% respectively.

Significant is the weight variation of carbonate limestones in Fetida Cave (Fig. 3A-B). The DC in B1 (Fig. 3A) exhibited higher values than in B2 (Fig. 3B); the weight loss reached 7% in 837 days of exposure. In B1, DC underwater is higher during the first part of the monitoring, whilst after 582 days in the cave an inversion of tendency was visible, and weight loss at the interface became higher.

Tablets in aerate conditions showed an initial weight loss, followed by weight gain. In B2, DC at the interface was higher than underwater, and this tendency was quite stable over time. In aerate conditions, tablets set horizontally (Ch) showed a significant weight loss in the first part of the monitoring, followed by weight gain. The general behaviour for the tablets in air, both horizontally and vertically oriented was similar; however, those horizontally oriented showed a higher weight loss (see cyan line in Fig. 3B). The weight variation observed in Terme Sibarite (Fig. 3C) exhibited higher values of DC underwater. In Ninfe Cave (Fig. 3D) the dissolution of marble was faster with respect to Istria limestone, both underwater and at the interface. In Acqua Fitusa Spring Cave the Carrara marble was the only lithology showing a certain degree of DC, which was exclusively visible at the interface zone (Fig. 3E). In Terme Sibarite, Ninfe Cave, and Acqua Fitusa Spring Cave it was difficult to observe weight variation in aerate conditions.

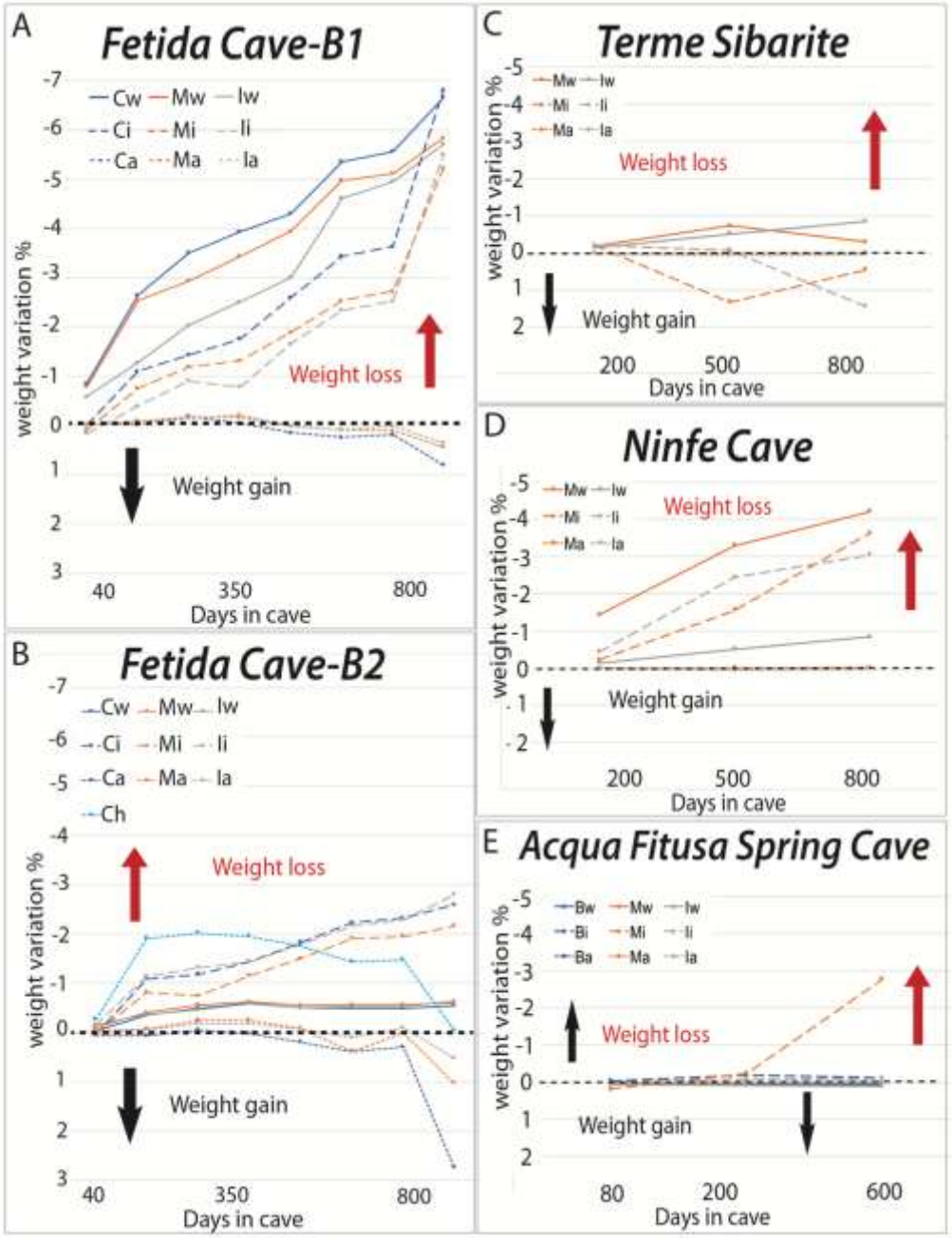

Figure 3: Weight variation (%) of tablets over time (days of exposure in cave), in A) Fetida Cave, monitoring site B1 (close to a sulphidic spring); B) Fetida Cave, monitoring site B2 (in the innermost portion of the cave); C) Terme Sibarite; D) Ninfe Cave; E) Acqua Fitusa Spring Cave. "C" means Altamura limestone and "B" Rudist breccias member of the Crisanti Formation (both host-rocks), "M" Carrara Marble, "I" Istria limestone, whereas "w" means underwater, "I" interface, and "a" air, "h" means horizontally oriented (cyan colour). Colours and lines help to discriminate lithologies (blue, orange, grey) and environmental conditions of exposure (continuous line means underwater, dashed line interface, dotted line air). Red arrow shows the area of weight loss and the black line the weight gain area.

4. Discussion and Conclusions

Field monitoring of DC and laboratory measurement of weight variation showed interesting results, demonstrating the importance of environmental parameters, essential key factors for the weight loss/gain. Overall, the gypsum tablets underwater and at the interface were easily dissolved, especially due to the undersaturation of water solution with respect to gypsum. As a matter of fact, the weight loss in aerate conditions was significantly lower.

In Calabria and Sicily, the DC rate seems to be controlled by lithology, and the weight loss of marble is favoured with respect to the other lithologies. In Terme Sibarite and in

Ninfe Cave, the dissolution is faster underwater, whereas in *Acqua Fitusa Spring* Cave it was faster at the interface.
The investigations carried out in Fetida Cave demonstrated the DC to have a different behaviour as a function of the vicinity to the sulphidic spring (located in B1). The average value of weight loss reached 7% close to the sulphidic spring (B1). In the first stages of monitoring (before 582 days of exposure), DC underwater was faster, whilst after day 582, DC became higher at the interface. On the contrary, in B2, located in the innermost portion of the cave, the higher DC was observed at the interface throughout the whole exposure. Overall, in aerate conditions it is possible to observe an initial weight loss, followed by weight gain. This behaviour is linked to the interaction of H_2SO_4 with the external surface of tablets, which tends to dissolve carbonate producing weight loss. Then the dissolved ion of carbonate (CO_3^{2-}) is replaced with SO_4^{2-} inducing the precipitation of gypsum ($CaSO_4 \cdot H_2O$), and subsequent weight gain of the tablet.
Significant is the weight loss observed on the horizontally oriented tablets in B2. From Figure 3B it is possible to observe how a few months after the exposure, the weight loss reached an average of 2%, due to the falling of gypsum moonmilk (pH 0-1) from the upper surface of tablets. After moonmilk removal, the weight variation exhibited the same tendency of the vertically oriented tablets (in aerate conditions).
The field monitoring of DC and weight loss/gain in the aforementioned systems will end in 2021, and final results will allow to clarify these preliminary outcomes.

Acknowledgments

Thanks to all the people who helped us during the field monitoring and documenting the cave environments. In particular, we thank Orlando Lacarbonara, Rosangela Addesso, Isabella Serena Liso, Luca Pisano, Marianna Mazzei. Thanks to Sergio Pispico to Santa Cesarea Terme spa director. Thanks to Giuseppe Martire, Carlo Forace, to the "Associazione Speleologica Liocorno" and to Terme Sibarite spa director. Thanks to Antonio Cesarini, and to the whole caving group of "Serra del Gufo".
Thanks to the members of the "Le Taddarite" of Palermo speleological association.
Thanks to Bartolomeo Vigna and Adriano Fiorucci from Politecnico di Torino for the geochemical analysis of water samples. Ilenia D'Angeli thanks the "Lions Club Megaride" (district 108 YA) and the "Stazione Zoologica Anton Dohrn" for the financial support in the framework of the "Paolo Brancaccio" award.

References

CORBEL, J. (1959). Erosion en terrain calcaire. Annales de Géographie, 68, 97-120.

D'ANGELI IM., PARISE M., VATTANO M., MADONIA G., GALDENZI S., DE WAELE J., (2019) Sulfuric acid caves of Italy: A review. Geomorphology, 333, 105-122.

D'ANGELI IM, GHEZZI D., LEUKO S., FIRRINCIELI A., PARISE M., FIORUCCI A., VIGNA B., ADDESSO R., BALDANTONI D., CARBONE C., MILLER AZ., JURADO V., SAIZ-JIMENEZ C., DE WAELE J., CAPPELLETTI M., (2019b) Geomicrobiology of a seawater-influences active sulfuric acid cave. PLoS ONE, 14(8): e0220706.

FORD D., WILLIAMS P., (2007) Karst hydrogeology and geomorphology. John Wiley & Sons, 562 p.

GABROVŠEK F., PERIC B. (2006) Monitoring the flood pulses in the epiphreatic zone of karst aquifer. Acta Carsologica, 35(1), 35-45.

GALDENZI S. (2012) Corrosion of limestone tablets in sulfidic ground-water: measurements and speleogenetic implications. International Journal of Speleology, 41(3), 149-159.

GALDENZI S., MENICHETTI M., FORTI P. (1997) La corrosione di placchette calcaree ad opera di acque sulfuree: dati sperimentali in ambiente ipogeo. In: P.Y. JEANNIN (Ed.), Proceedings of the 12th International Congress of Speleology, La Chaux-de-Fonds, 1, 187-190.

HIGH C.J., HANNA K. (1970) A method for the direct measurement of erosion on rock surface. British Geomorphological Research Group, Technical Bulletin 5.

MARIANI S., MANIERO M., BARCHI M., VAN DER BORG K., VONHOF H., MONTANARI A. (2007). Use of the speleogenetic data to evaluate Holocene uplifting and tilting: an example from the Frasassi anticline (northeastern Apennines, Italy), Earth Planetary Science Letters, 257(1-2), 313-328.

MIHEVC A., (2001) Speleogeneza Divakega krasa. Zalozba ZRC, Ljubljana, 148 p. šGypsum caves as indicators of climate-driven river incision and aggradation in a rapidly uplifting region. Geology, 43, 539-542.

PULINA M., SAURO U. (1993) Modello dell'erosione chimica potenziale di rocce carbonatiche in Italia. Memorie della Società Geologica Italiana, 313-323.

PRELOVŠEK M. (2012) The dynamics of the present-day speleogenetic processes in the stream caves of Slovenia. Carsologia, 15, 152 p.

SWEETING M.M. (1979) Solution and erosion in the karst of Melinau limestone in Gunung Mulu national park, Sarawak, Borneo. Proceeding of the 4th International Congress of Speleolgy in Yugoslavia. Lubljana, 227-232.

TRUDGILL, S., HIGH, C.J., HANNA, F.K. (1981). Improvements to the micro-erosion meter. British Geomorphological Research Group Technical Bulletin, 29, 3-17.

Sulphur stable isotope signatures from sulphuric acid caves of Italy

Ilenia M. D'ANGELI(1), Stefano M., BERNASCONI(2), Cristina CARBONE(3), Mario PARISE(4), Giuliana MADONIA(5), Marco VATTANO(5), Jo DE WAELE(1)

(1) Dipartimento di Scienze Biologiche, Geologiche e Ambientali, Università di Bologna, jo.dewaele@unibo.it (corresponding author), dangeli.ilenia89@gmail.com
(2) Geological Institute, ETH Zürich, stefano.bernasconi@erdw.ethz.ch
(3) Dipartimento di Scienze della Terra, dell'Ambiente e della Vita, cristina.carbone@unige.it
(4) Dipartimento di Scienze della Terra e Geoambientali, Università di Bari, mario.parise@uniba.it
(5) Dipartimento di Scienze della Terra e del Mare, Università di Palermo, marco.vattano@unipa.it, giuliana.madonia@unipa.it.

Abstract

The study of sulphur stable isotope signatures in Sulphuric Acid Speleogenetic (SAS) caves gave rise to interesting information on both H_2S sources and reactions involved in the sulphur cycle. In general, the stable isotope geochemistry of gypsum, sulphur and other sulphate by-products found in underground SAS environments, provides the most robust evidence of present-time and past SAS processes. Chemical signatures during sulphuric acid weathering can be influenced by microbial sulphate reduction (MSR) and/or thermochemical sulphate reduction (TSR). Studies on S isotope fractionation revealed large fractionations during MSR (from -30‰ to -70‰) with typical 34S-depleted sulphides, whereas TSR shows smaller variations or no fractionation (δ34S values of SAS by-products due to TSR are more or less similar to the original source of reduced sulphur). In the last two decades, the investigation on SAS caves around the world increased and produced interesting results. Italy hosts 25% of the worldwide known SAS caves, which are mainly located along the Apennine Chain, but also in Apulia, Sicily and Sardinia. In this contribution, we will report the new results from the study of the sulphur stable isotopes of sulphate and sulphur by-products found in 18 SAS systems in Italy.

1. Introduction

Chemical signatures of sulphuric acid speleogenesis in inactive-fossil caves are mainly preserved in the stable isotopes of sulphur, which can give important information regarding both the H_2S sources and involved reactions in the sulphur cycle.

In general, sulphur stable isotope investigations of gypsum and sulphur, found as by-products in underground environments, represent the most robust evidence of past SAS processes. Sulphur has four stable isotopes in nature (^{32}S, ^{33}S, ^{34}S and ^{36}S), but only ^{32}S (95%) and ^{34}S (4.2%) have mostly been used, mainly because the other two isotopes account for less than 1% (ECKARDT, 2001; CANFIELD, 2001). Nevertheless, some authors proved ^{33}S to represent a valuable tool in unravelling complex biogeochemical sulphur cycling processes (CANFIELD *et al.*, 2010; ZERKLE *et al.,* 2010).

In general, the isotopic composition of geological samples is expressed in $\delta^{34}S$, the ratio of ^{34}S and ^{32}S in ‰, normalized to the universal standard (Cañon Diablo Troilite: CDT), and the average values of $\delta^{34}S$ observed can vary significantly from -70 to +35 ‰.

One of the most striking chemical signatures of SAS is the often very negative value of $\delta^{34}S$ (down to -25‰) of gypsum which indicates that sulphate was produced by oxidation of sulphide produced by MSR (microbial sulphate reduction). These low $\delta^{34}S$ values were the first compelling evidence for the implication of hydrocarbons in the origin of H_2S in the Guadalupe Mountains in New Mexico (HILL, 1981). There, the hydrocarbons of the Delaware Basin provided the electrons for microbial sulphate reduction of the Castile Formation evaporites, demonstrated by a $\delta^{34}S$ shift from around +10‰ of these Permian gypsum deposits to around −20‰ for the H_2S (HILL, 1987, 1990).

Studies on S isotope fractionation during S oxidation have shown that the $\delta^{34}S$ shift can be very small, producing no fractionation at high T (OHMOTO & RYE, 1979) or small fractionation at low T (FRY *et al*., 1988). This means that the $\delta^{34}S$ values of SAS minerals (e.g., gypsum, Al-Fe-sulphates) due to TSR (thermochemical sulfate reduction) are more or less similar to that of the original source of reduced sulphur (BOTTRELL *et al*., 2001; SEAL, 2006). Nevertheless, as in the case of Cerna Valley (Romania), the wide range of $\delta^{34}S$ values have been proven to derive both from TSR of sedimentary sulfates and their reaction with methane, produced by microbial decay of nearby coal deposits (ONAC *et al.,* 2011).

On the contrary, sulphate reducing microbes preferentially use ^{32}S for their metabolic reactions and produce ^{34}S-depleted H_2S (STRAUSS, 1997), causing $\delta^{34}S$ values of sulphides to shift by as much as -70‰ (BRUNNER & BERNASCONI, 2005).

In general, the final $\delta^{34}S$ value depends on the initial isotopic signature of the sulphur source and many other factors such as e.g. sulfate reduction rate and concentrations of reactants. Similar to the Guadalupe Mountains (SPIRAKIS & CUNNINGHAM, 1992), low sulphur isotopic compositions of

gypsum have been found in Villa Luz Cave (Mexico) where H_2S most probably derives from microbial reduction of evaporites using electrons of hydrocarbons coming from the nearby oil fields (HOSE *et al.,* 2000). Further, $\delta^{34}S$ values of gypsum in Kraushöhle (Austria) (PUCHELT & BLUM, 1989; PLAN *et al.,* 2012) and Montecchio (Tuscany, Italy) (PICCINI *et al.,* 2015) are very low deriving from the fractionation of Triassic evaporites, due to microbial reduction and successive oxidation.

Recently, interesting investigations on sulphur isotopes have been carried out in some Italian SAS systems such as Frasassi (ZERKLE *et al.,* 2016) and Calabrian caves (GALDENZI & MARUOKA, 2019). They found sulphide $\delta^{34}S$ values ranging between -21 and -13‰, whilst sulphate $\delta^{34}S$ ranged between +16 and +23‰, demonstrating the deep-seated Triassic evaporites of the Burano Formation (15 to 17 ‰) to play an important role as dominant source of sulphate (GALDENZI & MENICHETTI, 1995).

During the last five years SAS by-products have been collected in several still-active and fossil cave systems in Italy, including Monte Cucco (MC), Acquasanta Terme (AT), Cavallone-Bove (CB), Capo Palinuro (CP), Monte Sellaro (MS), Cassano allo Ionio (CI), Santa Cesarea Terme (SCT), Acqua Mintina (AM), Acqua Fitusa (AF) caves (Fig. 1, to which the labels are referred). In addition, the sulphur isotope composition of bitumen (Maiella Mts., Abruzzo), Messinian and Triassic gypsum deposits have been investigated.

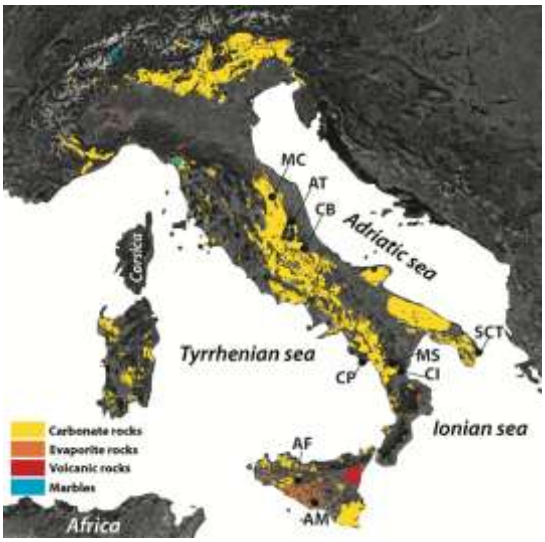

Figure 1: Study area displaying caves location. MC Monte Cucco (Umbria), AT Acquasanta Terme (Marche), CB Cavallone-Bove (Abruzzo), CP Capo Palinuro (Campania), MS Monte Sellaro (Calabria), CI Cassano allo Ionio (Calabria), SCT Santa Cesarea Terme (Apulia), AM Acqua Mintina (Sicily), AF Acqua Fitusa (Sicily).

2. Materials and methods

SAS minerals were collected directly in the field from broken pieces of deposits or provided by collections of the Circolo Speleologico Idrogeologico Friulano as in the case of Capo Palinuro.

A total of 91 mineralogical samples coming from Santa Cesarea Terme (7), Acqua Mintina (10), Acqua Fitusa (10), Cavallone-Bove system (17), Cassano allo Ionio (15), Capo Palinuro (4), Monte Cucco (17), Acquasanta Terme (3), Monte Sellaro (2), Messinian evaporite (1) and Triassic evaporite (1) and bitumen from Majella Massif (4) were powdered and analyzed at ETH Zurich to study ^{34}S stable isotopes. Of these 91 samples (excluded 4 samples of bitumen, 1 sample of Messinian and Triassic evaporites), 49 were constituted by gypsum (the most common by-product in SAS environment and observable in all the systems described in this paper), 16 by alunite (AM, CB, MC), 7 by sulphur (SCT, AM, CI, CP, MC, AS), 7 by jarosite (SCT, AM, CB, MC), 2 by celestine (AM), 1 by an assemblage of copiapite-pickeringite-tamarugite (CI), 1 by thenardite-eugsterite (AF), 1 by barite (MC), and 1 by baritina (MC) (Fig. 2). All samples were wrapped in tin capsules with V_2O_5 and converted into SO_2 in Thermo Fisher-EA 1112 coupled with a Thermo Fisher Delta V Isotope ratio mass spectrometer. Their distribution is reported in Figure 3.

3. Results and Discussion

Sulphur stable isotopic analyses of mineralogical samples (sulphur, gypsum, and Al-Fe-sulphates) collected in several SAS systems of Italy (Fig. 1) show distinctive distributions (Fig. 3) controlled by the interaction of hydrocarbon-related substances with deep-seated evaporites. These values can thus be compared with the end-member values of Triassic and Messinian evaporites, and bitumen deposits. Messinian gypsum (MG) from Bologna area shows a $\delta^{34}S$ value of 23.6‰, whereas the Triassic evaporites (TG) from Pietre Nere Formation in Apulia have a value of 15.1‰. Bitumen deposits (BIT) range between -18.9 and -17.2‰. The values of $\delta^{34}S$ in the various cave systems are listed below and range between: a) Monte Cucco -22.97 and 5.18‰; b) Acquasanta Terme -11.32 and -9.57‰; c) Cavallone-Bove -8.86 and 9.33‰; d) Capo Palinuro -25.85 and -17.28%; e) Monte Sellaro -10.46 and -9.32%; f) Cassano allo Ionio -28.15 and 15.77%; g) Santa Cesarea Terme -33.00 and -21.97‰; h) Acqua Mintina -14.18 and 1.31‰; Acqua Fitusa -2.53 and 23.57‰.

The most negative $\delta^{34}S$ values have been found in Santa Cesarea Terme, and are likely due to the mixing of hydrocarbon derived S-rich fluids with minor amounts of fluids deriving from the MSR of deep-seated Triassic gypsum. Monte Cucco and Cassano allo Ionio caves present a wide range of sulphur stable isotopes. As demonstrated by D'ANGELI *et al.* (2018), Monte Cucco showed phases of hypogene hydrothermal processes that probably influenced thermally the reduction of sulphates, as recorded in Cerna Valley (ONAC *et al.,* 2011).

Figure 2: Some of the mineralogical deposits collected in sulphuric acid speleogenetic caves in Italy. A) copiapite-pickeringite-tamarugite from Terme Sibarite spa in Cassano allo Ionio (Calabria); B) Sulphur crusts covering the walls and gypsum stalactites from Gattulla Cave in Santa Cesarea Terme (Apulia); C) sulphur from Acqua Mintina cave (Sicily); D) gypsum from Acqua Mintina (Sicily); E massive gypsum deposits from "La Grotta" in Monte Cucco (Umbria); F-G-H) alunite and jarosite deposits in Cavallone Cave (Abruzzo); I) Bitumen in some mine caves in the Majella Massif. A photo by Soledad Cuezva, B by Mario Parise, C-D by Marco Vattano; E by Jo De Waele; F-G-H by Maria Nagostinis; I) by Jo De Waele

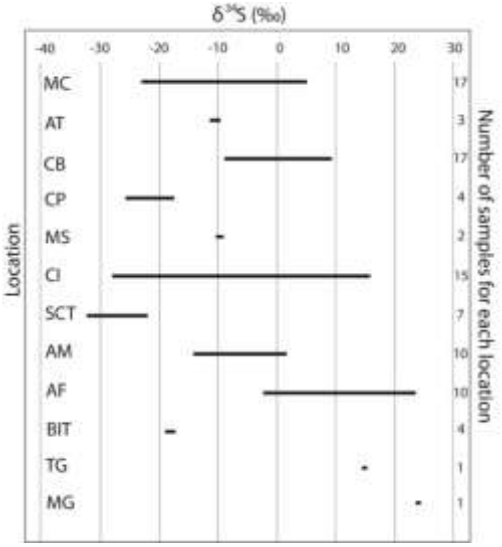

Figure 3: $\delta^{34}S$ values recorded in sulphur, gypsum and Al-Fe-sulphate deposits collected in several SAS systems of Italy. MC Monte Cucco (Umbria), AT Acquasanta Terme (Marche), CB Cavallone-Bove (Abruzzo), CP Capo Palinuro (Campania), MS Monte Sellaro (Calabria), CI Cassano allo Ionio (Calabria), SCT Santa Cesarea Terme (Apulia), AM Acqua Mintina (Sicily), AF Acqua Fitusa (Sicily), BIT bitumen collected in the Majella Massif area (Abruzzo), TG is the Triassic Gypsum from Pietre Nere in Apulia, and MG Messinian Gypsum from Sicily.

The samples collected in Cassano allo Ionio caves showed more or less the same distribution as those described by GALDENZI & MARUOKA (2019), and can be related to deep-seated Triassic evaporite reduction. Only one sample of gypsum collected in a recently discovered cave (called "Terme Sibarite Cave"), located close to the present sulphuric water table, recorded a positive value of 15.8‰.

4. Conclusions

Geochemical investigation using ^{34}S from Italian sulphuric acid speleogenetic cave systems shows wide variability in values of $\delta^{34}S$ ranging between -33 and +23.57‰. This great variability is the result of the geological and structural conditions of the investigated cave systems, characterized by an active Apennine chain with deep discontinuities well linked to deep-seated H_2S sources of sulphur (Triassic evaporites, sea water deep circulation, hydrocarbon tiers, volcanic activity, and the presence of sulphides). In addition, H_2S-enriched fluids might have undergone a different degree of microbial sulphate reduction (MSR) which was more efficient in the locations exhibiting negative values. The most negative values have been observed in the still-active Santa Cesarea Terme, a very peculiar system in which sea water mixes with rising sulphidic fluids producing characteristic geochemical patterns (D'ANGELI *et al.,* 2020). Nevertheless, our results are in agreement with those observed in Frasassi and Calabrian caves displaying a similar

tendency (ZERKLE *et al.,* 2016; GALDENZI & MARUOKA, 2019). This would demonstrate that the dominant source of H_2S are the Triassic evaporites located below the Apennine Chain, the privileged zone of sulphuric acid cave formation (D'ANGELI *et al.,* 2019). Despite that, the wide diversity might be explained by local interactions of fluids with other minor sources such as deep-seated hydrocarbon tiers, sedimentary sulphides (pyrite, marcasite, chalcopyrite), and volcanic activity (especially in Capo Palinuro).

Acknowledgments

Thanks to all the people who helped us during the field sampling. In particular, we thank Orlando Lacarbonara, Rosangela Addesso, Luca Poderini, Giuseppe Antonini, Paolo Forconi, and Maria Nagostinis. Thanks to the Circolo Speleologico Idrologico Friulano for the 4 samples from Capo Palinuro, a site which is difficult to access in the last years due to coastal landslides. Thanks to Sergio Pispico and to the Santa Cesarea Terme spa director, to Giuseppe Martire, Carlo Forace, and the "Associazione Speleologica Liocorno", and to the Terme Sibarite spa director. Thanks to Antonio Cesarini, to the whole caving group of "Serra del Gufo", and to the "Le Taddarite" cavers for the support during the fieldwork in Sicily.

References

BOTTRELL SH., CROWLEY S., SELF C., (2001). Invasion of a karst aquifer by hydrothermal fluids: evidence from stable isotopic compositions of cave mineralization. Geofluids, 1(2), 103-121.

BRUNNER, B., BERNASCONI, S.M., (2005). A revised isotope fractionation model for dissimilatory sulfate reduction in sulfate reducing bacteria. Geochim. Cosmochim. Acta 69, 4759-4771.

CANFIELD DE., (2001). Biogeochemistry of sulfur isotopes. Reviews in Mineralogy and Geochemistry, 43, 607-636.

CANFIELD DE., FARQUHAR J., ZERKLE AL., (2010). High isotope fractionations during sulfate reduction in a low sulfate euxinic ocean analog. Geology, 38, 415-418.

D'ANGELI IM., CARBONE C., NAGOSTINIS M., PARISE M., VATTANO M., MADONIA G., DE WAELE J., (2018). New insights on secondary minerals from Italian sulfuric acid caves. Int. Journal of Speleology, 47(3), 271-291.

D'ANGELI IM., PARISE M., VATTANO M., MADONIA G., GALDENZI S., DE WAELE J., (2019) Sulfuric acid caves of Italy: A review. Geomorphology, 333, 105-122.

D'ANGELI IM., DE WAELE J., FIORUCCI A., VIGNA B., BERNASCONI SM., FLOREA LJ., LISO IS., PARISE M., (2020). Hydrogeology and geochemistry of the sulfur karst spring at Santa Cesarea Terme (Apulia, southern Italy). Hydr. J., DOI: 10.1007/s10040-020-02275-y.

ECKARDT F., (2001). The origin of sulphates: an example of sulphur isotopic application. Progress in Physical Geography, 25(4), 512-519.

FRY B., RUF W., GEST H., HAYES JM., 1988. Sulfur isotopes effects associated with oxidation of sulfide by O2 in aqueous solution. Chemical Geology, 73, 205-210.

GALDENZI S., MENICHETTI M., (1995). Occurrence of hypogenic caves in a karst region: examples from central Italy. Environmental Geology, 26, 39-47.

GALDENZI S., MARUOKA T., (2003). Gypsum deposits in the Frasassi caves, Central Italy. J.Cav.Karst St., 65, 111-125.

GALDENZI S., MARUOKA T., (2019). Sulfuric acid caves in calabria (South Italy): Cave morphology and sulfate deposits. Geomorphology, 328, 211-221.

HILL CA., (1981). Speleogenesis of Carlsbad Caverns and other caves in the Guadalupe Mountains. In: BF. Beck, (Ed.) Proc. 8th Int. Congr. Spel., 1, 143-144.

HILL CA., (1987). Geology of Carlsbad Caverns and other caves in the Guadalupe Mountains, New Mexico and Texas. New Mex. Bur. Min. Min. Res. Bull., 117, 1-150.

HILL CA., (1990). Sulfuric acid speleogenesis of Carlsbad Caverns and its relationship to hydrocarbons, Delaware basin, New Mexico and Texas, AAPG Bull., 74, 1685-1694.

HOSE LD., PALMER AN., PALMER MV, NORTHUP DE., BOSTON PJ., DUCHENE HR., (2000). Microbiology and geochemistry in a hydrogen-sulphide-rich karst environment. Chemical Geology, 169, 399-423.

PICCINI L., DE WAELE J., GALLI E., POLYAK VJ., BERNASCONI SM., ASMERON Y., (2015). Sulphuric acid speleogenesis and landscape evolution: Montecchio cave, Albegna river valley (Southern Tuscany, Italy). Geomorphology, 229, 134-143.

PLAN L., TSCHEGG C., DE WAELE J., SPÖTL C., (2012). Corrosion morphology morphology and cave wall alteration in an Alpine sulfuric acid cave (Kraushöhle, Austria). Geomorphology, 169-170, 45-54.

PUCHELT H., BLUM N., 1989. Geochemische Aspekte der Bildung des Gipvorkommens der Kraushöhle/Steiermark Oberrh. Geol. Abh., 35, 87-99.

OHMOTO H., RYE RO., (1979). Isotopes of sulfur and carbon. In: HL. BARNES (Ed.), Geochemistry of Hydrothermal Ore Deposits, Wiley & Sons, 509-567.

ONAC BP., Wynn JG., SUMRALL JB., (2011). Tracing the source of cave sulfates: a unique case from Cerna Valley, Romania. Chemical Geology, 288, 105-114.

SEAL RR., (2006). Sulfur isotope geochemistry of sulfide minerals. Rev. Min. and Geochem., 61(1), 633-677.

SPIRAKIS CS., CUNNINGHAM KI., (1992) Genesis of sulfur deposits in Lechuguilla Cave, Carlsbad Caverns National Park, New Mexico. In: G. WESSEL, B. WIMBERLEY (Eds.), Native Sulphur-developments in geology and exploration. Am. Inst. Min. Metall. Petrol. Eng., 139-145.

STRAUSS H., (1997). The isotopic composition of sedimentary sulfur through time. Palaeo, 132, 97-118.

ZERKLE AL., KAMYSHNY A., KUMP LR., FARQUHAR J., ODURO H., ARTHUR MA., (2010). Sulfur cycling in a stratified euxinic lake with moderately high sulfate: constraints from quadruple S isotopes. Geochimica et Cosmochimica Acta, 74, 4953-4970.

ZERKLE AL., JONES DS., FARQUHAR J., MACALADY JL., (2016). Sulfur isotope values in sulfidic Frasassi cave system, central Italy: a case of a chemolithotrophic S-based ecosystem. Geochim. Cosmochim. Acta, 173, 373-386.

The future of Quaternary geomorphology lies underground

Trevor FAULKNER

GEES, University of Birmingham, Edgbaston, Birmingham, B15 2TT, UK. e-mail: trevor@marblecaves.org.uk

Abstract

Little detail is known about the Quaternary evolution of upland Britain and Ireland. Multiple glaciations shaped the landscapes, but the maximum extent of the last British-Irish Ice Sheet is still being clarified, and its verticality is poorly constrained in space and time. Almost nothing is known about earlier upland glaciations, because surface evidence was reworked. Help is at hand, by studying karst caves. Caves have a special 'museum' property to preserve evidence of palaeo-environments, from their location, morphology, hydrology, dimensions and contents. Caves develop at successively lower levels during each deglaciation, as recharge and discharge points follow glacially-eroded valleys downwards. Phreatic passage diameters and vadose canyon entrenchments record timescales, perhaps confirmed by sediment dates. Using integrated studies of 'museum' attributes and working backwards in time and upwards in elevation, cave history, the varying glacial, deglacial and interglacial climate regimes, and the uplift and erosion of the local topography, can be deduced, and extrapolated beyond the immediate karst area. Partial successes with this approach include landscapes in Wales, Yorkshire and Norway. Resolution of these histories requires a holistic multi-disciplinary collaboration among geological, geomorphological, sedimentological, glaciological, hydrological, climatological, seismological and speleological communities.

1. The geomorphological problem

Little is known about the detailed Quaternary evolution of upland Britain (Fig. 1), Ireland and other glaciated northern environments. What were: The horizontal and vertical extents of icesheets during each glaciation? The erosion rates of summits and valley floors? The relationships to relative sea levels and the isostatic responses during each deglaciation? How much land lost by erosion was then elevated above sea level during each succeeding interglacial? What effects did seismic and aseismic tectonic movements have on the landscapes? This knowledge is challenging to obtain from surface observations, because each glaciation reworks or destroys previous evidence.

2. Present knowledge

Glaciological events in Britain and Ireland since the Last Glacial Maximum (LGM) are partly known. The global LGM occurred c. 26,000 years ago, when eustatic sea level was lower by c. 130 m (PU CLARK *et al.,* 2009). The development of the British-Irish Ice Sheet (BIIS) around the time of its local LGM was asynchronous, with an early build up in Scotland, followed by later extensions and growths southwards that covered all Ireland and Wales and most of England, with ice streams that flowed 'down' the Irish and North Seas (CD CLARK *et al*., 2012). The oscillations between the LGM and the Younger Dryas Stadial are still being investigated (Fig. 2). Little is published about glacial initiation at Marine Isotope Stage (MIS) 5d, although more is known about its onset in Norway (LUNDQVIST, 1986). Earlier glacial extremities have only been studied in England far from the upland areas.

There is more knowledge of the horizontal extents of the Fennoscandian Ice Sheet (FIS; OLSEN *et al*., 2013) and the Laurentide Ice Sheet (LIS; Quaternary Science Reviews, 5, 1986) for the last few glaciations. These were much larger than the BIIS and easier to model from deep sea sediments. Their oscillations after each local LGM commonly occurred before the ice margins retreated to the present coastlines, giving less terrestrial ambiguity. Their detailed landscape changes caused by each previous glaciation remain unknown, but the total erosional effect of *all* the FIS glaciations has been estimated (LIDMAR-BERGSTRÖM, 1997). The smaller BIIS, in warmer latitudes, was much more dynamic in space and time and more difficult to decipher.

Figure 1: Suilven, viewed from Stac Pollaidh in Assynt, Scotland, an area with karst caves.

Later glaciations in N. Europe, including the BIIS, were reviewed by BOSE *et al.* (2012). SIMMS (2004) discussed erosion and isostasy in Ireland, distinguishing between mechanical erosion of siliciclastic rocks and chemical dissolution of limestones. The question remains: how did the local landscapes evolve before the LGM, during the first 99% of the Quaternary, from 2.6–0.026 million years ago? Study of pre-LGM upland geomorphology appears to be 'stuck'.

3. A karst geomorphological approach

Geomorphological history of glaciated northern uplands can be improved from evidence in local or adjacent limestone caves. These act as 'museums' of previous environments, from their location, hydrology, morphology, dimensions, and chemical, clastic and archaeological contents.

Figure 2: Lacustrine deposits under till, Glen Findhorn.

Location, hydrology, morphology, dimensions

Cave location relative to present fluvial drainage is key. Streams in vadose passages and sumps are commonly continuing to enlarge passages in harmony with erosion of the local landscape. Whilst streams are flowing in steep topography, they are likely to be sufficiently dilute, turbulent, and flowing fast enough, for dissolution to be beyond the chemical breakthrough point where unsedimented floor lowering and wall retreat rate are maximised for the ambient temperature and P_{CO2}. This is c. 1 mm per year at 10°C with 1% P_{CO2} (PALMER, 1991). During floods, dissolution might obey the Fast Rate Law (KAUFMANN & DREYBRODT, 2007) and be supplemented by significant mechanical erosion, increasing enlargement rates by an order of magnitude. The duration of this latest phase can be estimated from the local annual precipitation, its seasonality, and the size of the relevant catchment area, using dissolution rates for relatively low temperature and P_{CO2} (FAULKNER, 2006). Hydrological parameters might be deducible from the lengths of wall scallops (FAULKNER, 2013a). In vadose passages, dissolution rates can be checked against passage depth and width (CHECKLEY & FAULKNER, 2014). It can be estimated if an active passage enlarged in the Holocene, or if it started prior to that, if phreatic, or in a previous interglacial, if vadose. Relict vadose passages could have been active earlier in the Holocene, or if at high levels, during a previous interglacial, when catchment areas and sink entrances were higher, prior to glacial erosion.

Relict phreatic caves high above a valley floor, such as Victoria Cave in Yorkshire (Figs. 3 and 4), are unrelated to Holocene hydrology. However, they formed and enlarged under phreatic hydraulic control, when filled by flowing water. The last opportunity for this in glaciated landscapes was during the last deglaciation, when submerged by an ice-dammed lake as the ice down-wasted (FAULKNER, 2008). Several narrow spillways above Victoria Cave and along the southern edge of the limestone (Fig. 5) show where lake water jökulhlaups burst through the ice sheet that continued to the south (MURPHY *et al.,* 2015). Fig. 6 shows an enigmatic feature at Gully Cave, Giggleswick Scar, Yorkshire. The only conceivable explanation is that water from an ice-dammed lake sank into an inception fracture to initiate the cave. Flow was forced upwards from the initial phreatic conduit in the roof, to create rising cupolas in the limestone cliff and a moulin in the continuing ice sheet, which had previously sealed the cliff edge.

Figure 3: A distant view of Victoria Cave, Yorkshire, UK, high on the far hillside.

Figure 4: The excavated entrance to Victoria Cave.

Figure 5: A spillway on the southern edge of the Yorkshire karst. Figure 6: Rising cupolas above the relict phreatic conduit at the entrance to Gully Cave, Yorkshire Dales.

Figure 7: Scallop size records the last dissolutional phreatic flow regime during deglaciation in Elgfjellhola, Norway. Isostatic uplift then caused cm-scale tectonic movement that can be observed around the passage circumference, including where it displaced the wall scallop. Glove for scale.

Both deglacial and interglacial phreatic enlargement opportunities were necessarily available during previous

glacial cycles. They could also occur at the start of each interstadial, dependent on the extent of local downwasting. Surface evidence of these occasions is extremely rare, but might be retained in underground deposits (see below). Sharp slickensides record neotectonic movements after passages enlarged to present sizes (Fig. 7). In central Scandinavia, probably all phreatic caves record a tectonic movement, but none that are mainly vadose. Relating movement to a known seismic event gives the latest time that the passage drained, probably at an ice dam collapse.

Contents

The ages of contents place constraints on passage formation. Their composition provides information about the external environment when deposited. Commonly, internal deposits are younger than the containing passage and most chemical deposits formed after the passage drained. Speleothems can be dated. Trace elements elucidate the contemporary local environment. Corroded large speleothems could indicate dissolution when submerged during a subsequent deglaciation. Speleothem 'straws' would probably not survive dissolution and mechanical erosion by flooding, and therefore formed in the Holocene. Allogenic clastic deposits can commonly also be dated and provide more external information. For example, Broadway in County Pot, Yorkshire, contains stacked sediment layers, including flowstone above rounded cobbles (FAULKNER, 2016), which indicate multiple deposition events, probably related to cycles of glaciation, deglaciation and interglaciation.

Various layered stalagmite and clastic deposits In Victoria Cave represent all the glacial cycles back to before 600 ka in MIS15 (LUNDBERG *et al*., 2010), so that a large passage (Fig. 4) must have existed before then. The deposits' presence hints that the cave was not subject to interglacial flows since, otherwise they could have been washed away. MIS8 is represented only by a hiatus in speleothem deposition between MIS9 and 7, rather than by a significant clay layer. This shows that MIS8 ice was thinner or absent in Yorkshire, and perhaps in Britain, when compared with ice from MIS14 to MIS2. The absence of large mammal deposits during some interglacials suggests that the entrance was sporadically blocked by scree. An elephant tooth and other interglacial mammal remains preserved in the short relict Joint Mitnor Cave, S. Devon, UK (WILMUT *et al*., 2014, p. 106) suggests that it has been relict since MIS5e.

Deducing the timescales

The evolutionary history of multi-level caves in glaciated areas can commonly be estimated, even before dating internal deposits. Glaciation modified the local landscape, caves and hydrology by the erosional deepening and widening of glacial valleys and by removing upper passages and entrance areas. Deglacial seismicity created deeper fractures that allowed new passages to form at lower levels (FAULKNER, 2008). Hence, cave and surface evolution can be deduced by considering the external and internal hydrology and cave configuration at each interglacial, by working backwards in time and upwards in elevation. The dimensions of the active vadose canyons and active phreatic sumps can indicate their age after inception, with suitable wall scallops confirming estimated flow rates and flow speeds. Where the cave has keyhole morphology, with relict phreatic passages or levels above an active streamway, this next higher level probably formed during the last deglaciation. Any relict vadose passages might have formed in the previous interglacial. Higher relict phreatic passages and levels could have formed during the deglaciation before that. This reasoning can be applied up to the highest levels in the cave, where higher entrances commonly indicate earlier sinks and resurgences. Because each passage level was submerged by flowing water during each subsequent deglaciation, higher conduits tend to increase in diameter. However, where the surface was more protected, such as under cold-based ice at high altitude, cave hydrology could stay more constant, and the same phreatic conduits could just increase in size.

Integrated studies of karst cave development and the glacial impact on the local topography are needed to deduce these timescales. This requires a holistic multi-disciplinary collaboration among geological, geomorphological, sedimentological, glaciological, hydrological, climatological, seismological and speleological communities. For safety and conservation, collaborating teams of researchers and cave explorers are needed. Most disciplines reside in university departments, which might be unaware of the opportunities available from speleological science. Nevertheless, contacts between university and local caving clubs ought to initiate from the academic side, to ensure that relevant scientific projects are specified, implemented and suitably reported.

Recent applications

Several examples with similar methodologies correlated cave and local topographical evolution. WALTHAM *et al.* (2010) used information from several long caves in Kingsdale, Yorkshire, to equate the formation of surviving high-level passage fragments to the Anglian MIS12 glaciation. WALTHAM & LONG (2011) deduced from erosion rates and isostasy that the age of exposure of the cavernous Great Scar Limestone was c. 1.3 Ma. SIMMS & FARRANT (2011) and FARRANT & SIMMS (2011) studied landscape evolution in SE Wales. They showed that Ogof Draenen, with >70 km of passages, had at least four development phases. It comprises essentially three long separate stacked systems that individually drained southwards, northwards, then southwards again, in response to fluvial and glacial incisions of the valleys at each end. FARRANT *et al*. (2013) showed that thick fine-grained sediments in the cave derived from glacial meltwater, probably after MIS12, 10 or 6. FAULKNER (2013b) showed that Toerfjellhola in Norway probably started as two separate high-level palaeocaves after MIS12, which became connected by a common flow route during MIS5e. COOPER & MYLROIE (2015) interpreted the effect of glaciation on speleogenesis in the NE United States and HARMAND *et al. (*2017) concentrated on fluvial evolution and karstification south of the major icesheets. VERESS *et al.* (2019) have recently presented a review of global glaciokarst knowledge. WESTAWAY (2020) inferred the uplift history of the English Peak District from cave deposits and levels.

4. The future vision

Digital technology now produces custom-made maps. A future aim would create maps and Digital Elevation Models for the Earth's upland surface as it was in previous interglacials, at scales up to 1:50,000. The first issues would be of glaciated karst areas in the MIS5e (Eemian) interglacial, followed by maps to represent MIS7e, MIS9, MIS11 etc. This would permit better understandings of how the many long and complex cave systems in Britain, Ireland and elsewhere developed relative to the glacial erosion and uplift of the local landscape. Clearly, this information becomes more tenuous with age, and initial maps of earlier interglacials would only be feasible at smaller scales. However, with refinement, both the timescale and physical resolution should increase. A coupled aim should be to produce geological maps that represent the lithology exposed at the surface during previous interglacials.

Acknowledgement

The International Union for Quaternary Research is thanked for providing the opportunity to present the poster, as now expanded in this paper, at the XX INQUA Congress in Dublin, 25–31 July 2019.

References

BOSE M., LÜTHGENS C., LEE J.R. and ROSE J. (2012) Quaternary glaciations of N. Europe. *Quaternary Science Reviews*, 44, 1–25.

CHECKLEY D. and FAULKNER T. (2014) Scallop measurement in a 10m-high vadose canyon in Pool Sink, Easegill Cave System, Yorkshire Dales, UK and a hypothetical post-deglacial canyon entrenchment timescale. *Cave and Karst Science*, 41 (2), 76-83.

CLARK C. D. and 4 others. (2012) Pattern and timing of retreat of the last British-Irish Ice Sheet. *Quaternary Science Reviews*, 44, 112-146.

CLARK P.U. and 8 others. (2009) The Last Glacial Maximum. *Science*, 325, 710-714.

COOPER M.P. and MYLROIE J.E. (2015) *Glaciation and Speleogenesis: Interpretations from NE USA*. Springer.

FARRANT A.R. and SIMMS M.J. (2011) Ogof Draenen: speleogenesis of a hydrological see-saw from the karst of South Wales. *Cave and Karst Science*, 38 (1), 31-52.

FARRANT A.R., SIMMS M.J. and NOBLE S.R. (2013) Subterranean glacial spillways: an example from the karst of S. Wales, UK. *16th International Congress of Speleology Proceedings*, Vol. 3, 42-47.

FAULKNER T. (2006) Limestone dissolution in phreatic conditions at maximum rates and in pure, cold, water. *Cave and Karst Science*, 33 (1), 11–20.

FAULKNER T. (2008) The top-down, middle-outwards, model of cave development in central Scandinavian marbles. *Cave and Karst Science*, 34 (1), 3-16.

FAULKNER T. (2013a) Speleogenesis and scallop formation and demise under hydraulic control and other recharge regimes. *Cave and Karst Science*, 40 (3), 114-132.

FAULKNER T. (2013b) A methodology to estimate the age of caves in northern latitudes, using Toerfjellhola in Norway as an example. *16th International Speleological Congress Proceedings*, Vol. 3, 342-348.

FAULKNER T. (2016) Cave Science Field Meeting: Barbon and Easegill, UK. [In 2011]. BCRA Annual Review for 2015, 35-37.

HARMAND D. and 8 others. (2017) Relationships between fluvial evolution and karstification related to climatic, tectonic and eustatic forcing in temperate regions. *Quaternary Science Reviews*, 166, 38-56.

KAUFMANN G. and DREYBRODT W. (2007) Calcite dissolution kinetics in the system CaCO3–H2O–CO2 at high under-saturation. *Geochimica et Cosmochimica Acta*, 71, 1398–1410.

LIDMAR-BERGSTRÖM K. (1997) A long-term perspective on glacial erosion. *Earth Surface Processes and Landforms*, 22, 297–306.

LUNDBERG J., LORD T.C.and MURPHY P.J. (2010) Thermal ionization mass spectrometer U-Th dates on Pleistocene speleothems from Victoria Cave, North Yorkshire, UK: Implications for paleoenvironment and stratigraphy over multiple glacial cycles. *Geosphere*, 6 (4), 379-395.

LUNDQVIST J. (1986) Late Weichselian glaciation and deglaciation in Scandinavia. *Quaternary Science Reviews*, 5, 269–292.

MURPHY P.J., FAULKNER T.L., LORD T.C. and THORP, J. (2015) The caves of Giggleswick Scar - examples of deglacial speleogenesis? *Cave and Karst Science*, 42 (1), 42–53.

OLSEN L., FREDIN O.and OLESEN O. (2013) *Quaternary Geology of Norway. Norges Geologiske Undersøkelse*. Special Publication 13.

PALMER A.N. (1991) Origin and Morphology of limestone caves. *Geological Society of America Bulletin*, 103, 1–21.

SIMMS M.J. (2004) Tortoises and hares: dissolution, erosion and isostasy in landscape evolution. *Earth Surface Processes and Landforms*, 29, 477-494.

SIMMS M.J. and FARRANT A.R. (2011) Landscape evolution in southeast Wales: evidence from aquifer geometry and surface topography associated with the Ogof Draenen cave system. *Cave and Karst Science*, 38 (1), 7-16.

VERESS M. and 5 others. (2019) *Glaciokarsts*. Springer Geography.

WALTHAM T. and LONG H. (2011) Limestone plateaus of the Yorks. Dales glaciokarst. *Cave and Karst Science* 38 (2),65-70.

WALTHAM T., MURPHY P. and BATTY A. (2010) Kingsdale: evolution of a Yorkshire Dale. *Proceedings of the Yorkshire Geological Society*, 58 (2), 95-105.

WESTAWAY R. (2020) Late Cenozoic uplift history of the Peak District, central England, inferred from dated cave deposits and integrated with regional drainage development: A review and synthesis. *Quaternary International* 546, 20-41.

WILMUT J., PROCTOR C. and JEAN D. (2014) *Exploring the limestones of south Devon*. William Pengelly Cave Studies Trust.

The caves of Hellfjell, Norway, and their speleogenesis

Trevor FAULKNER

GEES, University of Birmingham, Edgbaston, Birmingham, B15 2TT, UK. e-mail: trevor@marblecaves.org.uk

Abstract

About 60 karst caves occur in semi-circular marble outcrops on Hellfjell and in linear outcrops east of Mosjøen, south Nordland, Norway. The cave passages lie within 30 m of the overlying surface and only a few have higher and older levels leading to palaeo resurgences. Most therefore unlikely survived the typical 40 m erosion of the Weichselian glaciation. Instead, most were initiated during the last deglaciation, forming by dissolution of conduit walls by meltwaters flowing from submerging ice-dammed lakes along fractures created by isostatic rebound during ice thinning. As deglaciation proceeded, dry-land catchment areas and flow rates increased as the lake meltwaters migrated from supraglacial streams into englacial conduits and finally into subglacial waterways towards the sea. Most caves later enlarged by vadose and sump dissolution in the Holocene. Caves with relict upper levels probably formed during the previous deglaciation. A seaway existed between Vefsnfjord and Elsfjord, as the ice margin retreated, and lower altitude caves that had just been formed were flooded, before early Holocene isostatic uplift raised them above sea level.

1. Introduction

Semi-circular outcrops of mica schist and metamorphic calcitic limestones of the Helgeland Nappe Complex in the Scandinavian Caledonides surround the southern part of the large unforested granite pluton of Hellfjell (809 m a.s.l.) in an anticlinal formation (Fig. 1). They contain an interesting set of c. 20 marble caves on the forested southern slopes. These range from 90–334 m a.s.l., with lengths up to 386 m and a total passage length of c. 1400 m, within 9 local areas containing c. 40 more caves, mainly east of Mosjøen in Vefsndal (FAULKNER, 2019). Their deglacial speleogenesis depended on a complex interplay among ice melting down from summits and retreating back from the coast, land uplift, seismic fracture creation, flowing ice dammed lakes, and marine incursion.

L Length (m); VR Vertical Range (m); XS mean Cross-Section (m^2); Vol Volume (m^3); A Altitude (m a.s.l.).

2. The longer caves on Hellfjell

Dripsteinhola / Loop Cave

L 386 VR 23 XS 4.8 Vol 1853 A 337 (Dripsteinhola entrance)

A small stream sinks into the highest marble band at the head of the dry Bergdal in Area 3, below the entrance to Loop Cave (Fig. 2). The Entrance Chamber is littered with blocks of mica schist, which forms its floor (Fig. 3). Meander Passage descends to a junction with the Main Tunnel. The stream enters and leaves through sumps in Wet Passage, near the Cross Roads. A draughting crawl leads to the short Dripsteinhola entrance shaft that is just 2 m below the ridge top. Most of this cave formed phreatically, from passage morphology, roof pendants, pillars and oxbows.

The Subway / Snowmelt Sink Cave

L 209 VR 12 XS 3.2 Vol 424 A 327

A stream from Hjortdal sinks into Snowmelt Sink Cave at a 5m-deep blind gully, 180 m SE of Dripsteinhola, but in the next marble band (Fig. 4). The relict Subway on the north bank descends with a sloping wall of mica schist. This forms the floor after a bend and reaches the stream at a sump, near the Six Ways junction. Scallop Passage becomes choked, but instead wet crawls lead to the sink entrance.

Engåselvgrotta

L 254 VR 9 XS 2.1 Vol 533 A 295 (Upper Entrances)

The First (impenetrable) Engåselv Rising from Bergdal and Hjortdal is from the lower edge of the second marble band (Fig. 2). The stream later sinks inside the Upper Entrance chamber to Engåselvgrotta near the edge of a wide marble band, but is not seen again until near the Lower Entrances (Fig. 5). A T-junction leads to the Link Crawl, the only known connection to the Middle Entrances and the rest of the cave. Chest Jam Rift leads into four large sub-parallel strike-aligned passages that connect to the Lower Entrances, below which the Engåselv resurges.

Høgligrotta L 248 VR 38 XS c. 6.3 Vol c. 1320 A 90

Høgligrotta in Area 4 is in a continuation of the narrow lowest marble band from Rokåsen, 5 km to the west. The distinctive noisy Doorway Entrance bounded by fractures is in a cliff 6m above a road (Fig. 6). It enters a larger passage with a view down into a roaring streamway. The passage swings east, passing descents on the left into the streamway, which sumps upstream. Crawls lead to the base of the smooth steeply-sloping Black Dyke Aven, where the Top Entrance is in a doline 50 m north of the Doorway. The cave carries the stream Grøftremelv from another doline, c. 100m farther north. Downstream, the passage descends steeply, becoming larger below the Roaring Pitch. It lowers over sediment to a choke, after the water flows down tiny slots to an impenetrable rising c. 160m away and c. 13 m lower.

3. Speleogenesis

The eastward back-wasting deglaciation of the Weichselian ice sheet as the depressed land uplifted isostatically was accompanied by coastal marine incursion. Lines connecting places with equal amounts of relative isostatic uplift since the end of the Younger Dryas (YD) period, 10,000 ^{14}C years BP (11,703±4 cal. a before 1950), are YD isobases (Fig. 1). They are roughly parallel to the coast, and increase eastwards at c. 1 m per km. Local sea-level curve shapes for YD isobases up to 185 m were estimated by FAULKNER (2018) from an assumed sea level curve for Velfjord, 60 km to the SW (FAULKNER & HUNT, 2009).

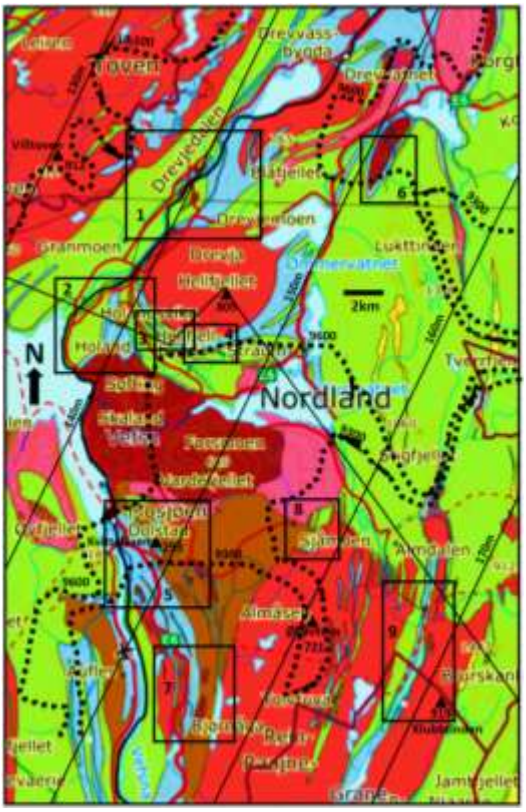

Figure 1: Hellfjell geology, showing: cave areas; YD isobases at 10 m intervals, from SØRENSEN et al. (1987) *(straight lines); Weichselian ice margin retreat stages, from BERGSTRØM (1995), with ages in ^{14}C years BP (dotted lines); and the profile via Hellfjell used in Fig. 7. Blue: marble. Green: mica schist. Other colours: igneous. Red lines: roads.*

Marine incursion up to the marine limit occurred at Hellfjell near the start of the Holocene. It has receded ever since, with continuing uplift. Inland encroachment can be derived from the YD isobase and the eastward recession of the western ice margin, as also shown on Fig. 1. The sea in Vefsnfjord inundated Drevjedal on the 140 m YD isobase to an altitude of 140 m at 10.0 ^{14}C ka BP. This incursion must have initially created a steep marine ice cliff where it melted the tidewater glacier, which was then still >300 m thick. Because the col at its north end is 110 m a.s.l., the whole valley was submerged and there was a direct sea connection between Vefsnfjord and Elsfjord to the north until c. 9.5 ^{14}C ka BP, when uplift rose the col above the sea.

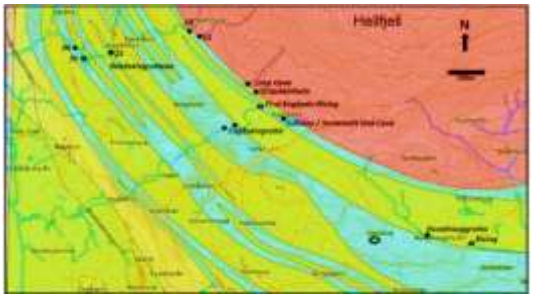

Figure 2: Hellfjell. Green: marble Yellow: schist Pink: granite.

Figure 3: Dripsteinhola / Loop Cave survey.

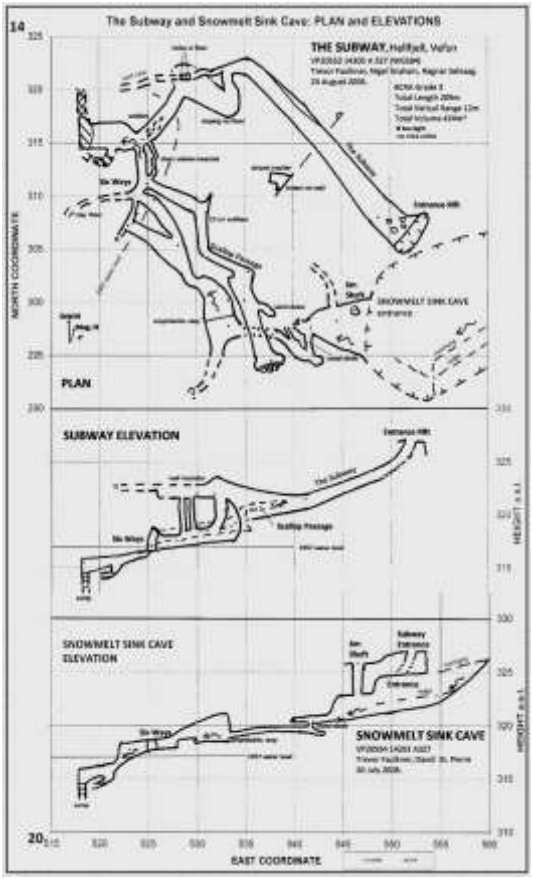

Figure 4: The Subway / Snowmelt Sink Cave survey.

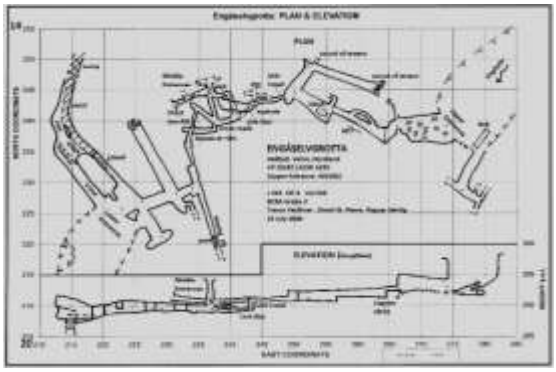

Figure 5: Engåselvgrotta survey

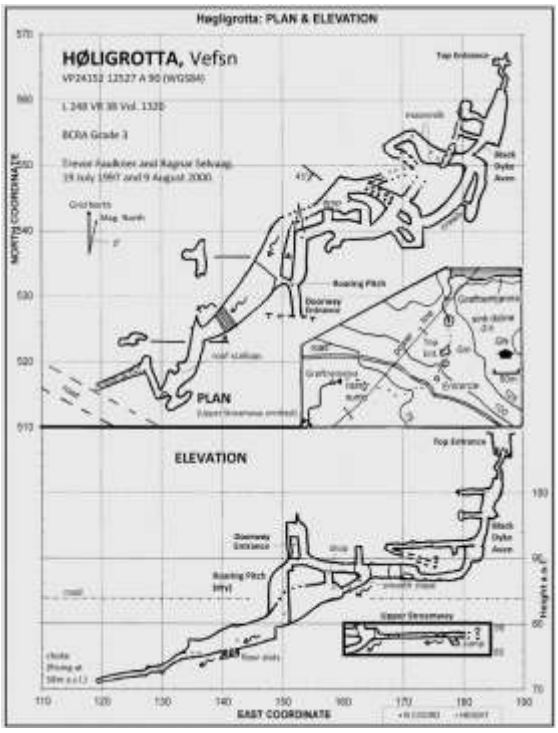

Figure 6: Høgligrotta survey

Contemporaneously with coastal back-wasting, the ice sheet melted by down-wasting onto the summits and later into the valleys. This necessarily created ice-dammed lakes (IDLs) around cold-based nunataks each summer, as plotted by FAULKNER (2005), from a formula derived from GRØNLIE (1975). Some IDLs grew to several 10s of km^2, with depths of several 100 m. It could take many 100s of years for them and the ice surface to lower past a point (such as a fracture entrance) in the mountains. The eastward and downward deglaciations are indicated in Fig. 7. This shows the local ice height and eastern margin at various times along a profile via the Hellfjell summit (Fig. 1), and as plotted against the YD isobase. It also shows the vertical extents of the 9 cave areas, discussed in more detail by FAULKNER (2019).

Caves in central Scandinavia commonly formed by dissolution by meltwaters flowing from submerging IDLs along fractures created by isostatic rebound during ice thinning (FAULKNER, 2006a; 2006b; 2008). The IDLs were initially static, but with downwasting, dry-land catchment areas and flows from the lakes increased. As well as flowing away as supraglacial streams on the distal side of overflowing lakes, the water could also flow out through the ice in englacial conduits, and later in subglacial waterways along warm-based Nye channels on the beds of the present surface streams towards the sea. Suitable fractures in marble beneath an IDL were inundated with flowing aggressive meltwater and enlarged by dissolution to create conduits up to 2 m in diameter within c. 1000 calendar years (FAULKNER (2006b). Wall scallops of length 3–20 cm that point downstream or to palaeo outlets record turbulent dissolutional flow speeds, as do deposited clastic sediments.

The deglaciation of Hellfjell is considered from Figs. 1 and 7. The summit of Hellfjell emerged as a nunatak at 10.9 ka, so that the caves in area 3 at c. 300 m a.s.l. near the 141 m YD isobase were submerged by an IDL on its southern side for c. 1 ka (c. 1700 cal. a), until c. 9.9 ka. This provided the time needed to form the phreatic passages with mean diameters ≤2.5 m in the three surveyed cave systems. The submersion of Høgligrotta at 90 m a.s.l. near the 144 m YD isobase continued until c. 9.6 ka, when the sea at 120 m a.s.l. forced the ice margin to retreat past the cave and its IDL must have collapsed at a jökulhlaup. This duration of 1.3 ka (1900 cal. a) gave time to form its phreatic parts prior to Holocene vadose entrenchment. However, the four cave surveys show relict upper levels that probably led to resurgences that were active during the MIS5e interglacial. The Doorway Entrance obviously functioned as a resurgence before the Roaring Pitch and lower passage formed. The higher levels in these caves were therefore likely formed by similar deglacial processes at the end of the MIS6 glaciation.

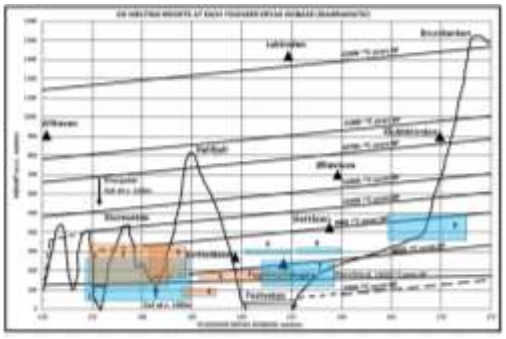

Figure 7: Ice sheet heights at various times along the profile in Fig. 1 plotted against the YD isobase, with several relevant summits included. The marine terminating western extremities of the later decaying ice sheet are shown by steep dashed ice cliff lines. The vertical extents of nine cave areas are shown in shaded boxes. 3 = Hellfjell. 4 = Høgli.

Its Top Entrance is only 109 m a.s.l., so the sea completely flooded Høgligrotta after its ice collapse. Marine abrasion might have shortened the Doorway Entrance as the sea fell to the 58 m altitude of its choked rising at 9.0 ka. The sea melted the ice south of Mosjøen at 9.3 ka, to inundate Vefsndal, where marine shells were found in raised beaches (GRØNLIE, 1975). He showed that melting was complete at 9.08 ka at 133 m a.s.l. at the 200 m YD isobase: the sea melted the tidewater glacier from one side, whilst ablation melted the remnant ice away on the other side. Between the 150–157 m YD isobases, the sea flooded to altitudes of 100–107 m, below the known karst caves in most areas. Although

there are no reports of marine shells in any of the lower caves in areas 1, 2 or 4, they can be anticipated in places protected from springmelt floods, as in Neptune's Cave in Velfjord (FAULKNER & HUNT, 2009).

Several surveys show entrances that are enlarged in width and height, compared with internal passages. These cannot be explained by collapse from simple frost heave, because fallen blocks would remain on the floor, and they are not tapering or are too high for marine abrasion. They therefore likely enlarged by freeze-thaw cycles and outward block pushing as an IDL descended past them during deglaciation, as discussed further by FAULKNER (2018). From Fig. 7, the ice sheet surface and its IDLs lowered by c. 100 m in 200 ^{14}C years, i.e., by c. 0.33 m cal. a^{-1}. With a typical winter ice lid 1.4 m-thick, a 2 m-high entrance would be in contact with ice during the period that such an IDL lowered 3.4 m, i.e., c. 10 years. The entrance enlargements are ≥3 m, suggesting widening of each wall at >0.15 m per year.

The deglacial chronology for the other cave areas was discussed by FAULKNER (2019). Small caves in the west of area 1 were likely created when water flowed through them from an IDL that survived for only 0.2 ka. Kumragrotta in the east of area 1 was probably submerged for 1 ka. A small phreatic roof level in a cave in area 2 was probably initiated whilst supplied from an IDL for 0.5 ka. Small caves in area 5 were probably submerged for only 0.3 ka before emerging above water level. Luktindgrotta (L 611 VR 65 XS 6.0 Vol 3666 A 302), near the 152m YD isobase in area 6, is the longest and most voluminous cave in the whole area. It formed below an IDL on the west side of Luktinden (A 1346), so that phreatic water flow started at c. 12.3 ka, when the ice margin was still west of adjacent coastal islands. The IDL lowered below the cave at 9.7 ka, giving a possible phreatic dissolution time of 2.6 ka (c. 3000 cal. a), easily providing the time needed to form the upper phreatic levels in the cave. Holocene entrenchment subsequently created a large vadose streamway. Small caves in area 7 were flooded for maximum times of 0.3–0.4 ka. Other small caves in area 8 are in a wide marshy area that is distant from local summits, so that their submerging IDL formed late in the sequence and lasted for only 0.3 ka. Ten caves in area 9, many with XS = c. 2 m^2, were probably initiated below an IDL on the western side of Klubbtinden that flooded them for 0.9 ka.

From this discussion, there is a trend of increasing cave L, XS and Vol with increasing time submerged by an IDL. This database is too small to propose precise empirical laws. However, some observations are relevant for deglacial phreatic dissolution, despite several complicating factors, including any MIS5e origin, entrance enlargement, and Holocene entrenchment with vadose passage dimensions related to catchment area (FAULKNER, 2009). There is a probabilistic relationship between explored length and mean cross-section, from the size of the human body and the time needed for any excavation. It seems that caves are only explorable, with XS ≥1 m^2, if they were submerged for at least 0.2 ka. Submersion for 1.3 ka created Høgligrotta, giving a mean radius increase rate of c. 1 mm a^{-1}. Luktindgrotta was submerged for 2.6 ka, giving a mean radius increase rate of c. 0.5 mm a^{-1}. Both these required dissolution rates seem reasonable in high-flow aggressive meltwater (FAULKNER, 2006b). Future study with a larger database should be able to distinguish between phreatic and vadose enlargement rates.

Each glaciation typically removes 40 m of bedrock from the upper and outer parts of caves (FAULKNER, 2008), so there were probably 'cave passages in the sky' above the existing caves. The survey elevations show that all these passages occur within 30m of the surface and only a few caves have higher levels leading to palaeo resurgences. This suggests that most of the passages were initiated during the last deglaciation. Following the FAULKNER (2009) hydrological classification, most are Combination caves, with relict phreatic levels above active vadose parts. Although no local relict vadose passages are known, shallow vadose streamways below relict phreatic levels probably existed in MIS5e, before being removed. An example of Weichselian entrance shortening prior to marine abrasion is provided by the Høgligrotta Doorway Entrance, which probably functioned as a resurgence during the MIS6 deglaciation and throughout MIS5e.

References

BERGSTRØM B. (1995) ELSFJORD. Kvartaergeologisk kart 1927 III. 1:50,000. Norges Geologiske Undersøkelse.

FAULKNER T.L. (2005) Cave inception and development in Caledonide metacarbonate rocks. PhD Thesis. Huddersfield.

FAULKNER T. (2006a) Tectonic inception in Caledonide marbles. Acta Carsologica, 35 (1), 7–21.

FAULKNER T. (2006b) Limestone dissolution in phreatic conditions at maximum rates and in pure, cold, water. Cave and Karst Science, 33 (1), 11–20.

FAULKNER T. (2008) The top-down, middle-outwards, model of cave development in Central Scandinavian marbles. Cave and Karst Science, 34 (1), 3-16.

FAULKNER T. (2009) Relationships between cave dimensions and catchment areas in Central Scandinavia: implications for speleogenesis. Cave and Karst Science, 36 (1), 11-20.

FAULKNER T. (2018) The ages of the Scandinavian caves. Norsk Grotteblad, (70), 15-33, 40.

FAULKNER T. (2019) The caves of Hellfjell and eastern Vefsn. Norsk Grotteblad, (72), 18-43.

FAULKNER T.L. and HUNT C.O. (2009) Holocene deposits from Neptune's Cave, Norway: environmental interpretation and relation to the deglacial and emergence history of the Velfjord–Tosenfjord area. Boreas, 38, 691-704.

GRØNLIE A. (1975) Geologien i Vefsnbygdene. Vefsn Bygdebok 1975, 417–483.

SØRENSEN R., BAKKELID S. and TORP B. (1987) Land Uplift. 1:5000000. Nasjonalatlas for Norge. Statens kartverk.

Why there are probably caves beneath the Norwegian Sea

Trevor FAULKNER
GEES, University of Birmingham, Edgbaston, Birmingham, B15 2TT, UK. e-mail: trevor@marblecaves.org.uk

Abstract
Norway has many littoral caves at various heights a.s.l., whose ages depend on the effects of glaciations and deglaciations on local sea levels. The height that the sea rose above present sea level in the early Holocene is the deglaciation marine limit (DML), which increased inland to a maximum of 163 m. Huge coastal caves above the local DML were formed during a glacial onset, when icesheets expanded rapidly, depressing the land ahead of the falling eustatic sea level. Their sizes were increased by upward stoping by rising sea levels. The glaciation marine limit was >120 m higher than the DML. Whilst Scandinavia was depressed isostatically, large forebulge areas, including around the Scottish islands of Shetland and St. Kilda uplifted, as local sea level also fell. This process reversed during deglaciations. During parts of both episodes, forebulge islands were surrounded by unfrozen sea water, so that small coastal caves could form during glacial onset. Larger caves formed during deglaciation, some continuing to exist b.s.l. at St. Kilda, and probably beneath Norwegian islands west of the hinge line.

1. Introduction
Norway has >300 littoral (coastal sea) caves at various heights above sea level (a.s.l), formed in schists, granites and other lithologies, some being huge (SJÖBERG, 1988). Their formation depended mainly on marine abrasion at the contemporary sea level. This was governed by the extent of glaciation during the Quaternary, when Scandinavian karst areas were sculpted by large strongly erosive icesheets (FAULKNER, 2017). Additionally, several well-known karst caves are actually hybrid, having entrances enlarged by marine abrasion (FAULKNER, 2005a). This paper discusses the age and formation of Norwegian littoral caves and considers the probability that some exist below sea level.

2. The formation of littoral caves
Norwegian glaciations started at the summits and spread westwards on to the continental shelf. Deglaciations started both by downwasting inland and by backwasting eastward margin retreats via the strandflat. Both processes started at high relative sea levels, because local isostatic depression exceeded falls in eustatic sea level throughout glaciation. The eastward retreat after the Last Glacial Maximum (LGM) was mapped by ANDERSEN & KARLSEN (1986), starting at 19,000 ^{14}C years BP from the NW extremity of the Lofoten Islands. VORREN *et al*. (2015) confirmed that this retreat from the continental shelf, which is <20 km wide locally (Fig. 1), started at c. 22.2 cal. ka BP. It reached inland Norway during the warm Bølling Interstadial after 13,500 ^{14}C years BP (14,692±4 cal. a B2k), when the sea flooded the depressed coastal areas and attacked the continuing ice cliff.

Younger Dryas isobases and marine limits
With less ice, the land rose rapidly in the early Holocene. YD isobases record equal amounts of uplift relative to present local sea level since the end of the Younger Dryas stadial, 10,000 ^{14}C years BP (11,703±4 cal. a B2k). SØRENSEN *et al*. (1987) mapped land uplift with linear isobases parallel to the northern coast (Fig. 1). The hinge line at a YD isobase of 0 m went from the western tip of Norway to Vesterålen. Earlier, the ice was thicker and the hinge line lay farther west. The maximum height that the sea reached inland is the local *deglaciation marine limit* (DML). This increased eastwards, peaking at 163 m at the 170 m YD isobase at 9890 ^{14}C years BP (Faulkner, 2018). It then reduced to 133 m at the 200 m YD isobase at 9080 ^{14}C years BP (Grønlie, 1975). Marine incursion was controlled by competition between uplift and the position of the ice margin. Thus, the 146m YD isobase sea level curve for Velfjord, derived by FAULKNER & HUNT (2009) and FAULKNER (2012), shows that all places to the east below a present 146 m altitude were inundated by the sea at the start of the Holocene, *providing that the ice had melted by then at that location*.

Valley glacier and mountain icesheet expansions at glacial *onsets* and glacial stadials depressed the land. This caused a rising local sea level ahead of the falling eustatic level, as at the Weichselian onset, when "*depression extended ahead of the ice margin*" (LUNDQVIST, 1986: p. 288) in the rapid Herning stadial at Marine Isotope Stage (MIS) 5d (115–100 ka). There is therefore another limit, the *glaciation marine limit* (GML), which is the maximum elevation that the sea reached inland before freezing or meeting an ice margin. OLSEN *et al*. (2001) found evidence of marine-influenced sediments dated from 35–24 ^{14}C ka BP at 260 m a.s.l. in north central Norway, at the 210 m YD isobase. This pre-LGM marine incursion was 120 m above the equivalent local DML, at an altitude that would have occurred there during deglaciation at 12,700 ^{14}C years BP without persisting ice. However, MANGERUD (1991) concluded that the MIS5d glaciation was as extensive as in the YD. Eustatic sea level was also probably higher, according to CREVELING *et al*. (2017). Thus, it probably caused the Weichselian GML at a height >120 m above the DML, during a high local sea level.

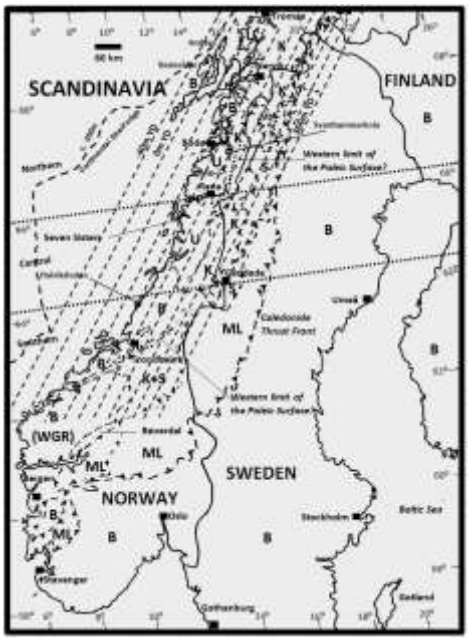

Figure 1: YD isobases at 40 m intervals (SORENSEN, 1987).

Shorelines

The amount of isostatic uplift produced by the denudation of mountains alone is a matter of continuing research, with views expressed that the equivalent of 70–85 % of lost land becomes elevated above sea level (WALTHAM & LONG, 2011). The YD and other conjectured shorelines are plotted against YD isobases in Fig. 2, together with the vertical ranges of some large karst and non-karst cave entrances. The main shorelines shown are those formed: a) after the onset of each major glaciation, when the new ice sheet was as extensive as at the YD and local sea level was rising; b) at the start of each interglacial, when the melting ice sheet was as extensive as at the end of the YD and local sea level was falling; and c) late in each interglacial, when ice was restricted to mountain glaciers and local and eustatic sea levels were almost static. For each stage, shorelines at the 150 m YD isobase are separated by 30 m of erosional uplift, assuming that a mean of 40 m of bedrock was removed at each of the last few glacial cycles. On this reconstruction, early interglacial shorelines coincide with the shoreline of the next but one major glacial onset at the 150 m YD isobase.

Icesheets flowing westwards smoothly eroded the eastern stoss slopes and caused ice plucking on the western lee slopes, causing coastline retreat. Each interglacial marine incursion then consolidated the process, creating the Norwegian strandflat (Fig. 3), which is commonly ≥25 km wide and within ±50 m of present sea level. It is commonly assumed that it formed primarily during the Quaternary, giving an average western cliff retreat rate ≥1 km per 100 ka. Retreats were probably much greater in each later more severe glaciation, when each hinge line retreat probably represents c. 15 m of YD isobases, from Fig. 2, a distance of c. 15 km due east. Glacial erosion along the northern and southern slopes of fjords and islands probably equalled the assumed minimum depth of valley deepening per 100 ka glacial cycle, giving a minimum rate of 40 m for the later retreats of cliffs aligned E–W. A hiatus in continuous sea level change can be observed as a raised beach, shoreline, terrace or platform (Fig. 4). Any that are now below sea level can be detected as submerged platforms.

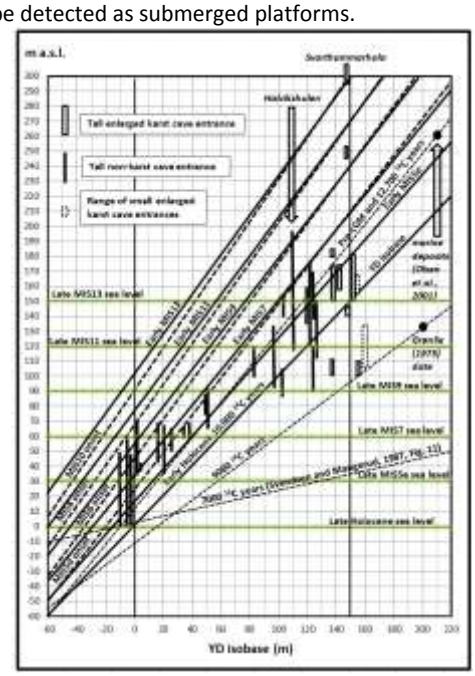

Figure 2: Conjectural shorelines plotted against YD isobases, showing the vertical ranges of large karst and non-karst cave entrances. Late interglacial: dotted. Early interglacial: solid. Glacial onsets: heavy dashed. Others: light dashed.

Figure 3: The Norwegian strandflat. Photo from the internet.

Formation mechanisms

The formation and demise of Norwegian littoral caves depend on competing processes. When not glaciated, the enclosing cliff is eroded by both marine abrasion and winter ice wedging, so that a cave only lengthens relative to cliff retreat if along a weak zone roughly orthogonal to the coast. Caves formed, and karst cave entrances modified, by the sea commonly taper both horizontally and vertically, showing the inward reducing power of marine abrasion (FAULKNER, 2005a). Lengths and entrance widths mainly depend on the time spent in the tidal range. Without ice wedging, the largest and longest caves should occur on coasts that face the open sea. Once a cave starts to form, ice-wedging accelerates enlargement by the spalling of the roof and walls. Collapse debris occupies c. 40 % more space than the original bedrock, but is partly removed by abrasion, tidal changes and movement outwards by ice as it expands prior to melting. These processes persist as long as the sea remains unfrozen in summer and is at the level of the cave or above it. Caves on islands facing north, south or east or farther inland along fjords in sheltered locations should be influenced more by ice wedging than by direct marine abrasion, resulting in narrower and shorter caves.

Figure 4: Two raised platforms viewed from the raised littoral cave Uamh nan Calman on the island of Lismore, Scotland.

Figure 5: Halvikshulen. Figures for scale. Photo from the internet.

Littoral cave classes

FAULKNER (2005a) estimated when >51 karst caves near the north central Norway coast became uncovered by the last ice sheet and how long they remained submerged by the sea. Five with enlarged entrances are above the local DML, as are seven in northern Norway (FAULKNER, 2018). Marine influences are demonstrated by enlarged entrances, non-laminated sand (FAULKNER, 2005b), holes bored by marine molluscs (FAULKNER, 2012), or shell deposits and barnacles attached to walls and roofs (FAULKNER & HUNT, 2009). Following diagrams by FAULKNER (2005a) of entrances enlarged by falling or rising sea levels, FAULKNER (2018) divided coastal caves into three classes:

1 Those below the DML and formed only during the Weichselian deglaciation with a *falling* local sea level, which typically have roof heights ≤5 m.
2 Those above the DML and formed during the onset of a glaciation or glacial stadial with a *rising* sea level, which have roof heights >>5 m.
3 Those below the DML, which were formed as class 2, but enlarged further during deglaciation.

Tall and wide non-karstic littoral cave entrances on the Norwegian coast and islands were described by HOLTEDAHL (1984), MØLLER (1985), and SJÖBERG (1988). Many roofs are well above the local DML, so they predate the Weichselian deglaciation as class 2 caves. Upward stoping by rising sea levels enlarged them during one or more glacial or stadial onsets, assisted by megatides caused by gravitational attraction from icesheets, when oceanic volume was smaller (VELAY-VITOW & PELTIER, 2020). Most cave floors listed by SJÖBERG (1988) descend deeper below collapsed rocks at the entrance, demonstrating that upward stoping by ice wedging continues when above sea level, and that bedrock floor altitudes are difficult to determine. Those entrances >>5 m high with floors below the local DML and any that are entirely below it also predate deglaciation, but were probably slightly enlarged by later deglacial marine abrasion and ice wedging as class 3 coastal caves, when the sea level fell past them.

If the shorelines in Fig. 2 are correct, the north-facing upper entrance to the hybrid karst cave Svarthammarhola at the end of Saltfjord at the 148 m YD isobase in northern Norway (Fig. 1), with its 311 m roof altitude, enlarged at the MIS10 onset or earlier. This was when it was greatly depressed isostatically, being 50 km inland from the present main coastline. The largest littoral cave in Europe is Halvikshulen (Figs. 1 and 5), near the 110 m YD isobase north of Trondheim. Its 78 m-high entrance, which spans 117–195 m a.s.l., is 340 m long and 250 m wide (SJÖBERG, 1988). Its roof is 65 m above the local DML, which is just 5 m above the assumed sea level at the MIS6 glacial onset, giving its youngest age of formation. Other tall caves were formed at or before MIS5d and some hybrid entrances enlarged before the LGM. Only the latest ages can be given, because the caves could have formed as the sea rose past them during an earlier glacial onset, with later enlargements until the latest glaciation that could raise sea level high enough. From Fig. 2, there were 17 main climatic episodes, from early MIS13 to the late Holocene, during which littoral caves could form or be enlarged. Eastward coastal cliff retreats per glacial cycle estimated above greatly exceed the length of any Scandinavian coastal cave. This suggests that even long class 2 caves can only survive succeeding major glaciations in positions well-protected from glacial plucking. Hence, the surviving tall caves facing west were much longer earlier in the Weichselian glaciation and are unlikely to predate most of it. Indeed, the protected entrances of most tall class 2 caves do face north or south. SVENDSEN & MANGERUD (1987) gave deglacial sea level curves extending inland near Trondheim for 155 km, which FAULKNER (2005a) interpreted for the 15–150m YD isobases farther north. Local sea level fell at 6.5–0.3 cm per year after 12 ka ^{14}C BP, taking 77–1667 years to fall 5 m. These seem reasonable timescales to erode class 1 caves. Those older and smaller are at higher YD isobases and elevations and those initiated later at low isobases and elevations are longer and wider.

Forebulge areas and submerged caves

A large forebulge area (Fig. 6) extended beyond the varying hinge line, towards the continental shelf during glaciation (FJELDSKAAR, 1994). Another lay around the Scottish islands Shetland and St. Kilda. Whilst Scotland and Scandinavia were depressed by 1–3 km of ice, the Scottish forebulge uplifted below ≤300 m of ice on these islands, whilst eustatic sea level also fell. This antiphase process reversed during deglaciations. The forebulge depressed farther below present sea level at each interglacial, as the successively lighter main landmasses rose higher after each glacial denudation and Shetland lowered in altitude, as shown by flooded valleys (called voes; FLINN, 1964). MYKURA (1976) reported the occurrence of offshore submerged platforms of probable earlier erosion surfaces, perhaps glacially-assisted, at depths of 9, 24, 45 and 82 m. These might correspond to local sea levels at MIS5e, 7, 9 and 11.

Although submerged sea caves are still unknown at Shetland, many huge tidal range littoral caves and geos occur on its NW coast. Calder's Geo Cave is 122 m long, 107 m wide, c. 8 m high and the largest natural chamber in Britain (DIXON, 2018). It shows that huge class 1 caves could form in interglacials when not protected by a strandflat. However, many submerged sea caves have been found by recreational divers at St. Kilda. This has no elevated littoral caves and a wave-cut platform 40-50 m b.s.l., as investigated by HARRIES *et al*. (2018). The caves variously extend to 180 m in length, with some class 2 roof heights being 25 m a.s.l., with some passage floors descending to 50 m b.s.l. Shorter partly submerged littoral caves on the island of North Rona extend to 65 m in length and 10 m in depth. The submerged

littoral caves at these islands within forebulge areas confirm their formation when mainland areas were glaciated. Class 2 initiation probably occurred early in interglacials during rising relative sea levels. Enlargement then continued during the interglacial, as sea level became almost static, until after the next glacial onset, when sea levels fell again. In Norway, the coasts and some small offshore islands at Lofoten and Vesterålen extend westwards into the YD forebulge area to the -20 m YD isobase (Fig. 1). Hence, class 1 caves could form at these places during uplift at glacial onset. Class 2 caves could form there during depression at early deglaciation. Shorelines were lower and the small islands larger when surrounded by unfrozen sea water at both times. These caves should continue to exist below present sea level, although some will be covered by soft sediments.

Figure 6: Forebulge areas

3. Conclusion

Littoral caves can only form when or if they are in the tidal range, they are not covered by ice, and their cave lengthening rate is greater than the cliff retreat rate. Competitions at all glacial stages among eustatic sea level, local isostasy and the ice margin determine the local relative sea level, showing that littoral caves can now occur above or below present sea level. Thus, there is a high probability that littoral caves continue to exist beneath the Norwegian Sea.

References

ANDERSEN B.G. and KARLSEN M. (1986) Glacial chronology – recession of the ice margin. 1:5000000. Nasjonalatlas for Norge. Kartblad 2.3.4. Statens kartverk.

CREVELING J.R., MITROVICA J.X., CLARK P.U., WAELBROECK C. and PICO T. (2017) Predicted bounds on peak global mean sea level during marine isotope stages 5a and 5c. Quaternary Science Reviews 163, 193-208.

DIXON K. (2018) Big! Descent 265, 33-35.

FAULKNER T. (2005a) Modification of cave entrances in Norway by marine action. 14th International Speleological Congress Proceedings, Athens. Paper O-69, 259-263.

FAULKNER T. (2005b) Nordlysgrotta og Marimyntgrotta. Norsk Grotteblad (45) 23–28.

FAULKNER T. (2012) Marin påvirkning og grottene ved Aunhatten og Langskjellighatten, Brønnøy. Norsk Grotteblad (58) 11-22, 48-49.

FAULKNER T. (2017) Are there any pre-Quaternary caves in Scandinavia? 17th International Speleological Congress. Proceedings Volume 2, 263-268 (Ed 1) or 269-274 (Ed 2).

FAULKNER T. (2018) The ages of the Norwegian caves. Norsk Grotteblad 70, 15-33, 40.

FAULKNER T.L. and HUNT C.O. (2009) Holocene deposits from Neptune's Cave, Nordland, Norway: environmental interpretation and relation to the deglacial and emergence history of the Velfjord–Tosenfjord area. Boreas 38 691-704.

FJELDSKAAR W. (1994) The amplitude and decay of the glacial forebulge in Fennoscandia. Norsk Geologisk Tidsskrift 74 (1) 2–8.

FLINN D. (1964) Coastal and submarine features around the Shetland Islands. Proc. of the Geol. Assoc. 75 (3) 321-339.

GRØNLIE A. (1975) Geologien I Vefsnbygdene. Vefsn Bygdebok 1975, 417–483.

HARRIES D.B. and 5 others. (2018) The establishment of site condition monitoring of the sea caves of the St. Kilda and North Rona Special Area of Conservation. Scottish Nat. Her. Res Report 1044. 213pp.

HOLTEDAHL H. (1984). High Pre-Late Weichselian sea-formed caves and other marine features on the Møre-Romsdal coast, W. Norway. Norsk Geol. Tidsskrift, 64, 75-85.

LUNDQVIST J. (1986) Late Weichselian glaciation and deglaciation in Scandinavia. Quaternary Sci. Rev. 5 269–292.

MANGERUD J. (1991) The Last Ice Age in Scandinavia. Striae 34, 15–30.

MØLLER J.J. (1985) Coastal caves and their relation to early postglacial shore levels in Lofoten and Vesterålen, north Norway. Norges Geol. Undersøkelse Bulletin 400 51–65.

MYKURA W. (1976) British Regional Geology: Orkney and Shetland. HMSO. 149pp.

OLSEN L., SVEIAN H. and BERGSTRØM B. (2001) Rapid adjustments of the western part of the Scandinavian Ice Sheet during the Mid and Late Weichselian - a new model. Norsk Geologisk Tidsskrift 81 93–118.

SJÖBERG R. (1988) Coastal Caves Indicating Preglacial Morphology in Norway. Cave Science 15 (3) 99–103.

SVENDSEN J.I. and MANGERUD J. (1987). Late Weichselian and Holocene sea-level history for a cross-section of western Norway. Journal of Quaternary Science 2 113–132.

SØRENSEN R., BAKKELID S. and TORP B. (1987) Land Uplift. 1:5000000. Nasjonalatlas for Norge. Statens kartverk.

VELAY-VITOW J. and PELTIER W.R. (2020) Out of the Ice Age: Megatides of the Arctic Ocean and the Bølling-Allerød, YD Transition. Geophysical Res. Letters 47 (23) 10 p.

VORREN T.O., RYDNINGEN T.A., BAETEN N.J. and LABERG J.S. (2015) Chronology and extent of the Lofoten–Vesterålen sector of the Scandinavian Ice Sheet from 26–16 cal. ka BP. Boreas 44, 445-458.

WALTHAM T. and LONG H. (2011) Limestone plateaus of the Yorkshire Dales glaciokarst. Cave & Karst Science 3 (2) 65-70.

The high-flow low-storage extreme in marble aquifers

Trevor FAULKNER

GEES, University of Birmingham, Edgbaston, Birmingham, B15 2TT, UK. e-mail: trevor@marblecaves.org.uk

Abstract

High grade marbles have negligible primary porosities after limestone metamorphism. Nevertheless, there are >2800 marble caves in Scandinavia, Scotland and North America. About a third consist of shallow vadose passages without pre-Holocene speleothems, which could not have survived the last glaciation. They therefore formed during the Holocene. However, other caves in Norway clearly pre-date the Holocene or survived several glaciations. These were initiated by phreatic 'pure' water flows from ice-dammed lakes through neotectonic fractures that were opened by isostatic rebound during deglaciation, many passages being horizontal even in vertical and angled foliations. Some flow routes were short enough and fractures wide enough for fast flow rates (shown by small sizes of later wall scallops) during tectonic inception to be immediately beyond rates required for chemical breakthrough or even for the Fast Rate Law. This was despite the absence of vegetation, resulting in little CO_2 in pure glacial meltwater. Phreatic passages enlarged at fast rates to ≤2 m diameter in the typical 1000 years duration of deglacial water flow, possibly followed by vadose entrenchment in the succeeding interglacial. The resulting marble aquifers have high flow rates and low storage capacity.

1. Main study area: central Scandinavia

Central Scandinavia comprises four allochthons of Caledonide nappe complexes in an area of c. 40,000 km². Metamorphic grades decline from amphibolite to greenschist facies eastwards, as the nappes are descended from the Helgeland Nappe Complex in Norway in the Uppermost Allochthon to the narrow Lowest Allochthon in Sweden, which overlies older crystalline basement. There are >1000 marble outcrops, commonly forming linear stripe karsts with lengths up to 53 km and widths from 3 to 3000 m (Fig. 1), containing >1000 caves. These commonly occur in groups along the outcrops at altitudes that appear randomly distributed. The area experienced multiple large Quaternary glaciations. These were likely warm-based most of the time, causing large-scale erosion of deep glacial valleys. There is no evidence of any existing pre-Quaternary caves. Toerfjellhola is perhaps the oldest cave in the area, probably dating from MIS12 (FAULKNER, 2013a).

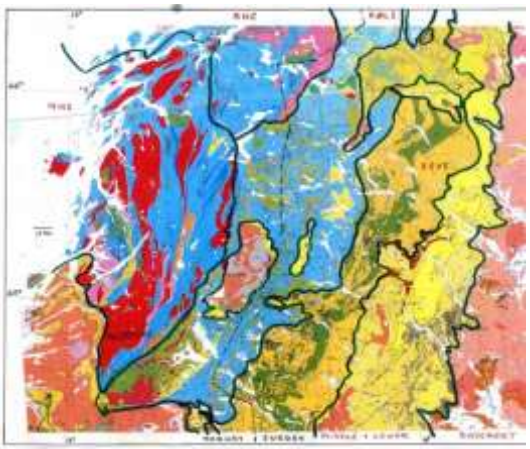

Figure 1: Central Scandinavia lithology and structure. Marble outcrops are shown in dark blue.

2. The cave inception problem

Aquifers in amphibolite-grade marbles in the mountainous Uppermost Allochthon (at least) are unlike those in sedimentary limestones. Negligible primary porosity and widely-spaced fractures produce zero matrix storage and no watertables. Metamorphism and folding removed the sedimentary bedding planes and much of the marble is vertically foliated or steeply inclined. Hence, speleogenesis is not explicable by the Inception Horizon Hypothesis (LOWE & GUNN, 1997) and there is no evidence of any hypogenic origin. However, there are several clues to the local speleogenetic processes. Long and deep caves are rare. The longest cave, c. 6 km, is Korallgrottan in Sweden in the lower metamorphic grade Upper Allochthon (ISACSSON, 1989) and the deepest, 180m, is Ytterlihullet in Norway (HEAP, 1975; FAULKNER, 2008a). However, the mean cave length is only 85m and the mean depth is only 9 m (FAULKNER, 2009a). Because these caves are epigean (Fig. 2), all except Ytterlihullet remaining within 55 m of the surface, this suggests that they evolved synchronously with the glacial topography. Many relict phreatic caves exist in 'impossible' situations, high on the sides of glacial valleys, without any present catchment area. Rather than being formed before the Quaternary glaciations, each of which removed up to 40 m of bedrock, and then being truncated by them, this suggests that they formed during periods of deglaciation. Enlargements during warm-based glaciation when submerged by subglacial lakes are unlikely, because such lakes would be slow moving and unaggressive, becoming saturated with calcite if overlying marble. The absence of relict vadose caves and the presence of only few large speleothems and few relict vadose passages suggest that most caves are relatively young.

3. The formation of neotectonic fractures

Despite crystalline 'hard rocks' in silicate lithologies being non-karstic and without effective primary porosity, they host millions of wells and boreholes world-wide with significant hydraulic yields. The fast flow rates through their fractures and the flow distances involved show that if some had formed in limestones, they could dissolve the limestone at a fast rate beyond that of the chemical breakthrough point determined by PALMER (1991), as discussed by FAULKNER, 2007a). It therefore follows that water flowing through newly-created fractures in crystalline metamorphic limestones could immediately dissolve the marble under a pre- or post-chemical breakthrough regime, as proposed in the Tectonic Inception Hypothesis (FAULKNER, 2006a).

Figure 2: The resurgence entrance to Eiterådalgrotta.

Figure 3: Deformed sediments on the Swedish High Coast.

Ice c. 3 km thick melted away at the end of the Weichselian glaciation. This caused rapid isostatic rebound that peaked at c. 0.5 m per year at the Baltic coast during the early Holocene (MÖRNER, 2003) and produced steep sea level curves at the Norwegian coast (SVENDSEN & MANGERUD, 1987). The rapid uplift created large earthquakes up to Magnitude 8, as evidenced by many examples of screes, rock splitting, soft sediment deformation (Fig. 3), mega-slides, talus (Fig. 4) and talus caves on the Swedish High Coast (MÖRNER & SJÖBERG, 2018). DEHLS *et al*. (2000) showed the widespread extent of neotectonic activity in Scandinavia. In Norway, 54 neotectonic movements were reported in non-karstic bedrocks by OLESEN *et al*. (2004). Additionally, FAULKNER (2005) recorded 56 seismic or aseismic centimetre-scale neotectonic movements in karst caves and outcrops in the Norwegian part of the study area (Figs. 5–9), when large blocks of marble shook and moved to slightly different positions. Holocene neotectonic displacements seen in phreatic passages were subsequent to the movement that created the same or a different inception fracture during deglaciation.

Figure 4: Talus created by the seismic 'blowing-up' of a hilltop roche moutonée above Boda Cave in Sweden.

Figure 5: Horizontal and near-vertical tectonic movements in Marimyntgrotta, north central Norway.

The distance of cave passages from the surface is not greater than one-eighth the depth of the local glacial valley in central Scandinavia (Fig. 10, from FAULKNER, 2007b). This applies in all Caledonide terranes, except in some deeper caves in northern Norway that were probably initiated along fractures created by long-range plate tectonics. Thus, caves formed along neotectonic fractures created during deglaciation that were deeper in steep topography, where seismic acceleration was greatest.

Figure 6: Horizontal opening of the base of a phreatic passage in Cliff Cave, north central Norway.

4. Deglaciation

The availability of water to submerge neotectonic fractures was investigated by deriving the deglaciation of the whole study area from basic principles at nine-time steps (FAULKNER, 2005). The decaying Weichselian icesheet necessarily generated sequences of ice-dammed lakes (IDLs; DAHL *et al.,* 1997), as occur in the mountains of SE Greenland at present (*Google Earth*). Study area analysis showed that all inland fractures and pre-existing caves were submerged by an IDL, typically for c. 1000 years, as the icesheet lowered by down-wasting. IDLs around nunataks at high levels were initially static, with pure meltwater. As the icesheets and IDLs lowered, catchment areas increased in size. Water was sucked via the fractures and out into supraglacial streams and englacial and subglacial channels in the ice (FAULKNER, 2021). By the time the IDLs lowered into valley bottoms, the inflowing streams carried significant sediments, leaving surface deposits with horizontal laminations that probably represent varves in some places (LUNDQVIST, 1972: Fig. 2).

Figure 7: Shattering at Cliff Cave entrance. Figure for scale.

Figure 8: Rotational tectonic movement in Beehive Cave.

Limestone dissolves in dilute flowing water, even when at 0°C with only atmospheric CO_2, at a 'normal' estimated maximum dissolution rate of 0.35 mm per year (FAULKNER, 2006b). This applies if the flow rate is high enough and the calcite concentration is low enough so that the chemical breakthrough point is exceeded (PALMER, 1991). However, the diameter of many phreatic passages in the study area is c. 2 m (Fig. 11), suggesting a radius increased of c. 1 mm per year for c. 1000 years. When water is <20 % saturated with calcite, as in meltwater, a Fast Rate Law applies that raises the dissolution rate by an order of magnitude (KAUFMANN & DREYBRODT, 2007). A rigorous treatment of the submergence timescales and phreatic passage sizes in the study area could thus provide the first practical support for the truth of the Fast Rate Law. However, the flows were turbulent, also causing mechanical erosion of mica schist and other impurities in the marble conduit walls. The present high speeds of flows through some local cave passages are shown by the small sizes of wall scallops (FAULKNER, 2013b) in Fig. 12. Thus, where vadose flows and phreatic flows through sumps continued in interglacials, high flow rates in relatively short conduits, even with low CO_2 above the tree line, could also cause dissolution and mechanical erosion at high rates.

Figure 9: Marble block moved after smoothing by glacial erosion on Elgfjell, north central Norway.

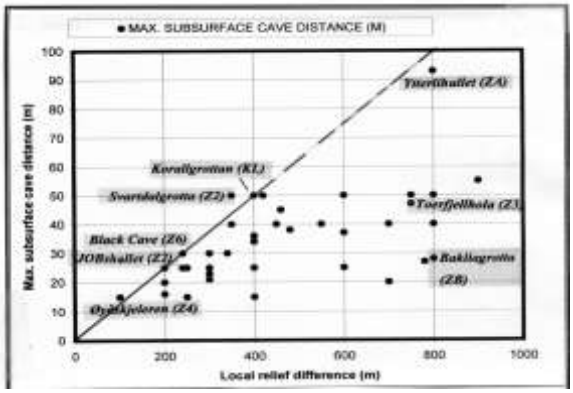

Figure 10: The sub-surface cave distance of caves in central Scandinavia plotted against the local relief difference.

Figure 11: 2 m-diameter phreatic passage in Jegerhullet, Norway, with a Holocene neotectonic movement.

5. Summary

Relict phreatic passages in marble caves in the non-Arctic Caledonides of New England (FAULKNER, 2009b; COOPER & MYLROIE (2015), Ireland, Scotland and Scandinavia (FAULKNER, 2009c) were formed along tectonic inception fractures created by deglacial earthquakes after rapid isostatic rebound. Ice-dammed lakes submerged marble karsts, allowing fast dissolution with turbulent flow, probably invoking the Fast Rate Law. The caves evolved and were removed during a 4-stage process that repeated during each glacial cycle (FAULKNER, 2008b). With open passages but negligible porosities and relatively low fracture densities in high- grade marbles, these aquifers respond rapidly after heavy rainfall (Fig. 13), but their low storage capacity allows floods to dissipate in a few hours.

Figure 13: High flow in Kvannlihola 2 in vertical stripe karst.

Figure 12: Longer scallops in the phreatic part of Fasett Resurgence Cave, Norway, indicate a deglacial flow speed of c. 1.1 ms^{-1}. Shorter scallops in the vadose part indicate a springmelt speed of c. 2.5 ms^{-1}. Photo by Alan Marshall.

References

COOPER M.P. and MYLROIE J.E. (2015) Glaciation and Speleogenesis: Interpretations from the Northeastern United States. Springer. 142 p.

DAHL R., SVEIAN H. and THORESEN M.K. (1997) Nord Trøndelag og Forsen: Geologi og Landscap. Norges Geologiske Undersøkelse. 137pp.

DEHLS J.F. and 5 others (2000) 1:3000000 Neotectonic map: Norway and adjacent areas. Geol. Survey of Norway.

FAULKNER T.L. (2005) Cave inception and development in Caledonide metacarbonate rocks. PhD. Huddersfield.

FAULKNER T. (2006a) Tectonic inception in Caledonide marbles. Acta Carsologica 35 (1) 7–21.

FAULKNER T. (2006b) Limestone dissolution in phreatic conditions at maximum rates and in pure, cold, water. Cave and Karst Science 33 (1) 11–20.

FAULKNER T. (2007a) The hydrogeology of crystalline rocks as supporting evidence for tectonic inception in some epigean endokarsts. Cave and Karst Science 33 (2) 55-64.

FAULKNER T. (2007b) The one-eighth relationship that constrains deglacial seismicity and cave development in Caledonide marbles. Acta Carsologica 36 (2) 195-202.

FAULKNER T. (2008a) Tilbake til Bryggfjelldalen. Norsk Grotteblad (50) 14-24, 36-37, 66-67.

FAULKNER T. (2008b) The top-down, middle-outwards, model of cave development in central Scandinavian marbles. Cave and Karst Science 34 (1) 3-16.

FAULKNER T. (2009a) Relationships between cave dimensions and local catchment areas in Central Scandinavia: implications for speleogenesis. Cave and Karst Science 36 (1) 11-20.

FAULKNER T. (2009b) Speleogenesis of the New England marble caves. 15th Int. Spel. Congress Proc., 2, 855-862.

FAULKNER T. (2009c) The general model of cave development in the metalimestones of the Caledonide terranes. 15th Intl. Spel. Congress Proc., Vol. 2, 863-870.

FAULKNER T. (2013a) A methodology to estimate the age of caves in northern latitudes, using Toerfjellhola in Norway as an example. 16th Int. Spel. Congress Proc., 3, 342-348.

FAULKNER T. (2013b) Speleogenesis and scallop formation and demise under hydraulic control and other recharge regimes. Cave and Karst Science 40 (3) 113-132.

FAULKNER T. (2021) Englacial conduits and crevasses in the artificial tunnel inside Langjökull glacier, Iceland. 18th International Speleological Congress Proceedings.

HEAP D. (1975) William Hulme Grammar School Report of Expedition to Nordland 1974. 27pp.

ISACSSON G. (1989) Cave deposits during glaciations and interglacials - an example from the Korallgrottan in Middle Sweden. 10th Intl. Spel. Congress Proceedings 217–218.

KAUFMANN G. and DREYBRODT W. (2007) Calcite dissolution kinetics in CaCO3–H2O–CO2 at high under-saturation. Geochimica et Cosmochimica Acta 71, 1398–1410.

LOWE D.J. and GUNN J. (1997) Carbonate Speleogenesis: An Inception Horizon Hypothesis. Acta Carso. 26/2 457–488.

LUNDQVIST J. (1972) Ice-lake types and deglaciation pattern along the Scand. mountain range. Boreas 1, 27–54.

MÖRNER N-A. (Ed.) (2003) Paleoseismicity of Sweden: a novel paradigm. Stockholm University. 320pp.

MÖRNER N-A. and SJÖBERG R. (2018) Merging the concepts of pseudo-karst and paleoseismicity in Sweden: A unified theory on the formation of fractures, fracture caves, and angular block heads. Int. Jnl. of Speleology 47 (3) 393-405.

OLESEN O. and 9 others. (2004) Neotectonic deformation in Norway and its implications: a review. Norwegian Journal of Geology 84 3–34.

PALMER A.N. (1991) Origin and Morphology of limestone caves. Geological Society of America Bulletin 103 1–21.

SVENDSEN J.I. and MANGERUD J. (1987) Late Weichselian and Holocene sea-level history for a cross-section of western Norway. Journal of Quaternary Science 2 113–132.

New chronological constraints on the intrakarstic fluvio-glacial fan of the cave Sous-les-Sangles (Bas-Bugey, France)

Stéphane JAILLET[(1)] & Edwige PONS-BRANCHU[(2)]

(1) Laboratoire EDYTEM, Université Savoie Mont Blanc, CNRS, Pôle Montagne, 73 376 Le Bourget-du-Lac, stephane.jaillet@univ-smb.fr (corresponding author)
(2) Laboratoire des Sciences du Climat et de l'Environnement, LSCE/IPSL, CEA-CNRS-UVSQ, Université Paris-Saclay, F-91191 Gif-sur-Yvette, France

Abstract

The age of the Last Glacial Maximum extension of the French north-western Alps is still under discussion. Lateral to the ancient glacial valleys, karstic galleries functionned as glacial sinkholes during the glacial retreat phases and are thus relevant recorders of these glacial phases. In the Bas-Bugey (Ain, France), the cave Sous-les-Sangles hosts a remarkable laminated detrital sequence associated with an ancient position of the Isère glacier in the "Cluse des Hôpitaux". Several U/Th alpha dates undertaken 20 years ago are revised here. Five new U/Th ICP-MS dates on speleothems frame the detrital complex, providing a terminus post quem (TPQ) and a terminus ante quem (TAQ) to this glacial invasion. The TPQ is dated 87.3 ± 3.9 ka (MIS 5.b.c) and the TAQ is dated 11.6 ± 4.3 ka (MIS 1). The laminated detrital sequence is thus better constrained and the glacial invasion could have only been deposited during MIS 4 (locally Würm II, first max) or MIS 2 (Last Glacial Maximum or locally Würm IV) stages. The cave Sous-les-Sangles has a strategic position to constrain maximum glacial extension during the last cold stages of the Quaternary in the French Alps.

Résumé

Nouvelles contraintes chronologiques sur le cône fluvio-glaciaire intrakarstique de la grotte Sous-les-Sangles (Bas-Bugey, France). L'âge de la dernière extension maximale glaciaire des Alpes nord-occidentales françaises est toujours discutée. En position latérale aux anciennes vallées glaciaires, des conduits karstiques ont fonctionné en pertes juxtaglaciaires durant les phases de retrait glaciaire et constituent des enregistreurs pertinents de ces phases glaciaires. Dans le Bas-Bugey (Ain, France), la grotte Sous-les-Sangles abrite une remarquable séquence détritique laminées associée à une position du glacier de l'Isère dans la cluse des Hôpitaux. Des datations entreprises il y a 20 ans (U/Th alpha) sont ici révisées. Cinq nouvelles dates U/Th MC-ICP-MS ont été entreprises sur des spéléothèmes encadrant l'ensemble détritique offrant un terminus post quem et un terminus ante quem à cette invasion glaciaire. Le TPQ est daté à 87,3 ± 3,9 ka (MIS 5) et le TAQ est daté à 11.6 ± 4.3 ka (MIS 1). La série détritique laminée est ainsi mieux contrainte et l'invasion glaciaire ne peut se situer que dans les stades MIS 4 (localement Würm ancien) ou MIS 2 (localement Würm récent). La grotte Sous-les-Sangles confirme sa position stratégique pour contraindre l'extension maximale glaciaire au cours des derniers stades froids du Quaternaire.

1. Introduction

The latest maximum glacial extension of the French north-western Alps (Würm) is still under discussion. Does it rather correspond to the ancient Würm (MIS 4) or to the recent Würm (MIS 2)? Lateral to the former glacial valleys, karstic galleries functionned in juxtaposed sinkholes. They are relevant recorders of these phases. South of the Jura, the Bas-Bugey is in a strategic position to record the French Alps glaciers maximum extension and the glacial retreat. The "Cluse des Hôpitaux" is an important valley currently drained by two diverging rivers. During the last glacial maximum, the cluse was invaded by a diffluence of the Isère glacier. The Upper Kimmeridgian limestone karst recorded this invasion. On the surface, the remains of the maximum glacial extension consist of till belts recognised at around 900 to 950 m above sea level (asl) in the Innimond sector and at around 850 to 900 m asl in the Ordonnaz sector (Kerrien *et al.*, 1990). The origin of these the Bas-Bugey glacial overflows has long been attributed to the Rhône (Kerrien *et al.*, 1990) and finally to Isère on the basis of petrographic analysis (Coutterand, 2010). In this sector, where glacial records are remarkable, an important karst develops: the Burbanche karst system (22 km) on the southern edge of the "Cluse des Hôpitaux" (Chirol, 1985; Chirolet Hugon, 2010; Hugon, 2013) (Fig. 1). We chose to analyse an exceptional sedimentary deposit at the Sous-les-Sangles cave (Fig. 2). It has already been the subject of extensive studies (Sbai *et al.*, 1995; Lignier *et al.*, 2002), but the precise chronology of the deposit remains to be established. This is the subject of this note.

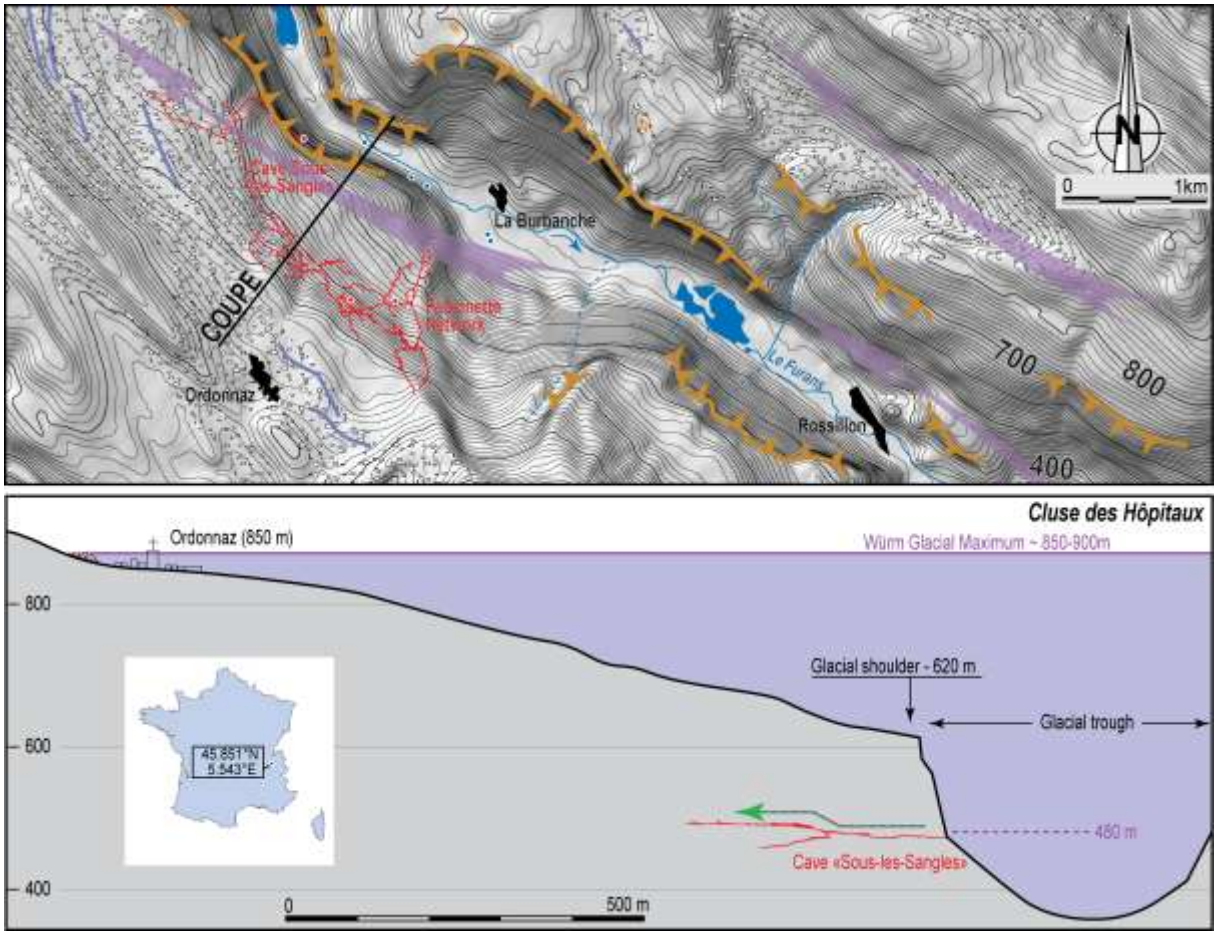

Figure 1: Location of the Sous-les-Sangles cave (plan and section) in the Bas-Bugey. Note the position of the horizontal cave in relation to the WGM (Würm Glacial Maximum) extension.

2. The karstic filling of the Sous-les-Sangles cave

At 475 m asl, the Sous-les-Sangles cave is a horizontal gallery developing in the lower third of the southern slope of the cluse. Underground, three major sedimentary formations have been identified (Fig. 3) (Lignier *et al*., 2002): (i) at the base, a morainal and fluvio-glacial filling composed of (I_{1-2}) dark, greenish, stratified sands, rich in quartz, mostly unworn (Sbai *et al*., 1995), covered in discordance by a coarser set (G_2) composed of decimetric blocks with a poorly sorted matrix. On top, a coarser sandy series (I_{2-3}), less stratified and partially channelled, lies in discordance (Lignier *et al*., 2002); (ii) on this set rests the sequence (G_3), composed of millimetre to multi-centimetre alternation of carbonate silts and clear clays over a thickness of more than 3 m: the Boulevarve. A detailed analysis of the laminations made it possible to propose a period of 350 years (Lignier *et al.*, 2002) for the setting. Closer to the entrance of the cavity, a set of clear morainic debris (iii) is identified in the "la Plage" sector (Lignier *et al*. 2002). This material has been largely reworked and washed away by the suffosion operation in the "La Plage" sector. In addition to these three types of deposits, there are also pre- and post-glacial speleothems. The cave was about 350 m below the surface of the glacier during its maximum extension. Under such a thickness, hydrological circulations are limited to the upper third of the ice mass or within the upper 100 to 150 m (Bini *et al*., 1998; Irvine-Fynn *et al.*, 2017). Considering these elements, juxta-glacial hydrological penetration is likely to occur when the ice surface is around 550 m, i.e. more than 250 m below the WGM line, i.e. well after the WGM.

Figure 2: The G_3 karstic infill is a 3 m thick sequence composed of millimetre to multi-centimetre alternation of carbonated silts and clear clays.

3. Contemporary filling of deglaciation

We propose the following deglaciation and endokarstic sedimentation scenario:

- **At the WGM (Würm Glacial Maximum)**, the glacial surface is at 850 m asl (Kerrien *et al*., 1990). Underground, the drain is flooded but does not experience significant hydrological circulation. On the other hand, sedimentary sets at the bottom of galleries are already present ($I_{1\text{-}2}$ and G_2 in particular, Lignier *et al*. 2002). These are intra-karstic fluvio-glacial cones dating from a previous glacial phase (Würm possible).
- **During a phase of retreat**, the ice surface stabilises at around 550 m. The sub-glacial flows are then around 480 m and allow hydrological exchanges with the karst in a juxta-glacial sinkholes position. The penetration of large water flow, carrying a fine detrital load and richly carbonated, leads to the sedimentation of the filling (G_3). Such a mechanism presupposes a certain equilibrium, an outlet downstream and a certain duration. These circulations are conditioned by the cavity altitude and therefore provide information on the glacial surface altitude, which itself give information on the glacier spatial extension.
- The further lowering of the ice surface ended this equilibrium **and the sedimentation stopped**. At the cave entrance, surface circulation can be lost underground with poorly sorted fluvio-glacial material. This coarser material indicates an increased hydrological competence, which can be attributed to a stronger hydraulic gradient. The proximity of the glacier front during the retreat dynamics may explain this temporary hydraulic gradient increase and thus in the importance of the water flows.
- Finally, **the glacier disappears** and the cavity recovers its hydrological functioning, still known today, with partial incision of the sedimentary deposits. Speleothems are set up and seal these sedimentary deposits in their partially dismantled state.

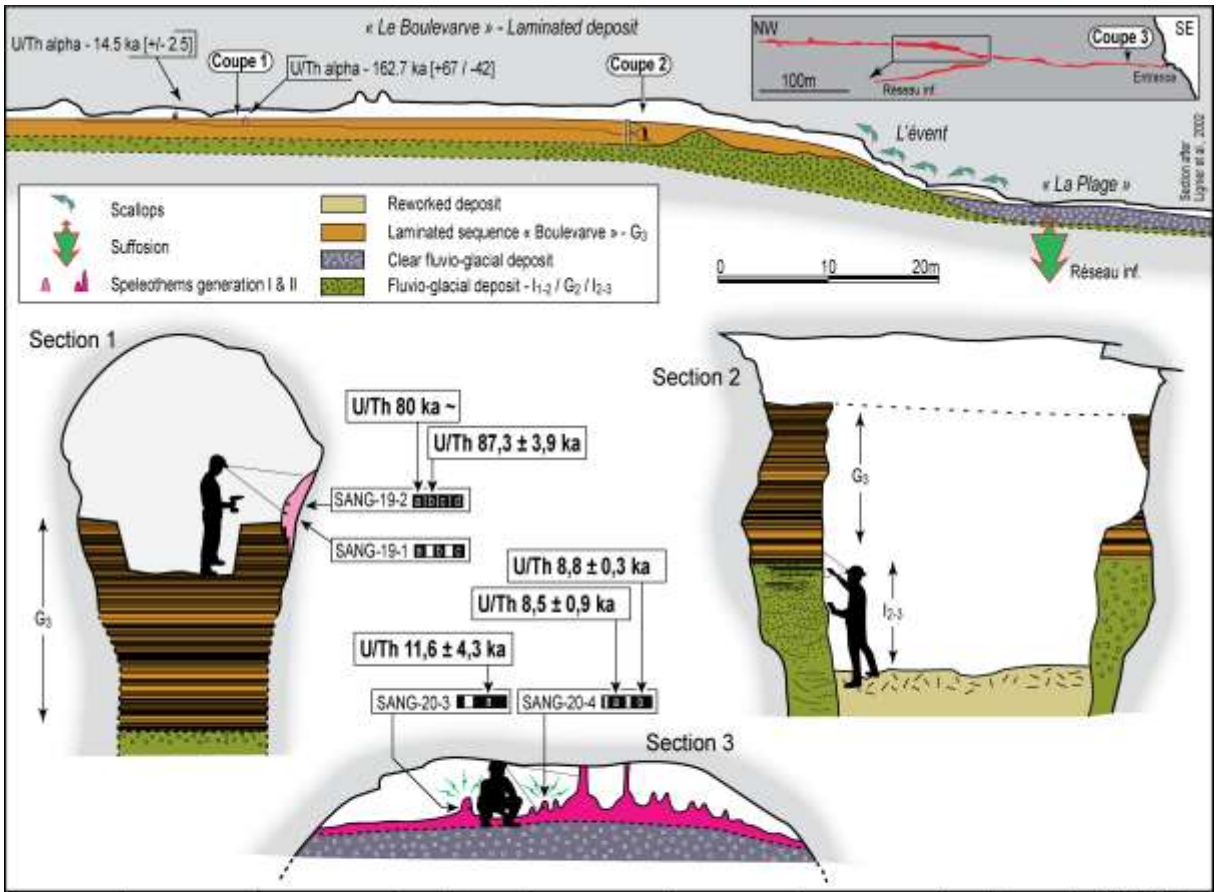

Sample	[^{238}U] ppm		[^{232}Th] ppb		δ^{234}U M (‰)		(^{230}Th/^{238}U)		(^{230}Th/^{232}Th)		Age (ka) 2019		$\delta^{234}U_T$		Age cor (ka) before 2019/2020	
SANG-19-2-a	0,125	0,00	43,27	0,51	340,64	5,63					~ 90				~ 80	
SANG-19-2-b	0,139	0,00	23,45	0,19	306,63	4,75	0,7736	0,00	13,98	0,03	93,55	0,9	392,5	7,4	87,32	3,87
SANG-20-4-b	0,273	0,002	3,05	0,02	430,66	2,55	0,1156	0,0007	32,22	0,18	9,17	0,07	441,5	2,6	8,76	0,27
SANG-20-4-a	0,255	0,002	11,42	0,09	437,34	3,26	0,1271	0,0008	8,84	0,06	10,06	0,09	447,9	3,5	8,46	0,89
SANG-20-3-b	0,216	0,002	51,59	0,42	368,70	2,18	0,2331	0,0008	3,04	0,01	20,22	0,11	381,0	5,1	11,60	4,29

Figure 3: Synthetic section of the cave Sous-les-Sangles with location of the studied sections. Table of the 5 U/Th dates with U and Th contents, activity ratios and ages. Raw ages were corrected ("Age cor" column) assuming a $^{230}Th/^{232}Th$ activity ratio for the detrital phase of 1.5 ± 50%. The data obtained show that the sedimentary ensemble belongs to the MIS 4, 3 or 2 stage.

4. New U/Th dates

For this reconstruction, we propose chronological constraints. U/Th dating (alpha method, Quinif, 1987) had made it possible to propose two dates framing the sequence and gave the following ages: 162.7 ka (+67 / -42) for a flowstone sealed by the G_3 deposit and 14.5 ka (+/- 2.5) for a stalagmite covering the G_3 deposit (Lignier *et al*., 2002). We have chosen to reuse these dates and supplement them with new analysis. For this purpose, three sections were invested. Section 1 is in line with the flowstone already dated. Analyses were performed at LSCE using a MC-ICP-MS and following the protocol described in Pons-Branchu et al., 2014. Two micro cores (SANG 19-1 and SANG 19-2) were dated, with for sample 2, an age of 87.3 ± 3.9 ka and a second age of approximately 80 ka. Near the entrance (section 3), two stalagmites (SANG 20-3 and SANG 20-4) were likewise cored and delivered the following Holocene ages: 11.6 ± 4.3 ka, 8.5 ± 0.9 ka, 8.8 ± 0.3 ka (Fig. 3). The speleothems SANG 20-3 and SANG 20-4 are shocked (fig. 4), i.e. they are marked by pebble impacts associated with the evacuation of clasts by flood waters. These impacts can only be identified on one side of the stalagmites and are evidence of the clean-up phase (coarse fillings with hydrological and sedimentary circulation) from the interior of the karst towards the valley. It is therefore not possible for glacial material to penetrate after the stalagmites establishment. These dates are terminus post quem and ante quem of the G_3 detrital sequence penetration. Consequently, the last glacial phase responsible for this detritic invasion took place at MIS stages 4, 3 or 2. Unfortunately, as it stands, it is not possible to distinguish between ancient Würm and recent Würm or even to correctly link this sequence to one of the stages of the glacial retreat. However, it has been possible to better constrain the relationship between the glacial dynamics in the valley and the invasion of sediments. The filling of the Sous-les-Sangles cave is an eloquent case that deserves further study. OSL analyses are planned to directly date the detrital deposits.

Figure 4: Micro-core drilling of the SANG 20-04 speleothem. Note the shocks (white dots in the green circle) showing the evacuation of the pebbles after growth.

References

BINI A., TOGNINI P., ZUCCOLI L. (1998) Rapport entre karst et glaciers durant les glaciations dans les vallées préalpines du sud des Alpes. *Karstologia*, 32, 7-26.

CHIROL B. (1985) Contribution à l'inventaire spéléologique de l'Ain, Jura méridional. *Spéléo01*, CDS Ain, 425 p.

CHIROL B., HUGON B. (2010) Le système Plaine du Bief – Falconnette – Source de la Burbanche (Jura méridional). *Grottes et Karsts de France*. Karstologia Mémoires n°10 (Audra dir.), pp.188-189.

COUTTERAND S. (2010) *Étude géomorphologique des flux glaciaires dans les Alpes nord-occidentales au Pléistocène Récent. Du maximum de la dernière glaciation aux premières étapes de la déglaciation*. Thèse, Université de Savoie, Chambéry, 468 p.

HUGON B. (2013) Réseau de la Falconette. Nouveau joyau du massif du Bugey, la Burbache, Ain. *SpéléoMagazine* n°82, topo HT, pp. 20-25.

KERRIEN Y., JUVENTI G., LORENCHET DE MONTJAMONT M., MONTJUVENT G., GAILLARD C. (1990) *Carte géologique de la France (1/50.000), feuille Belley* (700), Orléans, BRGM, Notice explicative par Kerrien Y., Montjuvent G., Combier J., Gaillard C., Girel J., Laurent R., Lorenchet de Montjamont M., 73p.

IRVINE-FYNN T., HUBBARD B. (2017) Glacier Hydrology and Runoff. *The International Encyclopaedia of Geography*, 18 p.

LIGNIER V., DESMET M. (2002) Les archives sédimentaires quaternaires de la grotte Sous les Sangles (Bas-Bugey, Jura méridional, France) ; indices paléo-climatiques et sismo-tectoniques. *Karstologia*, 39, 27-46.

PONS-BRANCHU E., DOUVILLE E., ROY-BARMAN M., DUMONT E., BRANCHU E., THIL F., FRANK N., BORDIER L. AND BORST W. (2014). A geochemical perspective on Parisian urban history based on U-Th dating, laminae counting and yttrium and REE concentrations of recent carbonates in underground aqueducts. *Quaternary Geochronology* 24, 44-53

SBAI A., EK C., DROUIN P., CHIROL B., ARIAGNO J.-C., PELISSON A., QUINIF Y. (1995) Les remplissages karstiques de la grotte Sous-les-Sangles : Sédimentologie et évolution spéléomorphologique d'une grotte du Jura méridional (France). *Quaternaire*, vol. 6, n°1, pp. 35-45.

A speleogenetic comparison between caves located in two neotectonic grabens in southern Greece.

Isidoros KAMPOLIS[1,2] & Kyriaki PAPADOPOULOU-VRYNIOTI[3]

(1) 1 School of Mining Metallurgical Engineering, Department of Geological Sciences, National Technical University of Athens, 9 Iroon Polytechniou, Athens, 15773, Greece – Greece
(2) Group of Palaeoenvironment and Ancient Metals Study, Institute for Nanotechnology Nanoscience, National Center for Scientific Research 'Demokritos', 10 Neapoleos, Athens, 15310, Greece – Greece
(3) Department of Geography and Climatology, Faculty of Geology Geoenvironment, National Kapodistrian University of Athens, Panepistimioupolis Zografou, Athens, 157 84, Greece – Greece

Abstract

The Corinth and Messiniakos gulfs represent two neotectonic grabens in Greece. The Corinth Gulf is a WNW-ESE bearing asymmetric graben of Upper Miocene age and separates the southern Central Greece from the northern Peloponnese. The Tyfion and Kapareli caves are located at the NE border of the Corinth Gulf, about 4 and 7 km from the closest coastline, respectively. On the other hand, the Messiniakos Gulf is an asymmetric graben of Late Miocene age striking NNW-SSE and borders the SW Peloponnese. The composite cave system of Selinitsa-Drakos is 46 km south of Kalamata City on the eastern coast of Messiniakos, 54 m from the sea. In order to compare the speleomorphology with the regional tectonic activity and assess the influence of geodynamics to speleogenesis, the development directions of the aforementioned caves were measured. For Selinitsa-Drakos system, these were exploited by the plan view maps whereas for Tyfion and Kapareli caves, they were measured during their survey. Also, 273 karstic/tectonic directions were measured around the cave entrances. Both cave groups are controlled by the regional tectonic history of the grabens and this can be seen in their development patterns. Finally, a common tectonic history is revealed for the whole area.

Fluviokarst on Quaternary eogenetic conglomerates; an example from Slovenia

Matej LIPAR(1) & Mateja FERK(1)

(1) Anton Melik Geographical Institute, Research Centre of the Slovenian Academy of Sciences and Arts, Ljubljana, 1000, Slovenia, matej.lipar@zrc-sazu.si (corresponding author), mateja.ferk@zrc-sazu.si

Abstract

Most of the eogenetic conglomerates in Slovenia are cemented remnants of Quaternary fluvio-glacial deposits. A high proportion of carbonate pebbles made the conglomerate prone to dissolution and karstic development. This includes the development of karst hydrology and geomorphological forms, e.g., dolines, pocket valleys and caves. Udin Boršt, one of the karstified conglomerate terraces in the north-western part of Slovenia, shows the additional development of fluvial geomorphology. Its overall distribution is not even and shows better development of fluvial geomorphology on the eastern/north-eastern side of the terrace. Whilst the first idea that a difference in the amount of percentage carbonate pebbles could cause this phenomenon due to mixing zones of the material from two different valleys, it was later noted that the elevation difference of the underlying impermeable Oligocene clay is the cause for this. We complement this idea that not just the elevation difference, but also the palaeotopography of the underlying clay, promoted the development of fluvial valleys and, in fact, had a predispositional effect on their spatial occurrence.

Résumé

Fluviokarst sur des conglomérats éogénétiques du Quaternaire ; un exemple en Slovénie. La plupart des conglomérats éogénétiques de Slovénie sont des restes cimentés de dépôts fluvio-glaciaires quaternaires. Une proportion élevée de galets de carbonate a rendu le conglomérat sujet à la dissolution et au développement ultérieur du karst. Cela comprend le développement de l'hydrologie karstique et des formes géomorphologiques, par exemple les dolines, les reculées karstiques et les grottes. Udin Boršt, l'une des terrasses de conglomérats du nord-ouest de la Slovénie, montre également le développement de morphologies fluviales. Sa distribution globale n'est pas uniforme et montre un meilleur développement de la géomorphologie fluviale sur le côté est / nord-est de la terrasse. Alors que la première idée selon laquelle une différence dans la quantité en pourcentage de galets de carbonate pourrait amener à ce phénomène en raison du mélange de matériaux issus de deux vallées différentes, il a été noté plus tard que la différence d'élévation de l'argile oligocène imperméable sous-jacente en est la cause principale. Nous aboutissons à cette idée que non seulement la différence d'élévation, mais aussi la paléotopographie de l'argile sous-jacente, a favorisé le développement des vallées fluviales et, en fait, a préparé leur répartition spatiale.

1. Introduction

Quaternary conglomerates in Slovenia reflect periodical deposition of fluvio-glacial material related to glacial and interglacial cycles. Carbonate Mesozoic rocks dominate in the catchments, so conglomerates mostly consist of carbonate pebbles cemented with the calcite. Periodical depositions of the material were followed by fluvial erosion, and consequently the older carbonate sediments appear as isolated terraces.

Karst that evolved on those terraces has been termed as 'conglomerate karst' (HABIČ, 1981; GABROVŠEK, 2005; KRANJC, 2005), 'shallow karst' (ŽLEBNIK, 1978), 'isolated karst' (HABIČ, 1981) and 'eogenetic karst' (LIPAR & FERK, 2011; FERK & LIPAR, 2012), and consists of a variety of karst geomorphological features including dolines, caves, pocket valleys and blind valleys. However, Udin Boršt terrace (Fig. 1) also exhibits fluvial topography, which dominates on its eastern and north-eastern part, expressed with steep valleys and gullies, forming so-called 'fluviokarst'.

The conglomerate of the Udin Boršt terrace was deposited on top of the impermeable Oligocene clay, which slopes down westwards and south-westwards. Consequently, the conglomerate deposits are generally thicker on the south-western part of the terrace, and notably thinner on the north-eastern part; this leads to the conclusion that a thin deposit of conglomerate and relatively shallow occurrence of the Oligocene clay beneath the conglomerate on the north-eastern part caused predominantly fluvial geomorphological regime. However, the question is whether these fluvial valleys could have been additionally influenced by the (palaeo)topography of the Oligocene clay that was present prior to deposition of the fluvio-glacial sediment (i.e., present day conglomerate). This paper illustrates the initial approach of field work mapping of the clay exposures and construction of the cross-section of the valley-ridge system in the north-eastern part of the terrace (Fig. 1).

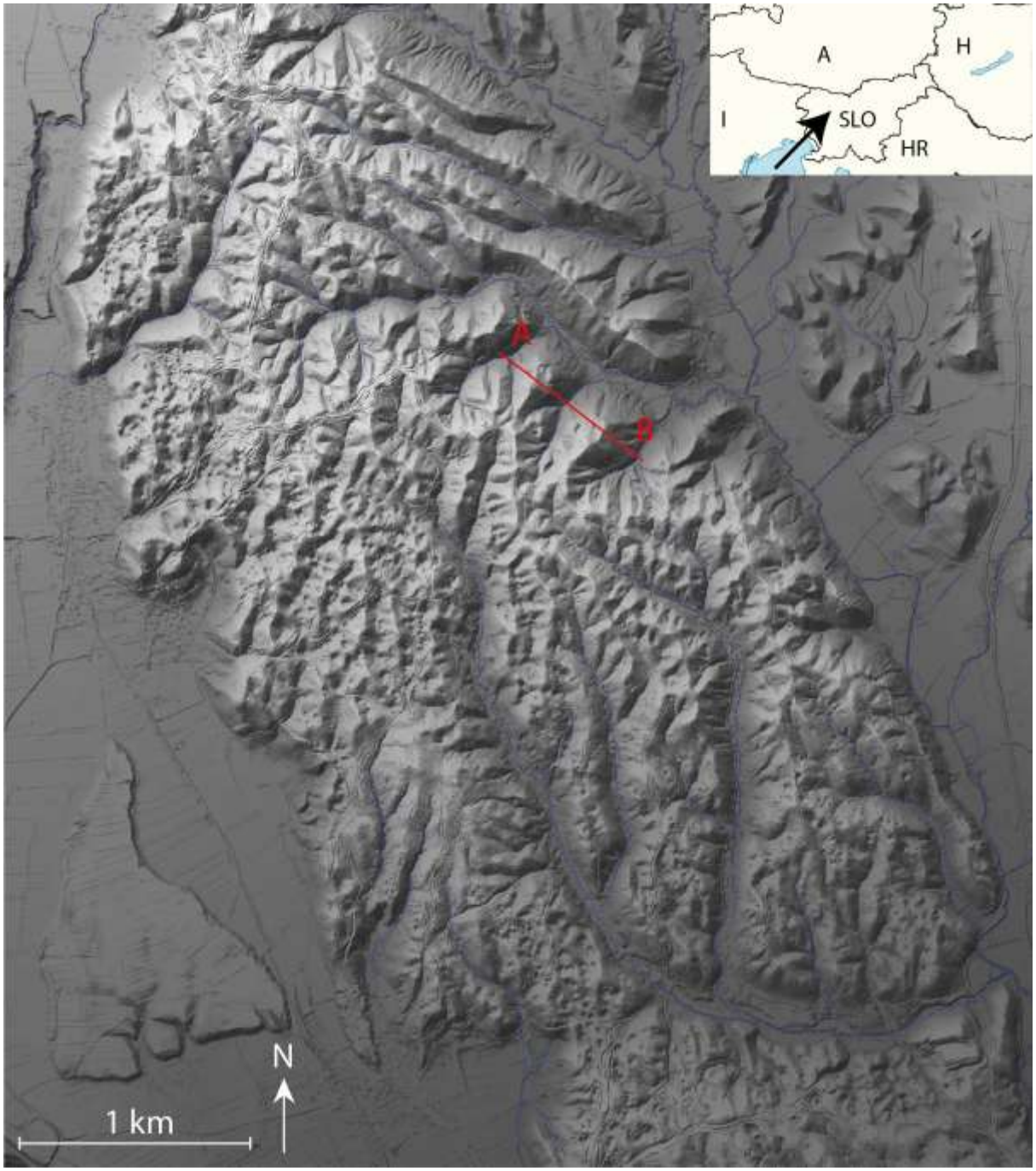

Figure 1: Digital elevation model based on LiDAR (source: ARSO, 2015) of the Udin Boršt terrace. Note the predominant fluvial geomorphology on its northeastern part and predominant karst topography on its southwestern part. A – B cross-section is shown in Fig. 3.

2. Materials and methods

Field work was conducted throughout the Udin Boršt terrace to map the exposures of Oligocene clay and Quaternary conglomerate. In several occasions, we used a hand drill to check for the Oligocene clay beneath the soil and residual sediment cover. Mapping was performed using SWMaps software on field, and then exported into Global Mapper software. Due to large errors in GPS elevation points from field, we adopted LiDAR data elevations to all the points for consistency and small error.

3. Results

The outcrops of the Oligocene clay and conglomerates have been mapped over the whole Udin Boršt terrace, but comparing the elevations of the exposed clay in relation to conglomerate around the whole terrace is problematic because the terrace has experienced neotectonic movement (MIHEVC *et al.*, 2015). We have therefore focused on a small section of the northeastern part of Udin Boršt (A – B cross-section in Fig. 1).

The exposure of the clay is, similarly to most of the valleys in Udin Boršt, restricted mostly to the floors of the valleys by on-going creek erosion (Fig. 2A). The lower parts of valley slopes are mostly covered by colluvium, but in places just above the colluvium, clay exposures were observed at the contact with the conglomerate, which is usually also seen as a steeper slope or a cliff-face. Springs are common at these contacts (Fig. 2B).

As the palaeotopography of the clay behind/underneath the conglomerate could not be observed, the overall topography of the clay within the valley floors could still be simply the result of the erosion postdating the deposition of the conglomerate. This led to the additional surveying of the ridges on both sides of the valley by sampling sediment up to 4 m in depth at multiple points with a hand-drill. We successfully found one occurrence of the clay 3 m deep underneath the soil and residual sediment that was left over after the denudation of the conglomerate on one of the valley ridges (Fig. 2C, Fig. 3).

Figure 2: Oligocene clay exposures: (A) – exposure of the clay at the bottom of the valleys by creek erosion; (B) – exposure of the clay at the contact with the upper lying conglomerate (note that these sections usually represent karst springs); (C) – clay occurrence underneath the soil and residual material on the ridge.

4. Discussion

Since conglomerate exposures were mapped in lower elevations on the valley slopes, the occurrence of the clay at higher elevations relative to the conglomerates in the same valley system confirms the presence of the palaeotopography of the clay. The 'palaeoridge' of the clay is illustrated as the ridge on the right hand-side in Fig. 3. Clear contacts of conglomerate and clay were found on both sides of the ridge, whilst the residual scattered non-carbonate pebbles within the loamy sediment at the drilling point on top of the ridge indicates the presence of conglomerate even above this point. MIHEVC *et al.* (2015) published a burial age of 1.86 Ma for the conglomerate of Udin Boršt, which represents enough formation-time for the great amount of non-carbonate residual material found on top of the ridge.

Furthermore, the Oligocene clay 'palaeoridge' within the present-day conglomerate ridge sparks the possibility that at least some present-day valleys can be re-activated palaeovalleys originating in the Oligocene clay before the initial burying by fluvio-glacial material. This suggests that occurrence and direction of particular valleys within the fluviokarst system of Udin Boršt was not led only by the shallow depth of the Oligocene clay on its eastern and north-eastern part, but also by its previous topography. Furthermore, the palaeotopography could partly explain the focusing of underground water in otherwise porous conglomerates with prevailing matrix porosity, and could therefore represent a complex and unique type of a 'fluviokarst' (for other processes that form fluviokarst see, e.g., FORD & WILLIAMS (2007)). The simplified proposed process suggests that the buried palaeovalleys collect and redirect underground water flow and cause (sub)vertical jointing of the conglomerate, which later evolves into present-day fluvial valleys. At the same time, the water still flows underground where the conglomerate is present and subsequently causes the formation of small caves at discharge points at the conglomerate-clay contact.

Nevertheless, a single find of the clay on the top of the ridge currently demonstrates only the possibility of the overall palaeotopographical influence. Further multiple-method approaches are necessary for detailed reconstruction of the palaeotopography, so that the pilot study within this paper can be developed to explain the Earth processes and their timing to form fluviokarst on

Quaternary carbonate conglomerates.

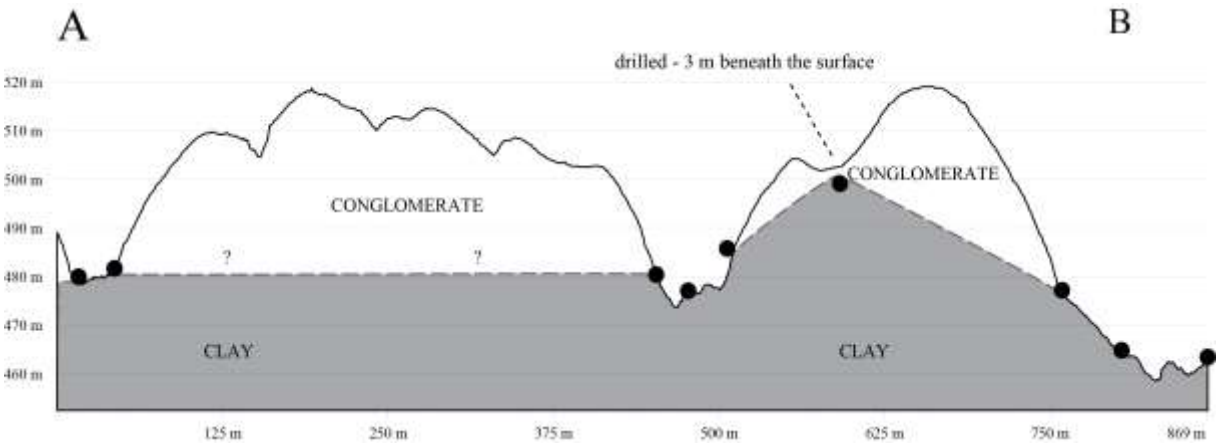

Figure 3: Cross-section (see Fig. 1 for location) of the fluvial valley within the conglomerate terrace. Black dots are locations of mapped clay on the field.

5. Conclusion

Field investigation of the impermeable Oligocene clay exposures confirmed the presence of its palaeotopography prior to fluvio-glacial material deposition (forming present carbonate conglomerate) and possible influence on later development of fluviokarst. Geomorphological features in the area therefore depend on several different components, including the depth of the conglomerate above the Oligocene clay, surface water seepage paths along fractures, horizontal and vertical contacts between karst and clay material, and the direction of groundwater flow which depends on the palaeotopography of the area.

Acknowledgments

The research on eogenetic conglomerates is funded by the Slovenian Research Agency research core funding Geography of Slovenia (P6-0101), Infrastructure Programme (I0-0031), fundamental research project Geomorphological peculiarities of AEOLianite KARST and their palaeoclimatic significance (N1-0162) and bilateral project Geomorphological characteristics on eogenetic carbonate rocks in Slovenia and United States of America (BI-US/19-21-005).

References

ARSO (2015) Online repository of LiDAR data (gis.arso.gov.si/). Slovenian Environment Agency.

FERK M., LIPAR M. (2012) Eogenetske jame v pleistocenskem karbonatnem konglomeratu v Sloveniji (Eogenetic caves in Pleistocene carbonate conglomerate in Slovenia). Acta geographica Slovenica, 52(1), 7-33.

FORD D., WILLIAMS P. (2007) Karst geomorphology and hydrology. John Wiley & Sons Ltd, Chichester, England, 562 p.

GABROVSEK F. (2005) Jame v konglomeratu: primer Udin Boršta, Slovenia (Caves in conglomerate: case of Udin Boršt, Slovenia). Acta Carsologica, 34(2), 507-519.

HABIČ P. (1981) Tipi krasa na Gorenjskem (Karst types in Upper Carniola). 12th meeting of the Slovene geographers. Geographical Society of Slovenia, Ljubljana, pp. 78-88.

KRANJC A. (2005) Conglomerate Karst in Slovenia : History of Cave Knowledge and Research of Udin Boršt (Gorenjsko). Acta Carsologica, 34(2), 521-532.

LIPAR M., FERK M. (2011) Eogenetic caves in conglomerate: an example from Udin Boršt, Slovenia. International Journal of Speleology, 40(1), 53-64.

MIHEVC A., BAVEC M., HÄUSELMANN P., FIEBIG M. (2015) Dating of the Udin Boršt conglomerate terrace and implication for tectonic uplift in the northern part of the Ljubljana Basin (Slovenia). Acta Carsologica, 44(2), 169-176.

ŽLEBNIK L. (1978) Kras na konglomeratnih terasah ob Zgornji Savi in njenih pretokih (Karstification of conglomeratic terraces along the Upper Sava River and tributaries). Geologija, 21, 89-9

Fractured speleothems as proxies for cave evolution

Alessia NANNONI[(1)], Marco ANTONELLINI[(2)], Bartolomeo VIGNA[(3)] & Jo DE WAELE[(2)]

(1) Department of Earth Sciences, University of Florence, Via La Pira 4, 50121, Florence, Italy, alessia.nannoni@unifi.it (corresponding author)
(2) Department of Biological, Geological and Environmental Sciences, University of Bologna, Via Zamboni 67, 40126 Bologna, Italy m.antonellini@unibo.it jo.dewaele@unibo.it
(3) Department of Environment, Land and Infrastructure Engineering (DIATI), Polytechnic of Turin, Corso Duca degli Abruzzi 24, 10129 Torino, Italy bartolomeo.vigna@polito.it

Abstract

Several fractured speleothems were studied in the Bossea cave (Piedmont, Italy) to infer the mechanisms that caused the rupture and their relationships with cave speleogenesis. The Bossea cave evolution is strongly controlled by a complex structural setting. It is a contact cave that developed along a detachment between meta-volcanic basement rocks and marbles laying on top. Downward erosion of the strongly deformed meta-volcanics led to the formation of giant halls in the downstream (touristic) part of the cave. The studied speleothems are located on both flanks of this downstream sector. All speleothems show fractures developed in uniaxial compression. Some fractured speleothems also show spalling and uplift of the concretions at the base. The deformation of these speleothems seems to be related to lateral focusing of vertical loads caused by the evolution of the arched cave roof. The sides of the rooms (abutments) are next to the detachment surface where speleothems rest on the highly weathered meta-volcanics, which can deform as the vertical load increases in response to roof collapses carving an arched ceiling profile. The cave ceiling evolution indicates an increasing instability of the downstream sector, a factor that should be considered in this show cave visited by over 30000 tourists every year.

1. Introduction

Broken speleothems are common structures in caves. However, their origin is difficult to infer because many processes may cause their formation (BECKER *et al.*, 2006; GILLI, 2005). Studies carried out in the past 50 years pointed to a co-seismic origin of these features, attempting to use them for neotectonics and paleo-seismological investigations (BRIESTENSKY *et al.*, 2014; FORTI, 2001; PLAN *et al.*, 2010). Other studies demonstrated that some examples interpreted as earthquake-induced were caused by other phenomena (BECKER *et al.*, 2006; GILLI, 2004). Overall, the processes that can lead to speleothem deformation can be divided in two types, speleogenetic and external ones (GILLI, 2004). The former type includes ground failure or creeping of the sediments underlying the speleothems, erosion at the base of the speleothem due to water flow, ice infill creep, rock decompression caused by *in situ* stress reorientation, mechanical failure of jointed blocks, and slope instability. The latter type of processes comprises human activities and active tectonics. Among the speleogenetic processes, mechanical failure is a phenomenon causing the most common cave morphologies, namely collapse or breakdown (FORD & WILLIAMS, 2007). The presence of the cave itself affects stress distribution in the rock surrounding the open passages. The distribution and the magnitude of cave breakdowns depend on many factors (HATZOR *et al.*, 2010): thickness of the rock cover, thickness and homogeneity of the rock layers (e.g. presence of marl layers), span of the opening, intensity of jointing, orientation of discontinuities, shear strength of discontinuities, strength of the intact rock, and groundwater conditions. The local structural setting, by controlling fault and joint distribution, bedding plane orientation and, consequently, water flow organization plays a fundamental role in cave speleogenesis and cave stability.

This contribution presents the first results of the investigation on the relationships between cave speleogenesis and the deformed speleothems found in an alpine cave system whose architecture and evolution are strongly controlled by the local structural setting. Some insights on current cave stability will also be presented. The studied cave, Bossea (NW Italy), is a show cave visited every year by 30,000 tourists and it hosts an underground scientific laboratory that has studied cave hydrology since the late 70s.

2. Geological setting, materials and methods

The Bossea cave (Piedmont, Italy) is a mid-altitude karst system developed in the Ligurian Alps. The surface is characterized by steep SE-facing slopes with bare rock outcrops and a thin soil cover. The development of the cave was strongly controlled by the Alpine tectonics (ANTONELLINI *et al.*, 2019). ENE-WSW striking subvertical faults put laterally in contact blocks of metamorphosed Mesozoic carbonates with the originally underlying metamorphosed Permian volcanoclastic and clastic rocks (quartzite and shale), limiting the areal development of

karstification. The carbonate and the clastic rocks sequence are also tectonically juxtaposed to the meta-volcanoclastics by a detachment (Fig. 1a). The detachment surface is antiformal with a hinge line plunging to ESE with a dip of 10-15°. The sequence made up of marble, quartzite, and shale is isoclinally folded. Consequently, bedding planes are steeply dipping (Fig. 1b). The meta-volcanics are strongly deformed and altered. The cave is 3 km long and is divided into an upstream and a downstream sector. In the former, the underground collector (TM, Fig. 1) flows in a canyon carved in the marble. The latter sector is a show cave and is characterized by large rooms and massive collapses (box in Fig. 1a, Fig. 1c). This part of the cave developed along the detachment surface (contact cave).

Deformed and fractured speleothem (stalagmites, stalactites, and columns) locations and dimensions were mapped inside the cave. Attitude of the fractures cutting the speleothems were measured with a Brunton™ geologic compass. Speleothem's base diameter, relative broken blocks movement, vertical and horizontal displacement along the fracture planes were also measured. The distance between the cave ceiling and the floor was measured at each speleothem location by means of a laser telemeter Leica Disto X. The structural data were plotted by using the Stereonet v.9.3.3 by ALLMENDINGER *et al.* (2012).

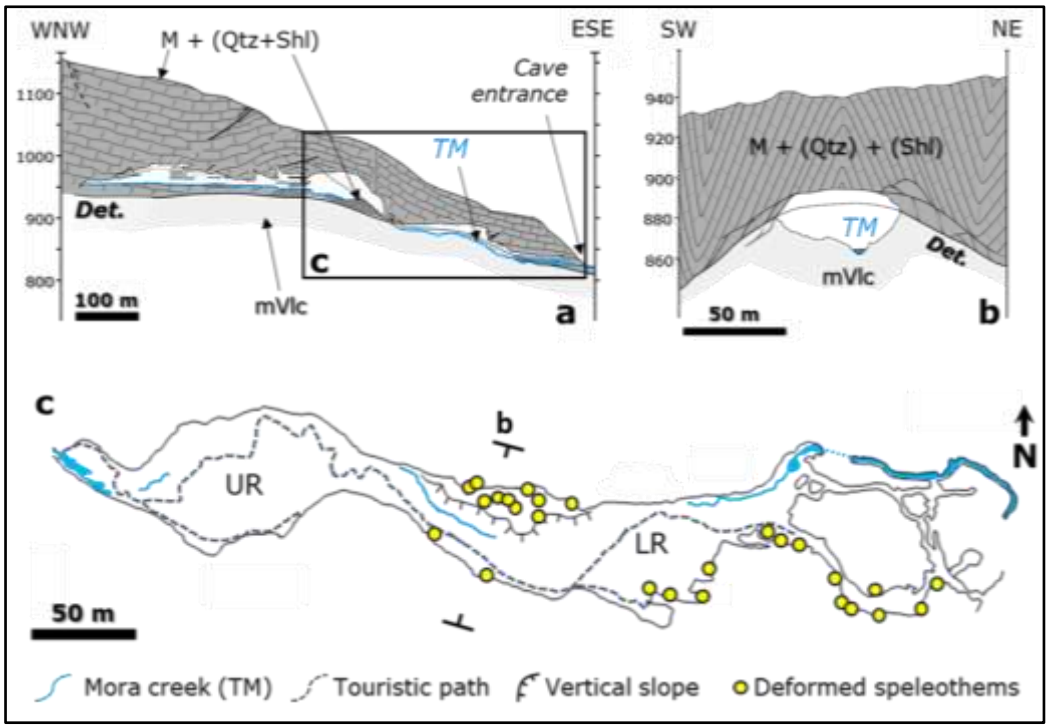

Figure 1: WNW-ESE (a) and SW-NE (b) simplified geological sections of Bossea cave, and plan view of the large rooms sector (c). The location of (b) and (c) are highlighted in (c) and (a), respectively. Labels: Det. = detachment, M = marble, Qtz = quartzite, Shl = shale, mVlc = meta-volcanics, TM = Mora creek, UR = upper room, LR = lower room. Modified after ANTONELLINI et al. (2019).

3. Results

Deformed speleothems are observed on both flanks of the lower part of the cave (i. e. Lower room, LR, and in the entry passage). Fractured concretions were not found nor in the upper room (UR), nor in the upstream part. The direction of displacement of the roof with respect to the speleothems is either northward or southward (Fig. 2a). Most speleothems show fractures that developed in uniaxial compression. These fractures are vertical and aligned with the principal compressional stress at the contact point (Fig. 2b, 2e). The uniaxial compression fractures open up at the roof contact point and propagate downwards. Some fractured speleothems, besides uniaxial compression fractures, show tilting, spalling, and uplift of the concretion at the base (Fig. 2c). Stress concentration at the roof-speleothem contact point caused intense fracturing, crystal cleavage gliding, and re-coloring (Fig. 2d). All speleothem contacts show predominantly contractional deformation (vertical downward) with a subordinate horizontal one (roof top-down). Some large speleothems show, in addition to uniaxial compression fractures, also spoon-shaped high aperture fractures at their base. These speleothems are observed next to steep slopes and rest on the strongly weathered and deformed meta-volcanics (Fig. 2f).

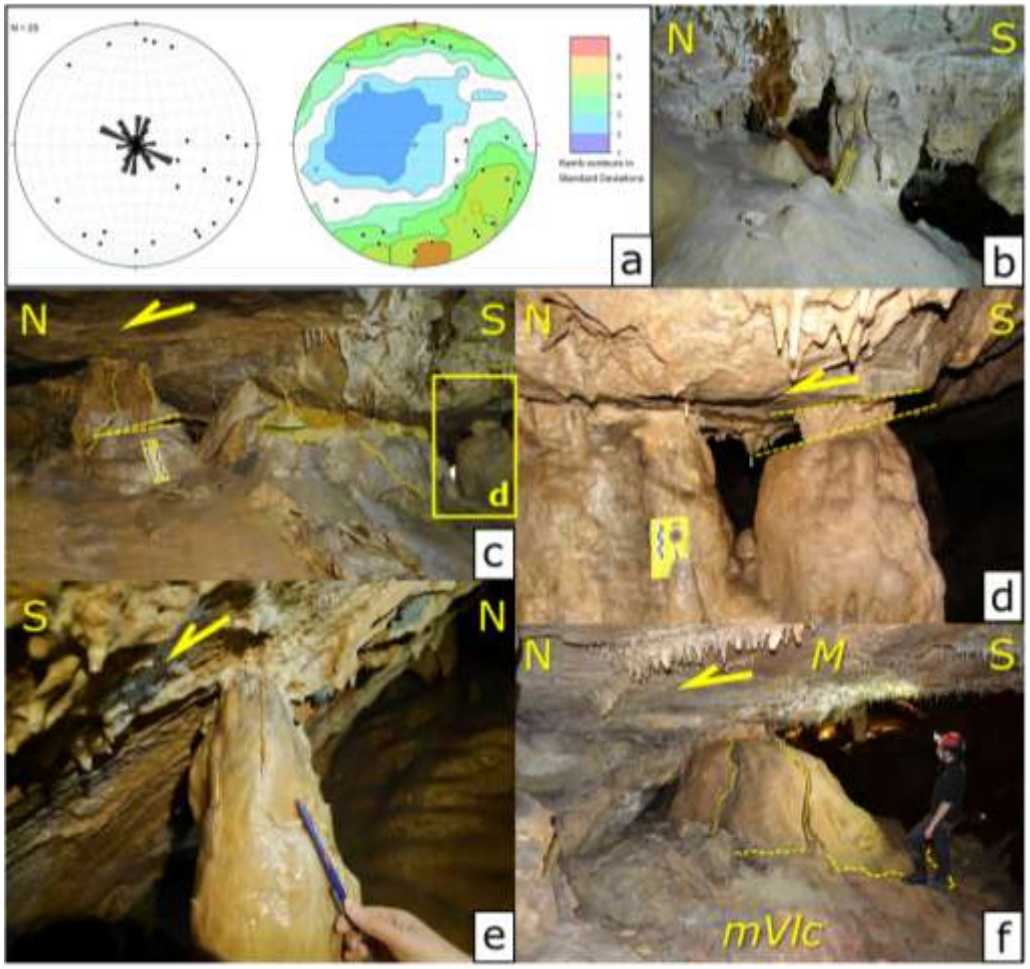

Figure 2: Slip vector diagram reporting the data of the deformed speleothems measured in Bossea cave (a). Morphological features in deformed speleothems: uniaxial compression fractures (b, e), uniaxial fractures and tilting (left column) and extrusion of material (central speleothem, c), calcite re-coloring and possible gliding along cleavage planes (d), high aperture spoon-shaped fracture at the base of a large speleothem (f). Yellow arrows show the roof relative movement with respect to the floor.

4. Discussion

A co-seismic origin for the deformed speleothems observed in the Bossea cave seems unlikely because slip vectors have no uniform orientation. The surface slope above the cave shows no evidence of instability so this factor could be also ruled out. It seems that the ongoing speleogenesis and the local structural setting concur to deform the speleothems. The cave development is progressing by erosion of the metavolcanics and roof collapses. This contributes to form an arched roof in the large rooms of the downstream sector. An arched roof causes the vertical loads to be focused on the abutments at the sides of the rooms. In particular, the gouge zone next to the detachment surface at the sides of the LR where roof and floor meet (Fig. 3b, 3d), represent an important weak element. The speleothems that grow close to the sides can be considered as “abutments or pillars” that deform as the lateral vertical load increases via roof collapse that tends to form an arched profile for the room ceiling. Moreover, these concretions rest on the top of the detachment gouge and highly weathered metavolcanics (Fig. 3e). If the speleothems grow over the metavolcanics on steep lateral slopes under uniaxial compression (load on the abutments due to the arched ceiling), landslides in the soft sediments at the base of these concretions can occur. This latter process is aided by the collapse of jointed strata and duplex blocks from the upper damage zone at the cave roof that contribute to form its arched profile (Fig. 3f). This hypothesis is coherent with the sense of movement of the roof respect to the studied speleothems (top down). Deformed concretions are not present in the UR because (Fig. 3c) the detachment is not outcropping.

The roof profiles of the UR and of the westernmost part of the LR seem less evolved towards an arched shape than the easternmost part of the LR, characterized also by less frequent rockfalls.

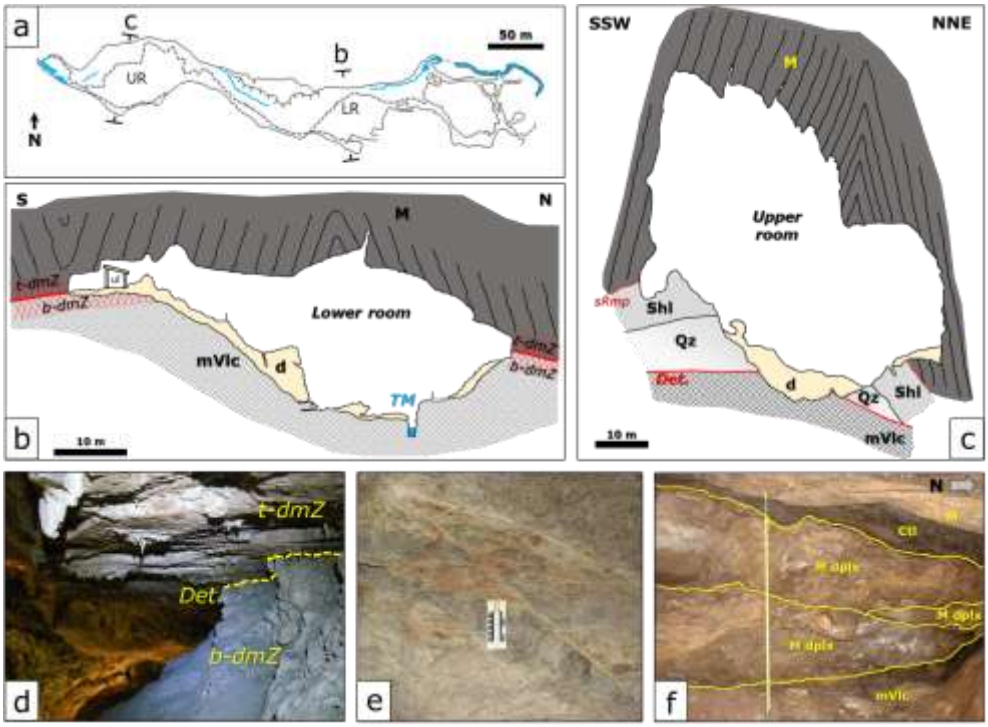

Figure 3: Map view of the LR show cave section (a). Geological cross-section of LR close to the underground scientific lab (ul, b). Geological cross-section UR (c). Outcrop of the detachment and the related damage zones inside the cave (d). Meso-structures of the bottom (e) and the top (f) damage zones. Labels: d = speleothem cover and clastic deposits, sRmp = secondary ramp, M dplx = marble duplex, Ctl = cataclasite. See Fig. 1 for mVlc, Qz, Shl, Det., b/t-dmZ meaning.

5. Conclusions

The investigation of the deformed speleothems of the Bossea cave confirmed the strong relationships between the complex local structural setting and speleogenesis. Overall, the ongoing cave evolution is controlled by important elements such as the detachment zone, the folded stratification, and the different mechanical properties of the rocks. This has implications for cave stability: speleogenesis is ongoing since the cave has not reached a stable roof configuration. The deformed speleothems are evidence of this process rather than an external perturbation (i.e. earthquakes). The cave profile evolution is unique for each sector, because it is strongly related to peculiar structures and morphologies, in fact the deformed speleothems are present in specific sites only.

References

ALLMENDINGER R.W., CARDOZO N., FISHER D. (2012) Structural geology algorithms: Vectors and tensors in structural geology: Cambridge University Press, UK, 302 p.

ANTONELLINI M., NANNONI A., VIGNA B., DE WAELE J. (2019) Structural control on karst water circulation and speleogenesis in a lithological contact zone: The Bossea cave system (Western Alps, Italy). Geomorphology 345, 106832.

BECKER A., DAVENPORT C. A., EICHENBERGER U., GILLI E., JEANNIN P. Y., LACAVE C. (2006) Speleoseismology: a critical perspective. Journal of Seism. 10.3, 371-388.

BRIESTENSKY M., STEMBERK J., ROWBERRY M.D. (2014) The use of damaged speleothems and in situ fault displacement monitoring to characterize active tectonic structures: an example from Západní cave, Czech Republic. Acta Carsologica 43.1, 129-138.

FORD D., WILLIAMS P. (2007) Karst hydrology and geomorphology, Ed. John Wiley & Sons. 562 p.

FORTI P. (2001) Seismotectonic and paleoseismic studies from speleothems: the state of the art. Geologica Belgica 4.3, 175-185.

GILLI E. (2004) Glacial causes of damage and difficulties to use speleothems as palaeoseismic indicators. Geodinamica Acta 17, 229-240.

GILLI E. (2005) Review on the use of natural cave speleothems as palaeoseismic or neotectonics indicators. C.R. Geoscience 337.13, 1208-1215.

HATZOR Y.H., WAINSHTEIN I., MAZOR D.B. (2010) Stability of shallow karstic caverns in blocky rock masses. Int. J. Rock. Mech. & Min. Sciences 47, 1289-1303.

PLAN L., GRASEMANN B., SPÖTL C., DECKER K., BOCH R., KRAMERS J. (2010) Neotectonic extrusion of the Eastern Alps: constraints from U/Th dating of tectonically damaged speleothems. Geology 38, 483-486.

Assessment of colored bacterial colonies on Azé and Blanot caves limestone walls

Stéphane PFENDLER(1) & Lionel BARRIQUAND(2)

(1) Université de Bourgogne Franche-Comté, CNRS, Laboratoire Chrono-environnement, 4, place Tharradin, F-25250 Montbéliard (corresponding author)
(2) Université Savoie-Mont-Blanc, EDYTEM, UMR 5204, Bâtiment « Pôle Montagne », 5 bd de la mer Caspienne, F-73376 Le Bourget-du-Lac cedex lionel.barriquand@wanadoo.fr

Abstract

Coloured bacterial colonizations were observed in Azé and Blanot caves (France) in both touristic and non-touristic areas. These proliferations were observed on moist walls and ceilings. In this study, we have characterized the bacterial developments using high-throughput sequencing. The results have highlighted that app. 80% of all DNA strands belong to the Actinobacterial phylum, followed by 12.5% of Proteobacteria. Three operational taxonomic units were highly dominant, representing 79.9% of the DNA sequences.

1. Introduction

Microorganisms are able to colonize almost any habitat on Earth, especially Prokaryotes. In fact, bacteria play a critical role in biogeochemical processes. Several studies have recorded bacterial communities that are inhabiting caves. Some of them are distinguished by physical peculiarities like bright colours. This is the case in the Azé and Blanot caves (France) where several (e.g., blue, pink, white, green, yellow) colonies proliferate on the moistest cave walls. The aim of this study is to characterize these colonies using next generation sequencing (Illumina MiSeq).

2. Material and methods

The observed bacterial communities in Azé and in Blanot caves were photographed using an Olympus Tough 4.0. In order to distinguish photosynthetic communities from non-photosynthetic biofilms, quantum yield measurements, corresponding phototrophs metabolism, were carried out. Before each sampling, five measurements were taken on each biofilm, which were previously placed for 30 min in the dark. Quantum yield parameter (Fv/Fm) was monitored using the photosynthesis yield analyzer mini-PAM (WALZ, Germany). Eleven non-photosynthetic colonies were scraped from the limestone walls with a plastic sterile tube, and maintained at -80 °C until total DNA extraction, amplification steps and sequencing. PowerBiofilm DNA Isolation Kit was used by MicroSynth AG following the manufacturer's instructions (MoBio Laboratories, Inc., Carlsbad, CA, USA). The polymerase chain reaction (PCR) amplification followed a two-step PCR protocol using a state-of the-art high fidelity polymerase. PCR amplifications were performed with the primers p23SrV_f1 (5'-GGACAGAAA- GACCCTATGAA-3'), p23SrV_r1 (5'-TCAGCCTGT- TATCCCTAGAG-3') and 16S 799 f (5' -AACMGGATTAGATACCCKG- 3') and 16S 1115 r (5' -AGGGTTGCGCTCGTTG- 3').

3. Results

In both Aze and Blanot caves, we have observed several biofilms (Fig. 1 A, B, C and D) colours (pink, blue, white and yellow). The observations using magnifying glass have permitted to show that some bacterial proliferation may be a mix of communities (i.e., blue and yellow colonies, visible on Fig. 1 A). The colonies can invade large areas of the caves (Fig. 1 E) and are able to retain water drops conferring them a shiny gold or silver aspect (Fig. 1 C and E).

Figure 1: Bacterial colonies growing on limestone walls exhibited several colours (blue (A, C), pink (B), yellow (A, D)). The colonies are able to retain water drops (C) that are reflecting the light (E).

DNA sequencing (Fig. 2) has permitted to record 1056 Operation Taxonomic Units (OTU). However, 79.9% of the DNA sequences were gathered in 3 OTUs, while the other 20.1% corresponded to low abundant OTUs (<1%). The two most abundant OTUs belong to the actinobacteria phylum (Actinobacteria_unclassified (43.9%) and a gender belonging to the Euzebya (33.7%)). The third most abundant phylum is represented by the Gamma-proteobacteria (Nitrosococcus, 2.4%), known as an ammonia-oxidizing bacterium. The results permitted to link the colour to an OTU. In fact, pink-coloured colonies belong to the Euzebia while blue, yellow and white spots are linked with the unclassified Actinobacteria.

Only one sample of blue colony was linked with the Euzebia. The second most abundant phylum was represented by the Proteobacteria (12.5%). The results have also highlighted that touristic activities have no influence on these bacterial communities (Fig. 3). In fact, there is no significant difference between bacterial colonies developing in the touristic part in comparison to the non-touristic areas. Moreover, no difference has been observed between the coloured colonies in Azé and Blanot caves. However, significant differences have been detected between the samples regarding their colour (Fig. 4), especially the pink biofilms versus the other colored biofilms.

	Biofilm colour	Pink	White	Blue	Yellow	Pink	Blue	Yellow	Blue	Pink	Blue
	Samples	bla1	bla2	Bla3	Bla4	azeNT1	azeNT2	azeNT3	azeT1	azeT2	azeT3
Number of DNA sequences	OTU 1	321	4870	5671	8203	135	7147	5586	6454	110	8042
	OTU 2	8589	983	580	245	8098	332	398	60	9036	1
	OTU 3	6	82	524	24	406	246	811	345	138	10
	bla: Blanot cave; aze: Azé cave; NT: non touristic area; T: touristic area										
	OTU 1: Actinobacteria_unclassified; OTU 2: Euzebya; OTU 3: Nitrosococcus.										

Figure 2: Abundance of DNA sequences per sample depending on the biofilm color.

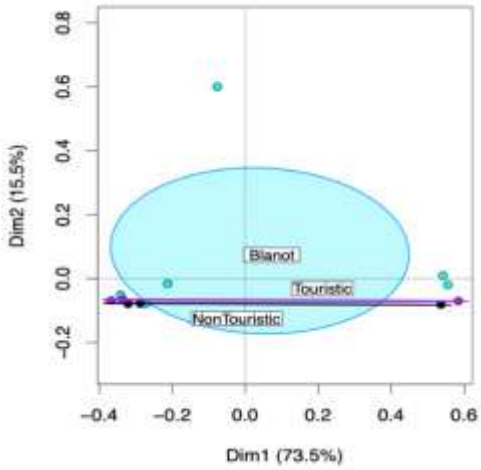

Figure 3: Principal coordinates analysis obtained using colonies that were sampled in both Azé (touristic and non-touristic areas) and Blanot caves (touristic area). A Bray-Curtis dissimilarity matrix was built and PERMANOVA was applied to this dissimilarity matrix. The result of PERMANOVA on the given Bray-Curtis dissimilarity matrix was shown under the Principal Coordinate Analysis (PCoA). The ellipses represent the area in which the centroid may be found (at 95% of probability).

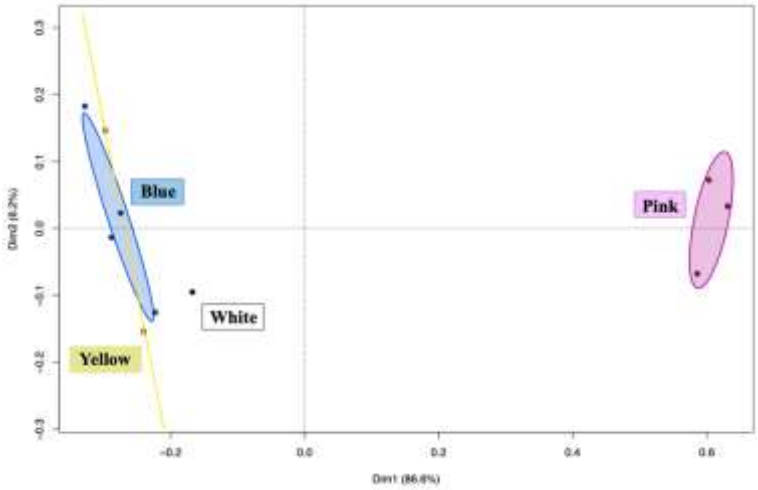

Figure 4: A principal coordinates analysis was performed depending on the colour of the sampled biofilms.

4. Discussion

Bacterial coloured biofilms developing in the Azé and Blanot caves were characterized as dominant Actinobacterial biofilm. This result is supported by the study of Porca et al. (2012). As well, Cuezva et al. (2009) reported high proportion of Actinobacteria but in a less extended proportion. However, Pašić et al. (2009) have reported that Proteobacteria were dominant. The variation in Actinobacteira proportion may be explain by the use of other molecular technics such as cloning or by the use of optical microscopy.

Cave microbial colonization is often related to touristic activities. However, this study has demonstrated that these communities may be considered as natural colony that grown independently of touristic tours.

Their expansion is probably conditioned by the physico-chemical parameters of the caves, in particular by high humidity conditions and the more or less regular presence of a water film. Thus the Balme Cave in Azé and the Cailleverdière Cave are instrumented to evaluate the environmental conditions conducive to the development of these biofilms. For a better understanding of these communities, a cultural approach (on Petri dishes) should be implemented. The definition of a model culture medium should make it possible to observe the growth mechanisms of these colonies and their impact on the cave walls. The latter can be significant and lead to an alteration of the casing and the anthropic traces that it may present (fig. 5). Thus, additional studies are needed to help understand the role of pigmented biofilms (Mulec et al., 2015).

Figure 5: Wall and graffiti dating from the end of the 19th century altered by biofilms in the Furtins cave (Berzé-la-Ville, France; picture by Serge Caillault).

5. Conclusion

Coloured bacterial colony developing on cave walls and ceilings is the consequence of bacterial biofilm proliferation, mainly composed by Actinobacteria and Proteobacteria. The two domain strains of Actinobacteria, representing more than 75% of the DNA strands sequenced, dominate all the biofilms. The unclassified actinobacteria gender is dominant for blue, yellow and white biofilm, while the Euzebia gender is dominant for pink coloured biofilm. These bacteria seem to be wild sprayed since no difference between the two caves was demonstrated.

Acknowledgments

First of all, we are grateful to the curators of the Azé and Blanot Cave, who kindly gave us permission to access the caves and to carry out all our field experiments. We also thank the Laboratory Chrono-Environment for their support and the association of the Azé cave for their financial contribution.

References

Lejla Pašic, Barbara Kovce, Boris Sket, Blagajana Herzog-Velikonja (2009). Diversity of microbial communities colonizing the walls of a Karstic cave in Slovenia. FEMS Microbiol Ecol, 71:50–60. DOI:10.1111/j.1574-6941.2009.00789.x.

Soledad Cuezva, Sergio Sanchez-Moral, Cesareo Saiz-Jimenez, Juan Carlos Cañaveras (2009). Microbial Communities and Associated Mineral Fabrics in Altamira Cave, Spain. International Journal of Speleology 38, 83-92.

Janez Mulec, Andreea Oarga-Mulec, Rok Tomazin, Tadeja Matos (2015). Characterization and fluorescence of yellow biofilms in karst caves, southwest Slovenia. International Journal of Speleology, 44 (2), 107-114. DOI:10.5038/1827-806X.44.2.1.

Ghost-rock karstification

Yves QUINIF[(1)] & Sophie VERHEYDEN[(2)]

(1) Service de Géologie fondamentale et appliquée, Faculté Polytechnique, Université de Mons, Rue de Houdain, 9, 7000-Mons, Belgium, yves.quinif2@gmail.com
(2) Department of Earth History of Life, Royal Institute of Natural Sciences (RBINS), Brussels, Belgium (corresponding author) sverheyden@naturalsciences.be

Abstract

Ghost-rock karstification or karstification by alteration of limestones with removal of the altered rock (ghost-rock) in a later stage has important differences with the classical way of cave formation by water progressively dissolving limestone and widening secondary voids, i.e., total-removal karstification. It often enables us to explain observed morphologies more easily than with the classical theory. The formation of caves from a ghost-rock occurs in two steps linked with two completely different palaeogeographical and palaeotectonic contexts. In Belgium, a first step occurred during Cretaceous when a flat surface enabled very slow underground water movements with partial dissolution of the limestone and formation of the ghost rock. The slow water movements also include possible convection loops related to low to medium-temperature geothermal water. A second step occurred in Cenozoic times during continental phases and when continental uplift increased the hydrological potential. Higher energetic water movements, phreatic or vadose, erode the residual alterite and creates a "speleological" cave. An example of such cave formation was observed *in situ* in the Quentin cave in Carboniferous limestones in Belgium. The cave formed in only a few months.

Résumé

La karstification par fantômisation. La karstification par fantômisation, ou par altération des calcaires avec élimination de la roche altérée (fantôme) à un stade ultérieur, présente des différences importantes avec la théorie classique de formation de grottes, c'est-à-dire l'eau qui dissout le calcaire et qui agrandit progressivement les fissures ou encore la karstification par élimination totale. La karstification par fantômisation permet souvent d'expliquer plus facilement les morphologies observées que la théorie classique. La formation de grottes à partir d'un fantôme de roche se fait en deux étapes qui sont à mettre en relation avec deux contextes paléogéographiques et paléotectoniques distincts. En Belgique, une première étape s'est produite au Crétacé, lorsqu'une surface plane a permis des mouvements d'eau souterraines très lents avec dissolution partielle du calcaire et formation du fantôme. Ces mouvements de l'eau dans l'aquifère peuvent se faire par boucles de convection liées à du géothermalisme de basse ou moyenne température. Une deuxième étape s'est produite au Cénozoïque pendant les phases continentales et lorsque le soulèvement des continents a augmenté le potentiel hydrologique. Des mouvements d'eau plus énergétiques, phréatiques ou vadoses, érodent l'altérite résiduelle et créent une grotte "spéléologique". La formation d'une grotte par évacuation de l'altérite a été observée *in situ* dans la grotte Quentin dans les calcaires carbonifères. La grotte s'est formée en seulement quelques mois.

1. A new karst genesis paradigm

Ghost-rock karstification is a new way of explaining the formation of caves and karst. Instead of the usually accepted theory (*total removal karstification*) of water (meteoric or deep hydrothermal) progressively dissolving the limestone and widening passages, ghost-rock karstification first leads to huge amounts of altered limestones that are 'washed away' by flowing water several million years later, which leads to the creation of caves. Moreover, this theory has the advantage of explaining observed incoherent passage width in caves or caves in hard materials such as quartzites, more easily than the classical theory. The concept of ghost rock as a primary step of cave formation was developed by the *Laboratoire de Géologie of the Faculté Polytechnique de Mons*, now known as *Faculté polytechnique de l'Université de Mons* in Belgium.

2. A two-step cave formation in distinct palaeoenvironmental contexts

The ghost-rock paradigm takes into account that karstification is in the first place a weathering process, just similar as for alumino-silicates. For carbonates, this weathering process partially dissolves the carbonates, especially the micritic part, while it leaves *in situ* not only the insoluble phase (clay minerals, quartz, siliceous cherts…) but also mostly sparitic carbonates (fossils, veins…). The weathering often occurs along structural discontinuities (bedding planes, fractures, faults….). The weathering leaves behind an altered isovolumic (= with the same volume) bedrock but with a porosity which can exceed 50% (Fig. 1). In several cases the ghost rocks are rich in organic

compounds that play a role in the bacterially mediated oxydo-reduction reactions, involving sulphides and leading to the production of sulfuric acids that 'boost' the karstification (QUINIF, 2014). Ghost-rock based cave formation takes place in two steps:

Step 1: Ghost-rock weathering
In Belgium, ghost-rock formation took place in a specific environmental context: low relief, hot and humid climate, important vegetation. These conditions are in fact those of the so-called *biostasy* phase, as defined by ERHART in 1967 (QUINIF et *al* 2014). The weathering takes place in the phreatic zone. The low hydrological potential, related to the low relief, makes that water is flowing extremely slowly. In deeper parts, the water may even follow phreatic thermal cells. The porosity necessary to initiate the weathering process is in our case offered by joints opened during Cretaceous extensional tectonic phases.

Step 2: Ghost-rock removal and cave formation
The second phase of karst genesis (Fig. 2) starts with changing environmental conditions of tectonic uplift and subsequent water-level lowering. A change in vegetation may influence the process with a decrease in the protection of the soils. This is the so-called *rhexistasy* phase as defined by ERHART in 1967. The creation of a hydrodynamical potential will induce a compaction of the porous altered rock or ghost rock leading to the creation of larger voids. These voids may migrate to the surface, following weathered structures and create surface collapses. Surface run-off waters may follow easy-to-erode pre-formed weathered networks to create a complex speleological system with underground rivers, pits and mazes. The water will find its way and resurge into lower lying valleys, creating the cave systems like we know them today.

Figure 1. Ghost rock in the Gauthier-Wincqz Quarry in Soignies, Belgium. The limestone, a massive Tournaisian (Mississippian) 'encrinite' was partially dissolved, especially its micritic part. The larger remains of the crinoid fossils give a granular aspect to the 'ghost'. Inside the ghost-rock, remains of unaltered or less altered limestone are observed, e.g., behind the hammer.

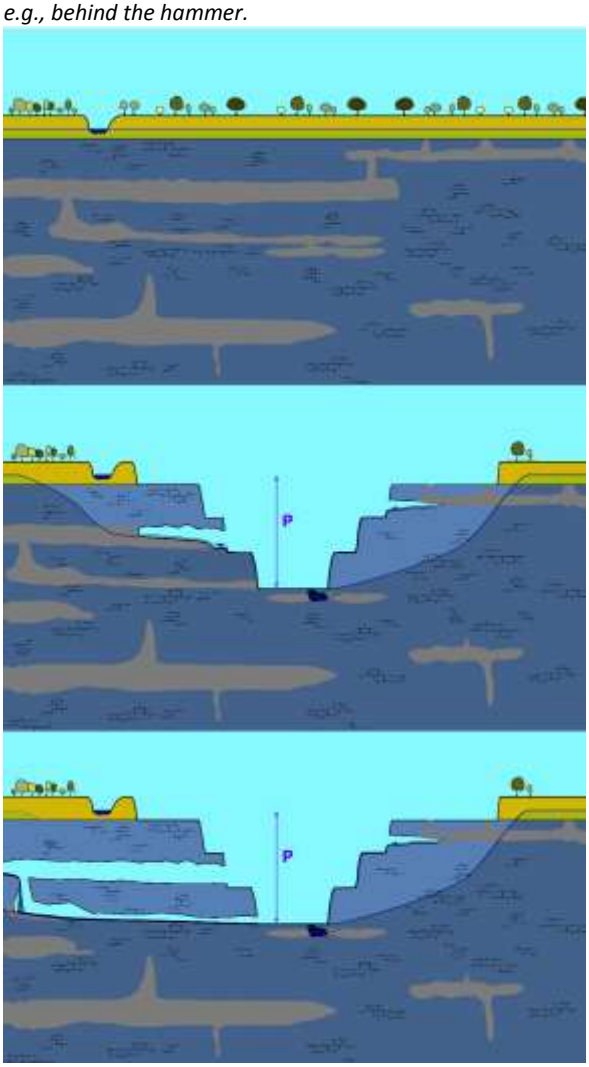

Figure 2. Evolution of a weathered or 'ghost-rock' karstified limestone as observed in the Nocarcentre Quarry (Ecaussinnes, Belgium). Above: Tertiary deposits cover in unconformity ghost-rock rich limestones that were karstified during Cretaceous. The residual ghost rock remained in place as long as the hydrodynamical potential was absent.
Middle: The digging of the quarry creates a hydrodynamical potential. Underground water flows from the surrounding aquifer into the quarry and 'washes away' the ghost rocks, creating 'speleological caves'.
Below: New underlying galleries form following the deepening of the quarry. This phenomenon mimics the natural process of deepening valleys.

The new concept has important consequences for several other aspects of karst and caves and even for cavers.

3. The consequences for caves (and cavers looking for new cave passages!)

Caves are older than previously thought…
In the classical karstification theory, Belgian caves were maximum ~10 Ma old, dating from Miocene age. Instead, the ghost-rock theory sets first karstification steps in Cretaceous times, when the weathering of the limestone pre-forms the future cave.
Looking for new caves? Better not digging into a ghost rock!

In contrast with the classical theory, the ghost-rock karstification does not enable to find an upstream or downstream part of a system, since it may be formed by irregular weathering of the limestone in any direction, depending on probably bacterial and chemical processes, and structural discontinuities. However, a river system may be organised afterwards by the water trying to find a passage and following successive altered levels. Of course, this means that digging into a ghost-rock will be probably less successful to find new open passages than digging in fluvial sediments, since the ghost rock indicates passages that were never emptied, while river sediments were deposited in already open passages. Best to be able to make the difference!

Relating cave levels with surface fluvial terrasses or erosion levels is hazardous

Since in the ghost-rock theory, flowing water tries to find a passage in the previously altered limestone, the opened passages were 'pre-figured' and are thus not progressively following the creation of the outside landscape as thought in the classical theory.

Key-holes and other roof channels are no proof of running water anymore.

Several macro and micro morphologies were observed inside ghost-rocks and are therefore no proof anymore for water flowing in open passages. Anastomosis and ceiling groves, key-hole galleries, ledges or terraces, ceiling channels or pockets are all morphologies that could have formed due to slow weathering and are no proof of running water in open passages (DUBOIS et *al*. 2014). Or said differently: Scallops and giant pothole patterns are the only 'sure' indication of flowing water.

Figure 3: Ghost rock in the quarry of Chansin (Namur Province, Belgium, DUBOIS & QUINIF, 2019). The ghost rock is surrounded by red lines. It seems be a gallery with a river deposit but this filling is in reality the residual alterite. The bedrock member affected by the weathering is a sandy limestone and the residual alterite is constituted essentially by sands with a great porosity.

4. Where is the ghost? A cave in a few months!

An important problem in proving the ghost-rock karstification in "nowadays" caves is that since these caves are open, it means that the alterite or weathered limestone or ghost-rock is gone. Most caves do not anymore contain the traces of the weathering and makes the ghost-rock karstification difficult to prove. However, some of them still do contain parts of weathered limestone such as Trabuc cave in Gard (BRUXELLES, 1997).

The best place to look for ghost-rock karstification is in quarries. In Belgium, 'ghost rocks' are observed in the quarries, such as in the Chansin quarry (Namur Province, Belgium) (Fig. 3) or in the quarries of the Hainaut region. The quarry of Nocarcentre (Soignies) in Belgium had several parts with altered limestones, so-called 'ghost rocks' (Fig 2). These parts were an important problem for the productivity of the quarries. Many springs were present, with water flowing out of the altered limestones, as a typical

consequence of the hydrological depression dome created by the pumping of the water by the quarry. After a few months, the water eroded the entire ghost rock and a classical–looking cave was born. We could enter the cave through a pit and navigate with a small boat on the river flowing on the compacted ghost rock residues. The water was coming from the not yet eroded ghost rock after several tens of meters (QUINIF, 2010). With the grotte Quentin, we witnessed the creation of a cave in a few months!
Nothing seems to be discriminating between a cave formed in the classical way and the cave formed from a ghost rock!

Remaining questions are numerous and one of them is: 'are all the current known caves formed following the ghost-rock theory?' or is it a continuum between several possibilities in-between two extremes of ghost-rock (partial dissolution & sudden void creation) and total removal karstification (direct removal of matter and progressive widening of voids) depending on the regional topographical and tectonic situation?

5. Conclusions and perspectives

It is now well demonstrated that in specific environmental context, the karstification will not follow the classical theory of total removal of the carbonates by flowing water, dissolving the limestone to progressively enlarge initial crack. Instead, the limestone is, in a first step, weathered and remains *in situ* with a larger porosity, a situation that can last millions of years. In a second step, driven by changing environmental conditions related to tectonic uplift or lowering of the piezometric water-level, the weathered limestone or 'ghost rock' is washed away by flowing water and a cave is formed.
The ghost-rock theory often enables better explanations for observed hydrological dynamics, i.e., buffer zones, that are difficult to explain in highly karstified rocks or the absence of evidence for high energetic waterflow, i.e., pebbles or scallops in large galleries.

Further studies should probably focus on the universality and prerequisite of the process in the karstogenesis and the spatial and temporal (chronology) extension of ghost-rocks as primary karstification step. Another important question remains about the process of partial dissolution and the role of bacteria in the decarbonation processes.
The relation with other processes, such as deep karst formation, ore mineralisations and oil and gas reservoir formation should be also further clarified. Several ghost-rocks in the organic -rich limestones in Soignies delivered an oily residue suggesting a possible reservoir function. In Belgium several karstic voids are filled with lead and zinc ores, that are a mix of smithsonite, limonite and other oxides. Their deposition history should be investigated in the light of ghost-rock karstification processes to have a more precise idea on how exactly the ores filled up the cavities.

References

BRUXELLES L. (1997) Karsts et paléokarsts du bassin de Mialet. *Karstologia* 30(2) : 15-24.

DUBOIS C., QUINIF Y, BAELE JM, BARRIQUAND L, BINI A, BRUXELLES L, DANDURAND G., HAVRON C., KAUFMANN O., LANS B., MAIRE R., MARTIN J., RODET J., ROWBERRY M.D., TOGNINI P. and VERGARI A. (2014)- The process of ghost-rock karstification and its role in the formation of cave systems. *Earth-Science Reviews* 131, 116-148.

DUBOIS C. and QUINIF Y., (2019) - The ghost-rock of the Chansin quarry (Belgium) – A remarkable example of pseudogallery. *Geologica Belgica*, 22/3-4, 175-181.

ERHART H. (1967) *La genèse des sols en tant que phénomène géologique*. Masson Ed., Paris, coll. Evolution des sciences, 90 p.

QUINIF Y. (2010) *Fantômes de roche et fantômisation. Essai sur un nouveau paradigme en karstogenèse*. Karstologia Mémoires 18, 183p.

QUINIF Y. (2014) La fantômisation, une nouvelle façon de concevoir la formation des cavernes. *Regards* 79, 42-72.

QUINIF Y., BAELE J.-M., DUBOIS C., HAVRON C., KAUFMANN O. et VERGARI A. (2014) – Fantômisation : un nouveau paradigme entre la théorie des deux phases de Davis et la théorie de la biorhexistasie d'Erhard. *Geologica Belgica*, 17, 66-74

.

.

Cellules de convection géothermiques et fantômisation

Yves QUINIF[(1)], Alain RORIVE[(2)], Luciane LICOUR[(3)], Grégory DANDURAND[(4)] & Laurent BRUXELLES[(5)]

(1) Service de Géologie fondamentale et appliquée, Université de Mons, rue de Houdain, 9, B-7000 Mons, Belgique, yves.quinif2@gmail.com
(2) Service de Géologie fondamentale et appliquée, Université de Mons, rue de Houdain, 9, B-7000 Mons, Belgique, alain.rorive@umons.ac.be
(3) Haute Ecole Provinciale de Hainaut-Condorcet, Dept d'Agronomie, rue Paul Pastur, 73, B-7500 Tournai) Tournai, Belgique. luciane.licour@condorcet.be.
(4) Inrap Nouvelle-Aquitaine (Poitiers) / UMR5608 TRACES (Toulouse). Gregory.Dandurand@Inrap.fr
(5) TRACES, UMR 5608 du CNRS, 5 allées Antonio Machado, 31058 Toulouse cedex 9. Laurent.bruxelles@inrap.fr

Résumé

L'initiation de la spéléogenèse a toujours constitué une énigme lorsqu'elle est considérée dans son contexte géologique. La découverte des fantômes de roche et surtout leur conception systémique dans le cadre de la karstogenèse conduit à reconsidérer cette initiation. La fantômisation est la division de la roche-mère en deux phases : une phase soluble exportée hors du système et une phase résiduelle constituant l'altérite. Les exemples des karsts de Lombardie et les paléokarsts du Hainaut ont montré que cette fantômisation se déroule plusieurs centaines de mètres sous la surface piézométrique. Le champ géothermique de Saint-Ghislain (Hainaut, Belgique) illustre une solution apportée à l'explication de l'initiation de la karstogenèse. Cet aquifère de calcaires et anhydrites carbonifères affleure au nord du Bassin de Mons et s'enfonce jusque 1700 à 4300 m de profondeur sous les formations houillères à la verticale de la ville de Saint-Ghislain, à l'ouest de Mons (Hainaut, Belgique). L'application de modèles thermo-hydrodynamiques à cet aquifère aveugle permet de considérer l'apparition de cellules de convection alimentées par le gradient géothermique. Ainsi, en fonction d'une perméabilité initiale et au-dessus d'une épaisseur limite, une circulation lente d'eau s'amorce et provoque la fantômisation que l'on peut alors rattacher à une spéléogenèse de type hypogène, l'énergie chimique étant ici apportée à la fois par les réactions bactériennes d'oxydo-réduction sur sulfures et la dissolution physique des sulfates. Le fantôme de roche se crée ainsi, l'altérite pouvant être érodée partiellement plus tard à la faveur de l'apparition d'un potentiel hydrodynamique, qu'il soit d'origine gravitaire ou, comme ici, d'origine géothermique.

Abstract

Geothermal convection cells and ghostrock karstification. The initiation of speleogenesis has always been an enigma when it is viewed in its geological context. The discovery of ghostrock and especially their systemic conception within the framework of karstogenesis leads to reconsider this initiation. "Ghosting" is the division of the bedrock into two phases: the weathering divides the bedrock in a soluble phase exported out of the system and a residual phase constituting the alterite. The examples of the karsts of Lombardy and the paleokarsts of Hainaut have shown that this ghosting takes place several hundred meters below the water table. The Saint-Ghislain geothermal field (Hainaut, Belgium) illustrates a solution to the explanation of the initiation of karstogenesis. This aquifer of limestone and carboniferous anhydrites outcrops north of the Mons Basin and sinks to a depth of 1,700 to 4,300 m under the coal formations vertically above the town of Saint-Ghislain, west of Mons (Hainaut, Belgium). The application of thermo-hydrodynamic models to this blind aquifer allows us to consider the appearance of convection cells fed by the geothermal gradient. Thus, depending on an initial permeability and above a limit thickness, a slow circulation of water begins and causes ghosting which can then be linked to a hypogenous type speleogenesis, chemical energy here being provided both by bacterial oxidation-reduction reactions on sulphides and the physical dissolution of sulphates. The phantom of rock is thus created, the alterite being able to be partially eroded later thanks to the appearance of a hydrodynamic potential, whether it is of gravity or, as here, of geothermal origin.

1. Introduction – Les fantômes de roche et les énergies mises en œuvre

La karstification par fantômisation se distingue de la karstification par enlèvement total (théorie « classique ») par le très faible potentiel hydrodynamique existant au départ de la karstogenèse. La formation des fantômes de roche se caractérise en effet par une attaque chimique séparant la roche mère en deux phases : une phase soluble exportée par les eaux souterraines et une phase résiduelle : l'altérite. La karstification classique, par enlèvement total, connaît quant à elle l'érosion à la fois des éléments solubilisés et les éléments solides détachés de la roche mère

par la dissolution de la matrice. Un exemple type est la dissolution de la partie micritique du calcaire et le résidu sparitique. Dans le cas de la fantômisation, ce dernier reste sur place au moins temporairement en la compagnie des insolubles et autres moins solubles : dolomite, minéraux argileux, silice. Le processus de fantômisation est bien connu dans le cas du granite où on l'appelle arénisation. La différence étant que les insolubles prennent largement la plus grande part dans l'altérite résiduelle : quartz, minéraux argileux secondaires, aluminosilicates résiduels. On a pensé longtemps que ce processus n'était pas de mise dans le cas des roches carbonatées. Or, les examens des paléokarsts en roches carbonatées dinantiennes de la province du Hainaut (Belgique) ont montré qu'il en est bien ainsi. Les formes souterraines gardent une altérite résiduelle formées de la partie moins soluble ; elle garde le volume initial, la perte de matière se manifestant par une augmentation de la porosité : c'est le fantôme de roche.

Figure 1 : Fantôme de roche (carrière du Clypot, Soignies, Belgique).

Cette distinction entre les deux types de karstogenèse se marque dans le concept thermodynamique de la karstification. La karstification, comme tout processus d'érosion, est le résultat d'une dissipation d'énergie. Parmi les types d'énergie concernée, l'énergie chimique est fondamentale car elle est la cause de la transformation de la roche mère. Elle tire sa source de réactions acide-base, l'acide pouvant être dû au CO_2 atmosphérique ou profond, aux sulfures qui s'oxydent en sulfates sous l'action de bactéries avec, comme corollaire, la présence d'acide sulfurique, en bref à la présence d'ions H_3O^+. Le second type d'énergie est l'énergie potentielle qui est la cause du mouvement de l'eau souterraine. Elle trouve sa source dans la gravité, le plus souvent invoquée, mais aussi dans le gradient géothermique, nous y reviendrons. Il manque encore un élément : la perméabilité initiale. En effet, les eaux souterraines doivent être capables de circuler au début du processus en l'absence d'érosion. Cette perméabilité initiale peut être due à une fracturation dont certaines familles directionnelles sont soumises à un régime tectonique en extension : c'est une troisième forme d'énergie de type mécanique. Il se peut que cette perméabilité initiale soit héritée d'une trop faible diagenèse, ou encore de la présence de cavités préexistantes.

Le gradient hydraulique joue le rôle fondamental dans le type de karstification. La fantômisation se satisfait d'un gradient hydraulique ΔH très faible puisque l'altérite résiduelle reste dans les formes souterraines sans être mécaniquement érodée dans cette première phase. Elle le sera lorsque le massif connaîtra l'augmentation de ce gradient (surrection, eustatisme, changement climatique). Son érosion mécanique aboutira alors à l'ouverture de cavités « spéléologiques ». Cette évolution qui part de l'altération chimique à l'érosion mécanique est une parfaite illustration de la théorie de la biorhexistasie d'ERHART (1967).

2. Le karst géothermique de Saint-Ghislain (Bassin de Mons, Belgique)

Un important aquifère constitué principalement de calcaires paléozoïques se situe dans le Bassin de Mons, structuré en fond de bateau comprenant des formations du Crétacé supérieur et du Paléogène incisées dans les formations paléozoïques du socle varisque (BOULVAIN & PINGOT, 2011). Sous les formations Houillères écaillées (Pennsylvanien et Serpukhovien), le Viséen et le Tournaisien regroupent des formations carbonatées (calcaires et dolomies) et sulfatées (anhydrite) d'une épaisseur avoisinant les 2.600 m d'épaisseur (Fig. 2). La karstification visible en affleurement au nord notamment grâce aux carrières des régions de Soignies et de Tournai se retrouve en profondeur, sans doute avec des différences morphologiques (dissolution des anhydrites, présence de brèches). Cet aquifère offre ainsi un modèle de karstification profonde dont les circulations ont été modélisées (LICOUR, 2012). En ce sens, il peut être considéré comme un holotype pour les circulations karstiques profondes.

En 1982, un sondage d'exploration géologique découvre de l'eau chaude artésienne au cœur du Bassin de Mons. Ce sondage recoupa vers 1.700 m de profondeur, dans les carbonates et sulfates viséens, des cavités et brèches très perméables contenant de l'eau à 70°C. Deux autres sondages (Douvrain et Ghlin) recoupèrent également les formations aquifères géothermiques. La configuration géologique visualisée par la figure 2 localise les zones d'infiltration au nord. Les eaux peuvent ainsi descendre au cœur de la structure où elles subissent le gradient géothermique normal (3°C/100 mètres). Il faut noter qu'aucune possibilité de sortie des eaux chaudes n'existe au sud, à l'est ou à l'ouest : l'aquifère s'ennoie profondément sous la nappe de charriage ardennaise sous la faille du midi. Les seules sources sont situées au nord de l'affleurement de l'aquifère et présentent des anomalies thermiques.
Ces constations ont conduit l'une d'entre nous (LICOUR, 2012) à concevoir un modèle de circulation des eaux dans l'aquifère suivant une ou plusieurs cellules de convection

thermique dont le moteur est la différence de température suivant la profondeur (Fig. 3). La quantification de ce modèle par un logiciel adapté prouve la vraisemblance de ces circulations, les seules pouvant expliquer la karstification profonde nécessitant une évacuation des eaux minéralisées. Verticalement, le mouvement de l'eau se fait suivant une descente par le mur de l'aquifère et une remontée par le toit. La modélisation dans une coupe verticale N-S indique l'initiation d'une cellule de convection dans un plan vertical (Fig. 3). Le mouvement peut être initié par le gradient géothermique à partir d'une épaisseur d'aquifère dont la valeur est fonction de la perméabilité initiale.

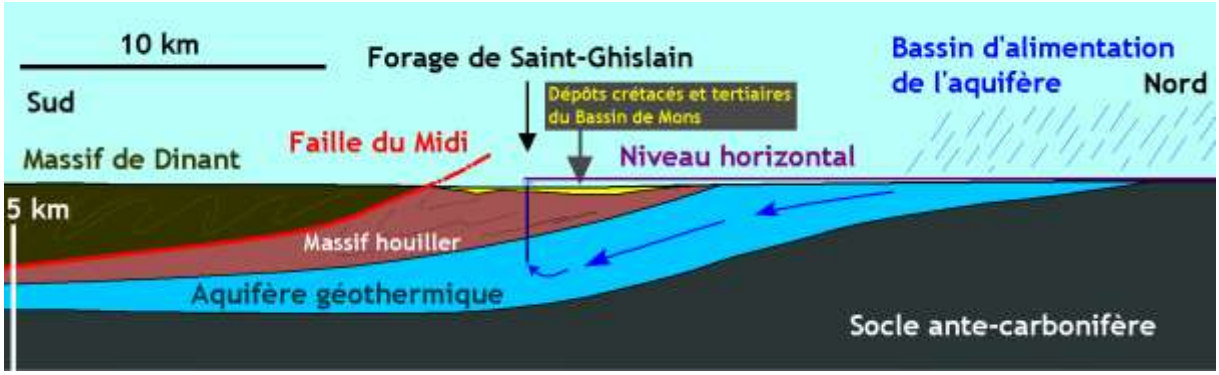

Figure 2 : L'aquifère géothermique du Hainaut. Cette figure est une coupe géologique interprétative orientée du nord vers le sud, à partir des données géologiques récoltées en affleurement, des forages et des investigations géophysiques. Les formations formant l'aquifère géothermique sont formées des calcaires, dolomies et anhydrites datant du Carbonifère inférieur. Elles reposent sur le socle primaire ante-carbonifère et sont surmontées par les formations du Carbonifère supérieur. Les eaux sont artésiennes au niveau des sondages forés dans le Bassin de Mons, étant à une altitude inférieure à la zone d'alimentation de l'aquifère.

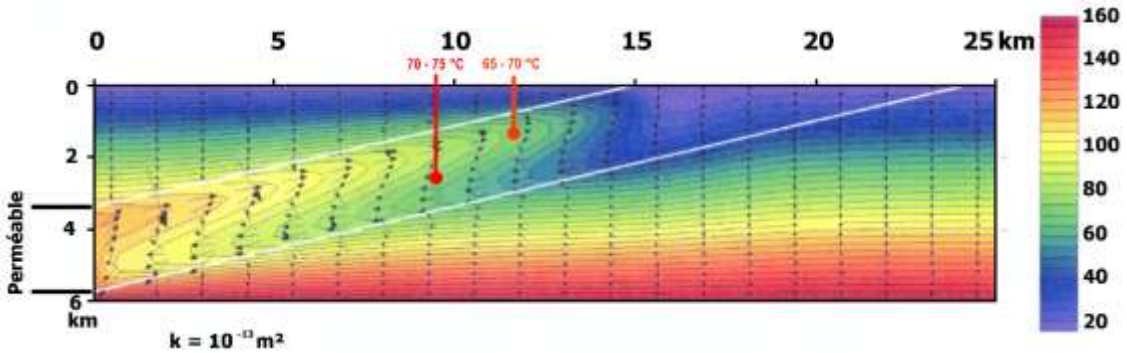

Figure 3 : Modèle de couche perméable inclinée à mur et toit imperméable et surface libre. A droite, l'échelle de température. Les deux lignes rouges verticales indiquent les positions des sondages de Saint-Ghislain et de Douvrain.

Les valeurs de discrétisation et des paramètres utilisés sont : 1. 25 km de long, soit 250 colonnes de 100 m, 6 km de profondeur, soit 60 rangées de 100 m ; gradient géothermique de 2,5 °C/100 m, soit 10 °C en surface et 157,5 °C au fond ; une porosité de 5 % et une perméabilité de 10^{-13} m² pour la couche perméable, une porosité de 2 % et une perméabilité de 10^{-20} m² pour les couches imperméables. La géométrie de l'aquifère a été calquée sur celle de l'aquifère du Carbonifère hennuyer. Les valeurs choisies sont adéquates pour l'initiation de la convection verticale. Le mouvement peut être initié par le gradient géothermique à partir d'une épaisseur d'aquifère dont la valeur est fonction de la perméabilité initiale.

3. La karstification de type fantôme de roche à moteur géothermal

Seule hypothèse expliquant la karstification profonde dans l'aquifère de Saint-Ghislain, le gradient géothermique génère ainsi des cellules de convection. Cette hypothèse résulte de la configuration géométrique de cet aquifère qui constitue un cul-de-sac au sud, en profondeur, avec des zones d'infiltrations et des exutoires limités aux régions d'affleurement septentrionales. Les mesures de température dans les sources et les sondages ainsi que leur distribution géographique conforte cette hypothèse. En outre, les grands « puits naturels du Houiller » apportent un argument supplémentaire à l'existence de cette karstification profonde (QUINIF, 1995 ; QUINIF & LICOUR, 2012). Ces formes géantes verticales, larges de plusieurs dizaines de mètres et profondes parfois de plus d'un kilomètre transpercent les terrains houillers et trouvent leur origine dans la karstification sous-jacente. On peut les considérer comme des fontis géants. Leurs remplissages, qui

ont révélé les iguanodons de Bernissart, situent leur genèse au Crétacé.
La question de l'initiation de cette karstification se pose maintenant. Comme nous l'avons écrit ci-dessus, une perméabilité initiale et les deux types d'énergie sont nécessaires.
1. La perméabilité initiale est due dans ces roches compactes à une fracturation ayant joué en extension lors d'une phase de l'histoire géologique. Or, le Crétacé offre cette possibilité (QUINIF *et al*., 1997). Cette chronologie est en parfait accord avec celle du fonctionnement des puits du Houiller daté par la paléontologie. À cette profondeur, déjà acquise aux temps crétacés, seul le calcaire se fracture, l'anhydrite réagit de façon plastique.
2. L'énergie chimique est fournie, outre le CO_2 superficiel, par les réactions rédox affectant les sulfures (HAVRON *et al*., 2007). Les températures de l'aquifère ont favorisé en outre l'activité bactérienne.
3. Le gradient de potentiel est ici dû non pas à la gravité comme pour beaucoup de karsts mais à la chaleur, le gradient géothermique.

Lors de l'initiation, les vitesses de circulation de l'eau dans les cellules de convection étaient très faibles. Nous sommes donc amenés à penser que c'est une karstogenèse de type fantômisation qui a eu lieu. Ensuite, la formation des fantômes de roche touchant les évaporites, une dissolution physique simple s'est ajoutée à ce processus. La dissolution d'une partie de la roche mère a engendré par la suite des brèches d'affaissement, rencontrées par les forages.

4. Conclusion

L'aquifère de Saint-Ghislain, grâce à ses caractéristiques géologiques, fournit un modèle de karstification profonde. L'évolution en subsidence depuis les temps post-varisques nous le montre non affecté par l'érosion qui aurait suivi une surrection, effaçant les formes primitives de la karstification par fantômisation. Nous nous trouvons ici dans le cas de la karstification hypogène prouvée dans de nombreuses configurations géologiques (AUDRA et *al*., 2004 ; KLIMCHOUK, 2009). L'apport des considérations présentes est le concept d'initiation de la karstogenèse par fantômisation au sein de cellules de convection géothermiques. Pour cela, il faut une formation aquifère karstifiable dont l'épaisseur, la profondeur et la perméabilité initiale se situent dans la gamme de valeurs citées plus haut. Ainsi que nous l'avons déjà démontré dans une autre publication, ce mécanisme éclaire la genèse des résurgences vauclusiennes (DANDURAND et *al*., 2019).

Références

AUDRA P. et HOFMANN B. A. (2004) Les cavités hypogènes associées aux dépôts de sulfures métalliques (MVT). *Le Grotte d'Italia*, 5, 35-56.

AUDRA P., BIGOT J.-Y. & NOBÉCOURT J.-C. (2010) Hypogenic caves in France. Speleogenesis and morphology of the cave systems. *Bulletin de la Société géologique de France*, t. 181, 4, 327-335.

BOULVAIN F. et PINGOT J.-L. (2011) Genèse du sous-sol de la Wallonie. *Classe des Sciences, Académie royale de Belgique*, 190 p.

ERHART H. (1967) *La genèse des sols en tant que phénomène géologique*. Masson Ed., Paris, coll. Évolution des sciences, 90 p.

HAVRON C., BAELE J.-M. et QUINIF Y. (2007) Pétrographie d'une altérite résiduelle de type « fantôme de roche ». *Karstologia*, 49, 25-32.

DANDURAND G., QUINIF Y., GUENDON J.-L. et GRUNEISEN A. (2019) Sources vauclusiennes et fantômes de roche. *Karstologia*, 74 : 31-46.

KLIMCHOUK A. (2009) Morphogenesis of hypogenic caves. *Geomorphology*, 106, 1–2, 100-117.

LICOUR L. (2012) *Relations entre la géologie profonde et le comportement hydrogéologique du réservoir géothermique du Hainaut (Belgique)*. Thèse de doctorat, Université de Mons Ed. : 372 p.

QUINIF Y. (1995) Le Puits de Flénu (Belgique). La plus grande structure endokarstique au monde (1200 m) et la problématique des puits du Houiller. *Karstologia*, 24, 29-36.

QUINIF Y. and LICOUR L. (2012) The karstic phenomenon of Bernissart pit and the geomorphologic situation in the Mesozoic times. In: *Bernissart Dinosaurus*, Ed. Pascal Godefroit. Indiana University Press, 50-61.

QUINIF Y., VANDYCKE S. et VERGARI A. (1997) Chronologie et causalité entre tectonique et karstification - l'exemple des paléokarsts crétacés du Hainaut (Belgique). *Bull. Soc. Géol. Fr.*, 168, 4, 463-472.

Active water cave Vodna jama v Lozi and Loza Unroofed Cave – a case of morphogenesis in the Slavina Corrosional Plain (SW Slovenia)

Astrid ŠVARA[1,2], Andrej MIHEVC[1] & Nadja ZUPAN HAJNA[1,3]

(1) Karst Research Institute ZRC SAZU, Titov trg 2, 6230 Postojna, Slovenia, astrid.svara@zrc-sazu.si (corresponding author), mihevc@zrc-sazu.si, zupan@zrc-sazu.si.
(2) University of Nova Gorica, Graduate School of Karstology, Vipavska cesta 13, 5000 Nova Gorica, Slovenia.
(3) International Union of Speleology – UIS, Titov trg 2, 6230 Postojna, Slovenia.

Abstract

The Slavina Corrosional Plain is a leveled karst area located between Postojna and Pivka Basin, Karst Plateau, and Vipava Valley, developed in Eocene, Paleocene, and Cretaceous Limestone. The northern part was influenced by allogenic waters, forming a distinctive contact karst geomorphology, among which caves are present, running towards the south. Vodna jama v Lozi is a 7.7 km long active water cave (between 550 m and 470 m a.s.l.). On the surface, an unroofed cave filled with sediments appears (between 630 m and 580 m a.s.l.), named Loza Unroofed Cave. Extending at least 4.3 km on the karst surface, it represents the longest known and studied unroofed cave in Slovenia, classified as a Valuable Natural Feature. The distinctive relict cave channel without a ceiling is up to 10 m deep and 30 m wide. A geomorphological map was produced by LiDAR imaging, cartographic measurements and sediment sampling. The sedimentary methods and X-Ray Diffraction (XRD) were used to determine the origin of sediments. By the analyses, we could prove, that the sediments in the Loza Unroofed Cave were brought into the cave by an allogenic river(s) sinking into the Slavina Corrosional Plain from the North or north-west part of the Postojna Basin. Furthermore, we assume regarding its position, sediment contents, and direction of water flow, to be a precursor of Vodna jama v Lozi, now an active epiphreatic cave about 100 m deeper.

1. Introduction

Geographical, Geological and Hydrological settings

The research area represents an NW part of the Dinaric karst which is the main morphological type of the Dinaric Mountains (MIHEVC & PRELOVŠEK, 2010). The Slavina Corrosional Plain is a karst area with individual peaks from altitude 640 m to 750 m, which on the N borders with the Postojna Basin, with a mean altitude of 550 m. The Postojna Basin comprises of Lower to Middle Eocene flysch rocks and Quaternary alluvium intercalations - river terraces and weathered flysch deposits (MELIK, 1951; PLENIČAR, 1963 and 1970; GOSPODARIČ, 1988). The Slavina Plain is at its contact with the basin developed in Paleocene to Eocene limestones, Cretaceous to Paleocene limestones, and in its main part in Upper Cretaceous limestones (generalized and marked with green color in Fig. 1). From a geological point of view, the Slavina Plain represents the Komen Thrust Sheet predominantly with NW-SE Dinaric and Transverse-Dinaric faulting, common for the structural unit of External Dinarides (PLACER, 2008). The Postojna Basin has impermeable properties with waters gathering in streams and flowing towards its borders. The Rakuljščica Stream has a proven underground water connection from the Sajevče Ponor at the end of the Sajevče Blind Valley (marked with white color in Fig. 1) through the caves Markov spodmol and Vodna jama v Lozi towards the Timava River (HRIBAR *et al.*, 1955), representing the Adriatic Sea Drainage Basin (ARSO, 2020).

Active cave Vodna jama v Lozi and the Loza Unroofed Cave

Due to geological and hydrological settings, contact karst geomorphic features have been forming in the Slavina Plain, along with (epi)phreatic speleological features, influenced by allogenic waters loaded with flysch derived sediments - composed mainly by pebbles, sand, silt, and clay (GOSPODARIČ *et al.*, 1970; MIHEVC, 1991a, 1991b, 1999 and 2006). One of the most representable features is the active cave Vodna jama v Lozi and the denuded cave Loza Unroofed Cave (Fig. 1).

The active water cave Vodna jama v Lozi (Cad. No. 911) is a (sub)horizontal cave, which is through a sump connected to the cave Markov spodmol (Cad. No. 878), together forming a 7.7 km long cave (CAVE REGISTER, 2020). The cave is developed between the approximate elevations of 550 m and 470 m, leaning towards SW. In the cave Markov spodmol, where the (epi)phreatic features are well developed, walls and ceiling are covered with scallops, showing a reworking of a fast river flow (Fig. 2), along with several cave lakes, sumps, and other dissolutional features. This cave is representing an intermittent ponor of the Rakuljščica Stream, today acting as such only at high waters. In the cave, several clastic sediment stacks of mainly channel and slack-water facieses appear. A profile was sampled for the paleomagnetic dating method, which gave an age range of its deposition between 0.78 – 2.58 Ma (ZUPAN HAJNA *et al.*, 2010 and 2020). The continuation part – the active cave

Vodna jama v Lozi is on the other hand represented by many clastic sediment accumulations, affecting the overall appearance of the cave which along with many water sumps and changing stream paths makes it more difficult to research.

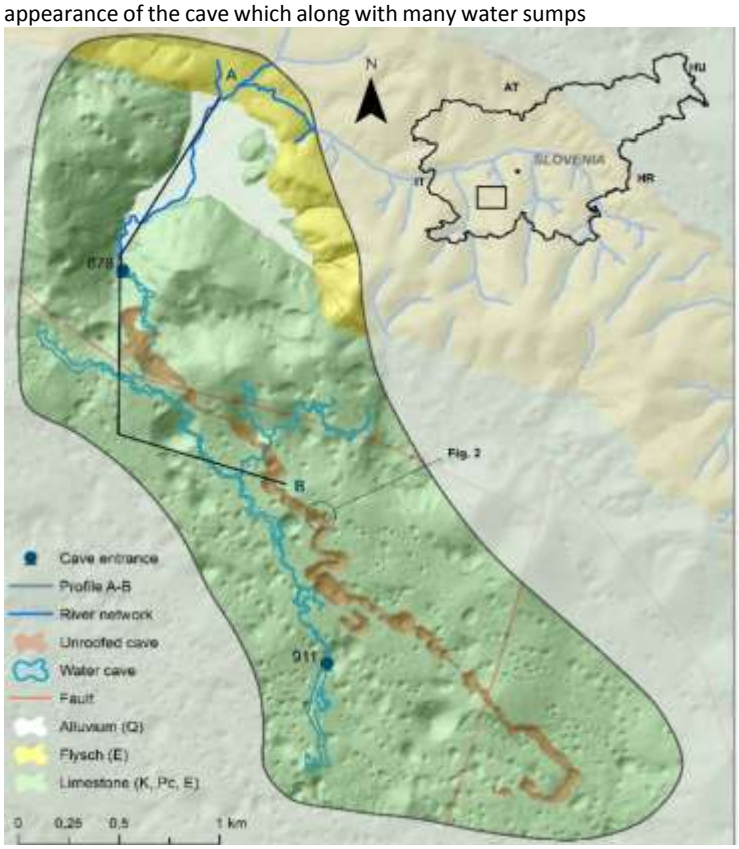

Figure 1: Location of the Loza Unroofed cave and active caves Vodna jama v Lozi (Cad. No. 911) and Markov spodmol (Cad. No. 878), on the Slavina Corrosional Plain, NW Slovenia with locations of Figures 4 and 5. Schematic cross section A-B. Source: GOV (Lidar and OGK geology) and Slovenian Cave Cadaster.

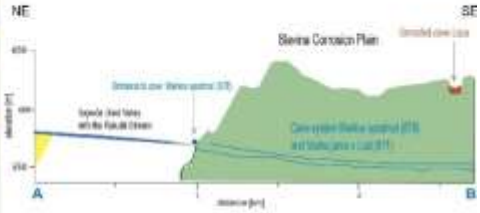

The (sub)horizontal Loza Unroofed Cave has an up to 30 m wide and 10 m deep cave channel, largely filled with allogenic clastic and allochthonous cave sediments. It is exposed on the surface between the elevations of 630 m and 580 m (MIHEVC, 1991a, 1991b, 1999 and 2006). In the approximate vicinity of the denuded cave, a side passage opens with a preserved ceiling. A section of fine clastic sediments was sampled for the paleomagnetic dating method, which revealed its age to be older than 4 Ma (ZUPAN HAJNA *et al.*, 2020).

Figure 2: Scallops in the cave Markov spodmol, showing phreatic genesis (Photo: GEDEI, 2015).

2. Materials and methods

The TTN5 topographic map in scale 1:5000, high-resolution LiDAR map, DMV digital elevation and shaded relief models, from the Slovenian Environmental Agency (ARSO), were used for geomorphological mapping of the research area, along with computer work on ArcMap and Adobe Illustrator software. Reviewing the existing information on cave reports and plans was done in the Slovenian Cave Cadaster at the Karst Research Institute ZRC SAZU in Postojna. Selected allogenic fine-grained sediments (e.g. clay, silt, sand) were sampled by a basic hand/machine drill. The X-ray powder diffraction (XRD) method helped us to determine the mineralogical composition of allochthonous clastic sediments which gave us information about their provenience. Both analyses were performed at the Karst research institute ZRC SAZU in Postojna on the Bruker XRD D2 Phaser system. By observing, mapping, and comparison of the geomorphic cave features in the active and unroofed cave, along with other analyzing methods, a morphogenetic review was made.

3. Results and conclusions

In the active caves Vodna jama v Lozi and Markov spodmol, the known orientation of the scallops, the type of sediment deposition, and the location of the ponor along with the underground river flow, gave us the idea to compare the active caves with the denuded cave in their vicinity, exposed about 100 m above on the surface. The cave Vodna jama v Lozi is represented by quite vast channels and chambers, mainly filled with allogenic sediments (flysch pebbles, sand, silt, and clay). Slack-water sediment facies and cap muds of the latest floodings are mainly covering the variety of depositions, which are in places uncovered by stream incisions. In several higher parts of the cave, stalagmites are deposited on top of the allogenic sediments, which can be inclined due to sediment creeping bellow. The paragenetic overprint is shown by the leveling of the ceiling, in places covered by half-tubes (Fig. 3), anastomoses, and pendants, while on the walls mainly as alluvial notches on several heights.

Figure 3: Half-tubes as paragenetic dissolutional forms in the active cave`s ceiling (Photo: TIČAR, 2020).

The Loza Unroofed Cave has its bottom channel mainly covered by clastic sediments, which are at different depths mixed with flowstone and limestone gravel as chips, derived from the degradation of the cave ceiling and walls due to denudation. In slightly inclined parts of the channel or along channel slopes, small outcrops of flowstone were found, many times easily weathered leaving only small remnants, hard to detect. The channel is frequently meandering and exposing some cave chambers in forms of collapse dolines. In one of them, a cave wall is preserved, with a stalagmite sedimented on top of a flowstone shelf, which was once deposited on top of an allogenic sediment stack/dome (Fig. 4). Along the preserved wall, a slightly tilted up to 3 m high flowstone deposit (stalagmite/stalactite) was observed (Fig. 5).

Figure 4: Stalagmite and a flowstone-shelf deposition, preserved in the unroofed cave (Photo: TIČAR, 2020).

Figure 5: Flowstone deposit, preserved in the unroofed cave (Photo: ŠVARA, 2020).

The active cave Vodna jama v Lozi has about 80 m altitude difference in its 7.7 km of length, which shows an average descent of 10.4 m in 1 km of its length, whereas the Loza Unroofed Cave has a 50 m altitude difference in its 4.3 km of length, which represents an average descent of 11.6 m in 1 km of its length. That said, by both representing an approximate descend of 1 m in the length of 100 m which corresponds to a horizontal cave typology, and with both of them generally following a Dinaric NW-SE direction (Fig. 1) along with displaying similar geological and geomorphological features, we can assume, that the unroofed cave is a precursor, a relict passage of the active caves Markov spodmol and Vodna jama v Lozi, formed as (sub)horizontal leveled passages, like others found in similar contact karst areas in its vicinity.

4. Future research

Since the ongoing Ph.D. study will be conducted within this area, many ideas for future research are planned. Hopefully, in the Loza Unroofed Cave, we will manage to conduct further analysis of allogenic sediments covering its bottom channel, comprising of XRD and XRF analysis (giving us more information about the provenience) and electrical resistivity imaging along several cross-sections (giving us exact information on the depth of the sediment cover whereas the total dimensions of the former channel). In the active cave, further studies will comprise of detailed analysis of at least one other sediment profile in the cave Markov spodmol, where sampling for paleomagnetic dating methods and others – if suitable, will be performed). After further analysis, an even clearer picture of the Slavina Corrosional Plain contact karst morphogenesis will appear.

References

ARSO (2020) *Drainage Basins*.- [Online] Available from http://gis.arso.gov.si/atlasokolja/profile.aspx?id=Atlas_Okolja_AXL@Arso [Accessed on October 24th, 2020].

CAVE REGISTER (2020) *Cave Register of the Karst Research Institute ZRC SAZU and Speleological Association of Slovenia*. Postojna, Ljubljana.

GEDEI P. (2015) *Hlajenje v Markovem spodmolu*.- [Online] Available from https://www.petergedei.com/sl/portfolios/hlajenje-v-markovem-spodmolu/[Accessed on December 8th, 2020].

GOSPODARIČ R. (1988) Paleoclimatic record of cave sediments from Postojna karst. *Annales de la Société géologique de Belgique* 111, pp. 91-95.

GOSPODARIČ R., HABE F., HABIČ P. (1970) Orehovški kras in izvir Korentana. *Acta carslogica* 5, no°2, pp. 97-108.

HRIBAR F., HABE F., SAVNIK R. (1955) Podzemeljski svet Prestraniškega in Slavenskega ravnika. *Acta Carsologica* 1, pp. 91-147.

MELIK A. (1951) Pliocenska Pivka. *Geografski vestnik* 23, no°1, pp. 17-39.

MIHEVC A. (1991a) *Morfološke značilnosti ponornega kontaktnega krasa: izbrani primeri iz slovenskega krasa*. Master thesis. Faculty of Arts, Department of Geography, Ljubljana, 206p.

MIHEVC A. (1991b) Morfološke značilnosti ponornega kontaktnega krasa v Sloveniji. *Geografski vestnik* 63, pp. 41-50.

MIHEVC A. (1999) Unroofed caves of Slavenski ravnik. In: Mihevc A. (Ed.) *7th International Karstological School, Classical Karst, Roofless caves. Guide-booklet for the excursions*, June 1999, Postojna, Speleological Association of Slovenia and Karst Research Institute ZRC SAZU, pp. 9-14.

MIHEVC A. (2006) Brezstropa jam ana Slavenskem ravniku. In: Boštjančič J. (Ed.) *Slavenski zbornik. Slavina*. Kulturno društvo Slavina, pp. 27-34.

MIHEVC A., PRELOVŠEK M. (2010) Geographical Position and General Overview. In: Mihevc A., Prelovšek M. & Zupan Hajna N. (Eds.) *Introduction to the Dinaric Karst*, Collegium Graphicum d.o.o., Ljubljana, pp. 6-8.

PLACER L. (2008) Principles of the tectonic subdivision of Slovenia. *Geologija*, 51 no°2, pp. 205-217.

PLENIČAR M. (1963) *Osnovna geološka karta - tolmač za list Postojna* L33-77, Geološki zavod, Ljubljana, 52p.

PLENIČAR M. (1970) *Tolmač osnovne geološke karte 1:100.000, List Postojna*. Zvezni geološki zavod, Beograd.

ZUPAN HAJNA N., MIHEVC A., PRUNER P., BOSÁK P. (2010) Palaeomagnetic research on karst sediments in Slovenia. *International Journal of Speleology*, 39 no°2, pp. 47-60.

ZUPAN HAJNA N., BOSÁK P., PRUNER P., MIHEVC A., HERCMAN H., HORÁČEK I. (2020) Karst sediments in Slovenia: Plio-Quaternary multi-proxy records. *Quaternary International* 546, pp. 4-19.